Spatio-temporal approach to transport dynamics in the mammalian brain ventricular system

Dissertation

for the award of the degree

"Doctor rerum naturalium"

of the Georg-August-Universität Göttingen

within the doctoral program Genes and Devolpment

of the Georg-August University School of Science (GAUSS)

submitted by

Regina Johanna Faubel

from Göttingen

Göttingen 2013

Thesis Committee

Prof. Gregor Eichele, Gene und Verhalten, Max-Planck-Institut für biophysikalische Chemie, Göttingen

Dr. Reinhard Schuh, Molekulare Entwicklungsbiologie und Molekulare Organogenese, Max-Planck-Institut für biophysikalische Chemie, Göttingen

Prof. Dr. Burkhard Morgenstern, Institut für Mikrobiologie und Genetik und Bioinformatik, Georg-August-Universität, Göttingen

Members of the Examination Board

Referee: Prof. Gregor Eichele, Gene und Verhalten, Max-Planck-Institut für biophysikalische Chemie, Göttingen

2nd Referee: Reinhard Schuh, Molekulare Entwicklungsbiologie und Molekulare Organogenese, Max-Planck-Institut für biophysikalische Chemie, Göttingen

Further members of the Examination Board

Prof. Dr. Ernst A. Wimmer, Entwicklungsbiologie, Georg-August-Universität, Göttingen

Prof. Dr. Anastassia Stoykova, Molekulare Neuroentwicklungsbiologie, Max-Planck-Institut für biophysikalische Chemie, Göttingen

Prof. Dr. Eberhard Bodenschatz, Hydrodynamik, Strukturbildung und Biokomplexität, Max-Planck-Insitut für Dynamik und Selbstorganisation, Göttingen

Date of oral examination: Monday, November 22nd, 2013

Declaration

Herewith, I confirm that I have written the present PhD thesis independently and with no other sources and aids than quoted.

Göttingen, September 30th, 2013 Regina Faubel

Jedes Werden in der Natur, im Menschen, in der Liebe

Muss abwarten, geduldig sein. Bis seine Zeit zum Blühen kommt.

Dietrich Bonhoeffer

Zusammenfassung

Das Antizipieren täglich wiederkehrender, zirkadianer Ereignisse scheint dem Leben auf der Erde große evolutionäre Vorteile zu bieten, da beinahe alle Eukaryonten eine zirkadiane Uhr als internen Zeitgeber entwickelt haben. Die zirkadiane Uhr ist eine zell-autonome Eigenschaft, die zellulären Funktionen einen 24-Stunden Rhythmus auferlegt. Diese Oszillation ist genetisch determiniert und kann darüber hinaus auch durch äußere Faktoren wie Lichtperioden und Nahrungsaufnahme gesteuert werden. Seit Jahrzehnten verhelfen unzählige Studien das Ausmaß zirkadianer Regulation zu erfassen und somit humane Pathologien zu verstehen und zu behandeln. Die zirkadiane Dynamik von Substanzen in der Zerebrospinalflüssigkeit (ZSF) jedoch ist bisher weitgehend unerforscht. ZSF umspült das Gehirngewebe, wird homöostatisch über die Plexus chorioidei (ChPx) ausbalanciert und übt weitreichende Effekte auf die Physiologie, Erhaltung und Regeneration des Gehirns aus. Spezialisierte Zellen des Gehirngewebes bilden stabförmige Ausstülpungen, sogenannte Zilien, die eine synchronisierte Schlagbewegung ausführen und somit eine beständige und gerichtete Bewegung von ZSF bewirken und somit ZSF-Komponenten im Gehirn verteilen.

Diese Arbeit befasst sich mit der Frage nach zirkadianer Dynamik von diversen Regulationsmechanismen der Präsenz von ZSF-Komponenten. Zunächst wurde in einer Analyse des ChPx-Transkriptoms zirkadiane Regulation verschiedener Transportsysteme ermittelt, die den Austausch von Ionen, Nährstoffen, Toxinen und Metaboliten zwischen Gehirn und Blut vermitteln, u.a. die Produktion von ZSF selbst. Auch die enzymatische Prozessierung gewisser ZSF-Komponenten durch den ChPx scheint auf klar definierte Zeitfenster beschränkt.

Unter den zirkadian regulierten Komponenten des ChPx befinden sich Transkripte, welche zur Schlagbewegung der Zilien beitragen und somit maßgeblich an der gerichteten Fortbewegung von ZSF-Komponenten beteiligt sind. Dies verleitete zur Annahme, nicht nur der Transport in das ZSF, sondern auch die Verteilung von Substanzen erfolge zirkadian. Um dieser Frage nachgzuehen, wurde ein System zur Mikroorgankultur verbunden mit computergestützter Analyse etabliert, um die Schlagrichtung von Zilien und daraus resultierende Strömungen zu bestimmen. Es stellte sich heraus, dass die Zilien in Mikrodomänen organisiert sind, wobei die Schlagrichtung der Zilien innerhalb einer Mikrodomäne die Flussrichtung des darüber liegenden Volumens vorgibt. Die Mikrodomänen sind derart arrangiert, dass sich ein charakteristisches Strömungsmuster

ergibt, welches schnelle, effiziente und regional begrenzte Fortbewegung von Substanzen ermöglicht und in diversen Mausstämmen finden ist. Änderungen des Musters in Abhängigkeit von der Tageszeit und der Funktionalität des zirkadianen Uhrengens Bmal1 deuten auf eine zikradiane Dynamik der ZSF-Strömung hin.

Zusammenfassend werfen die Ergebnisse dieser Arbeit verschiedene Aspekte zirkadianer Regulation von funktionalen, erhaltenden und regenerativen Prozessen des Gehirns auf, welche auf das Verständnis humaner Pathologien sowie die Verabreichung von Medikamenten weitreichende Auswirkungen haben könnte.

Summary

Anticipation of daily recurrent, circadian events seems to be of high evolutionary advantage for life on earth since most eukaryotic organisms evolved internal timekeepers, the so called circadian clocks. The oscillation of the mammalian circadian clock is genetically determined and adapts to external cues. The circadian clock is a cell autonomous characteristic and subjects the presence and function of numerous proteins to specific time windows during the day. For decades of years, molecular and physiologic studies on rodent tissues and cells elucidated the extent to which the circadian clock orchestrates diverse functions throughout the day and helped in understanding and treatment of human pathologies. However, circadian dynamics of substances in the cerebrospinal fluid (CSF) are largely unexplored. CSF embeds the brain parenchyma, exerts far-reaching effects on brain physiology, maintenance, and regeneration. CSF is homeostatically balanced by the choroid plexus (ChPx). Specialized cells cover the parenchyma and anchor rod-shaped protrusions, the so-called cilia that by synchronized beating induce translocation of CSF and its compounds.

This work addresses the mechanisms underlying circadian regulation of CSF components. Analysis of the ChPx circadian transcriptome revealed circadian regulation of a variety of transport systems that mediate exchange of ions, nutrients, toxins, and metabolites between CSF and blood as well as CSF-secretion itself. Moreover, evidence was found that endocrine functions and enzymatic breakdown might be constrained to defined time windows. A finding of far-reaching impact is circadian oscillation of ciliary components. This led to the assumption that, once arrived in the CSF, translocation of CSF components might be circadian regulated. This question was addressed by establishing a micro-organ culture system and computational analysis in order to determine cilia beat orientation and cilia-induced flow of beads. Apparently, cilia beat direction is organized to micro-domains and produces a characteristic flow pattern above the cilia carpet implicating the presence of efficient and regionally restricted trafficking pathways via the CSF. This flow pattern is conserved between strains but seems to depend on the time of day. Genetic deletion of the major clock gene Bmal1 results in huge changes of the flow pattern suggesting the circadian clock as regulator of the daytime-dependent reorientation of cilia beating.

Altogether, these data suggest circadian regulation of CSF-mediated processes of maintenance, functioning, and repair of the brain that should be considered for understanding of human pathologies and pharmaceutical targeting of the brain. Moreover,

the finding of the highly complex ciliary transport system sheds a new light on copmartmentation and translocation of nutrients, toxins, and hormones in the mammalian brain.

I. List of Content

II. List of Figures

III. List of Tables

IV. List of Abbreviations

A	anterior
Ace	angiotensin-converting enzyme
ACTH	adreno-corticotrohin
Aoc2	amine oxidase, copper containing 2 (retina-specific)
ATP	adenosin triphosphate
Atp1b2	Atpase, Na+/K+ transporting, beta 2 polypeptide
AVP	arginino-vasopressin
BBB	blood-brain barrier
BBSome	Bardet-Biedel Syndrome proteins
Bmal1	*aryl-hydrocarbon receptor nuclear translocator-like*
°C	degree celsius
cAMP	cyclic adenosine monophosphate
CAR	carbonic anhydrase
CCG	clock controlled gene
ChPx	choroid plexus
ChPxlat	choroid plexus from the lateral ventricle
ChPx4	choroid plexus from the fourth ventricle
Clock	*circadian locomotor output cycles kaput*
Clc2	cardiotrophin like cytokine
Cry1	cryptochrome 1 (photolyase-like)
Cry2	cryptochrome 2 (photolyase-like)
CSF	cerebrospinal fluid
CT	circadian time
D	dorsal
Dbp	D-box binding protein
DIC	differential interference contrast
DMEM	Dulbecco`s modified Eagle Medium
ECM	extracellular matrix
Elovl5	ELOVL fatty acid elongase 5
FMO	ferredoxin-mono-oxidase
fps	frames per second

fz3	frizzled homolog 3
g	gravitation constant
G	gauche
GRP	glucagon related polypeptide
Hlf	hepatic leukemic factor
ISF	interstitial fluid
ISH	*in-situ* hybridization
KCNJ13	potassium channel, inwardly rectifying subfamily J, member 13
L:D	Light:Dark
min	minutes
Npas2	neuronal PAS domain 2
p	posterior
PBS	phosphate-buffered saline
PCP	planar cell polarity
PCR	Polymerase chain reaction
Per1	Period1
Per2	Period2
Per3	Period3
POR	P450 (cytochrome) oxidoreductase
Prok2	prokineticin 2
Prokr2	cognate prokineticin receptor 2; Gpcr173I1
PVN	paraventricular nucleus
qPCR	quantitative polymerase chain reaction
Reverbα	Nr1d2 nuclear receptor subfamily 1,group D, member 1
Reverbβ	Nr1d1 nuclear receptor subfamily 1,group D, member 2
Rorα	Retinoic related orphan receptor alpha
RNA	ribonucleic acid
SCN	suprachiasmatic nucleus
sec	seconds
Slc	solute carrier
Tef	tyrotroph embryonic factor

Tgfα	Transforming growth factor α
TTL	transcriptional and translational loop
V	ventral
VIP	vasoactive intestinal polypeptide
VPAC2	vasoactive intestinal polypeptide receptor 2
Wnt	Wingless related MMTV integration site
ZT	*Zeitgeber* time

1 Introduction

1.1 Circadian rhythms: from genes to behavior

1.1.1 The mammalian circadian clock

Physiologic and behavioral functions in mammals are subjected to daily recurrent, rhythmic variation. This rhythmicity is regulated to a certain extent by the intrinsic circadian (from Latin *circa* (=about) and *dies* (=a day)) clock. The circadian clock consists of interlocked transcriptional and translational feedback loops (TTLs) involving clock genes and clock gene products. Clock genes encode transcription factors and regulatory factors that exhibit cell-autonomous oscillation in a circadian manner. Due to the circadian regulation of their activity, clock genes impose a circadian rhythm to the expression of a range of so called clock-controlled genes (CCGs) (reviewed by Mohawk et al., 2012; Partch et al., 2014). Almost all tissues and organs harbor an intrinsic circadian clock (termed peripheral clocks) that oscillates independently even after organs are removed from the organism (Guilding and Piggins, 2007). These peripheral clocks are hierarchically coordinated by the master circadian clock of the suprachiasmatic nucleus (SCN), a small nucleus residing in the hypothalamus of the mammalian brain in proximity to the third ventricle (Rusak, 1979; Rusak and Zucker, 1979).

Moreover, environmental signals, so-called *Zeitgeber* may direct clock oscillation and this way mammals can be entrained to periodic signals. Mice kept under light:dark (L:D) cycles of 12:12 hours entirely accommodate to this rhythm in the absence of other entraining cues such as intake of food, exercise, and temperature (Bobrzynska and Mrosovsky, 1998; Coleman and Francis, 1991; Damiola et al., 2000; Edgar and Dement, 1991; Glaser and Stanewsky, 2005 Peek et al., 2012). The resulting coordination of physiological and behavioral functions throughout the day allows anticipation and therefore an optimal adaptation of the organism to daily recurrent environmental cues.

1.1.2 The molecular clockwork

Autonomous oscillation of the TTLs (Fig.1.1.2) is sustained by a small number of core-clock genes (Buhr and Takahashi, 2013; Dardente and Cermakian, 2007). Aryl-hydrocarbon receptor nuclear translocator-like (*Bmal1*) is maximally expressed at protein level around the transition from the dark phase to the light phase. The BMAL1 protein heterodimerizes with circadian locomotor output cycles kaput (CLOCK) (Vitaterna et al., 1994) or its paralog

neuronal PAS domain protein 2 (NPAS2) (Reick et al., 2001) to activate transcription at E-box elements. E-box elements are part of the promoter regions of many clock-controlled genes and also of certain core-clock genes that form a negative feedback loop (Fig.1.1.2), such as *period1-3* and *cryptochrome*1-2 (photolyase-like) (*Per1-3, Cry1*, and *Cry2*). Upon translation, CRY1-2 and PER1-3 accumulate in the cytoplasm. These transcription regulators are activated in the late light phase and shuttle into the nucleus where they inhibit transcription at E-box elements and as consequence their own expression (Tamanini et al., 2005). The transcriptional repression is terminated by degradation of CRY1-2 and PER1-3.

A second loop involves the *retinoic acid orphan receptors* (*RORα, RORβ* and *RORγ*) that are transcriptional activators of *Bmal1*. Activity of BMAL1 induces expression of the E-box regulated *nuclear receptor subfamily 1 group D member 1* (*Rev-erbα*) that constitutes an additional inhibitory feedback loop by directly repressing ROR-mediated transcription of *Bmal1*. Genetic deletion of the major clock gene *Bmal1* strongly impairs clock oscillation whereas loss of other clock genes is at least partly compensated by homologues (Saini et al., 2011).

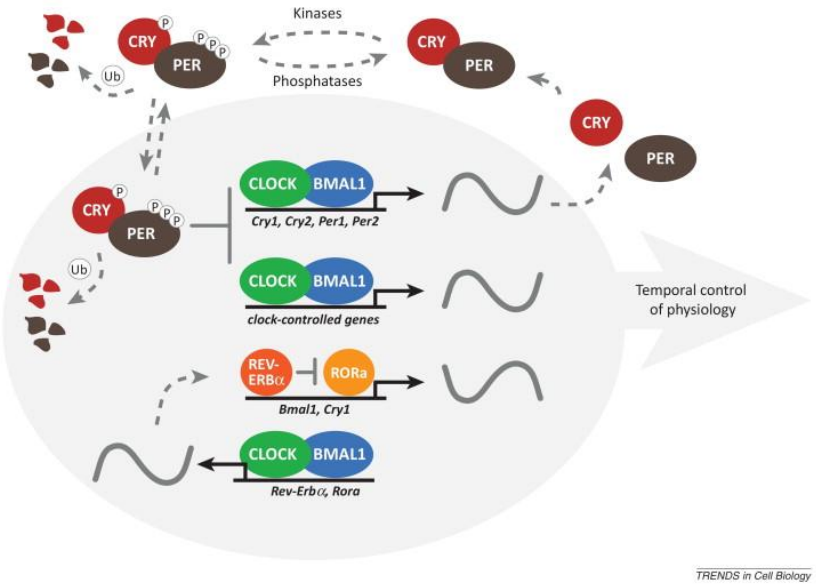

Fig.1.1.2 Simplified scheme of the molecular clockwork. Physiologic processes are temporally coordinated as a consequence of the alternation exhibited by the main core-clock genes, which are the activating transcription factors CLOCK and BMAL1 and the repressing transcription regulators PER1-3 and CRY1-2 (from Partch et al., 2013).

Further E-box regulated genes are *D-box binding protein (Dbp), hepatic leukemic factor (Hlf),* and *tyrotroph embryonic factor* (*Tef*). Even though in vitro studies revealed a small but

measurable impact of these homologues on the period of clock oscillation (Ukai-Tadenuma et al., 2011), genetic deletion studies showed that the encoded transcription factors are not essential for the oscillation of the circadian clock (Gachon et al., 2004). Nevertheless, they mediate circadian rhythm of genes that are involved in a variety of physiologic functions (Gachon et al., 2006; Wang et al., 2010). Because the circadian role of *Dbp, Hlf,* and *Tef* is to impose circadian oscillation to physiologically relevant CCGs they are rather considered to be clock output genes then core-clock genes.

In addition to the core-clock components, posttranslational modification fine-tunes the clock oscillation. Degradation of clock gene products is induced by F-box and leucine-rich repeat protein 3 (FBXL3)-mediated ubiquitination of CRY by the SKP1-CUL1-F-box protein (SCF) E3 ubiquitin ligase complex (Siepka et al., 2007) and by phosphorylation of PER by casein kinase 1 ε (Meng et al., 2008). BMAL1-activity is regulated by SUMOylation (Cardone et al., 2005). Also chromatin remodeling and RNA Polymerase II binding are implicated in fine-tuning of clock oscillation (Hardin and Panda, 2013).

A range of external and endogenous cues interferes with the circadian oscillation of clock genes and therefore has the potential to reset the clock or change the amplitude (Hirayama and Sassone-Corsi, 2005; Hirota and Fukada, 2004). The integration of these cues is mediated by intracellular signal transduction paths. Light pulses at night-time activate the extracellular signaling regulated kinase pathway and thereby induce phase shifts of the SCN clock. Blood-borne signals have been shown to phase-shift the clock oscillation in fibroblasts (Balsalobre et al., 1998). A range of individual signals has been identified that bear the potential to shift the clock e.g. cAMP, glucocorticoid hormones, and Ca^{2+} (Balsalobre et al., 2000; reviewed in Saini et al., 2011).

1.1.3 Humoral communication of the SCN

In the absence of environmental clock-entraining factors, the SCN is crucial for the synchronization of the individual clocks throughout the body. Mechanical ablation of the whole SCN (Moore and Eichler, 1972; Mosko and Moore, 1979; Rusak, 1979; Stephan and Zucker, 1972) as well as SCN-specific genetic disruption of *Bmal1* (Husse et al, 2011a) abolishes circadian rhythm in rodents. However, peripheral clocks keep their rhythm when kept under L:D conditions (Guo et al, 2006; Husse, 2011b). This indicates that they are

directly entrained by light or indirectly by light-induced inhibition of locomotor activity (Hughes and Piggins, 2012; Mrosovsky, 1999; Redlin and Mrosovsky, 1999).

Following ablation of the host SCN, transplantation of SCN is sufficient to restore circadian behavior (Aguilar-Roblero et al., 1986; DeCoursey and Buggy, 1989; LeSauter et al., 1996; Saitoh et al., 1987; Sawaki et al., 1984). Furthermore, in mice with a genetically manipulated clock, circadian rhythm in behavior can be rescued by transplantation of wildtype-SCN (Sujino et al., 2003). This finding raises the question whether neuronal connections mediate this rescue. Encapsulation of SCN-transplants inhibits the outgrowth of neurites but not the diffusion of endocrine signals from the SCN. Encapsulated SCN-transplants were able to restore the circadian rhythm in locomotor activity showing that endocrine, diffusible signals mediate the circadian regulation of the locomotor activity (Silver et al., 1996).

Several endocrine factors have been identified that are released from the SCN, bind to receptors that are located in close proximity to the third ventricle, and exert an inhibitory action on locomotor activity. These are transforming growth factor α (Tgfα), cardiotrophin like cytokine (Clc2), and prokineticin 2 (Prok2) (Kramer et al., 2001; Kraves and Weitz, 2006; Li et al., 2006). In the absence of the cognate receptor for Prok2, Prokr2, the overall locomotor activity and specifically the timing of the locomotor activity are strongly impaired. SCN-explants obtained from these animals showed normal circadian clock oscillation, indicating that Prok2 is not a regulator of the core-clock itself but acts as an output signal of the SCN and directly affects the locomotor activity (Prosser et al., 2007). Finally, neuropeptidergic release from the SCN has been shown to be essential for the synchronization of the individual cells of the SCN (Freeman and Herzog, 2011).

Genetic deletion of the *vasoactive intestinal peptide receptor 2* encoding for VPAC2 abolishes circadian rhythms in behavioral and metabolic functions of mice (Harmar et al., 2002). The ligand of VPAC2, vasoactive intestinal peptide (VIP), is highly expressed in the SCN and has the potential to phase shift the circadian clock of SCN-neurons in vitro (Reed et al., 2001). Genetic deletion of VIP revealed it`s role for the synchronization of SCN-neurons in vivo as well (Vosko et al., 2007). Further, systematic in vitro and transplantation studies revealed that the synchronizing effect of VIP and, in addition, of arginino-vasopressin (AVP) and gastrin-releasing peptide (GRP) involves an extracellular pathway that does not require neuronal connections between SCN-cells (Maywood et al., 2011; Hughes et al., 2011).

1.1.4 Assessing the functions of peripheral clocks

The circadian clock imposes oscillation to physiologic functions by direct or indirect regulation of circadian genes (Fig.1.1.4). The numerous individual functions oscillate most efficiently when synchronized. The synchronization is mediated by an interplay of neuronal connections between certain regions of the brain and peripheral organs (Hirota and Fukada, 2004; Maywood et al., 2007) as well as by humoral circadian cues that circulate in blood (Guo et al., 2005) and brain extracellular fluid (Maywood et al., 2011). The finding that fibroblasts maintain their circadian rhythm in vitro (Welsh et al., 2004) raised the question whether intrinsic clock oscillation has an impact on circadian regulation.

A fusion protein between either PER1 or PER2 and Luciferase expressed in rodents serves to visualize oscillation of the circadian clock (Welsh et al., 2004; Yamazaki et al., 2000). Tissue explants from such mice exhibit a robust circadian rhythm as measured by bioluminescence (Abe et al., 2002). SCN-explants maintain this rhythm when they are cultured. By contrast, bioluminescence rhythms in peripheral dampen after few days. However, this dampening is not caused by loss of clock oscillation but by progressive desynchronization of the individual cells (Yamaguchi et al., 2003). These observations support the view of the SCN as master clock that synchronizes the peripheral semiautonomous clocks and directly or indirectly imposes a rhythm to slave oscillators (Guilding and Piggins, 2007).

Circadian oscillation affects about 5-10% of the transcriptome (Ramsey et al., 2007). Studies on the proteome showed an even more pronounced effect of circadian regulation with about 10-20% of the proteome being regulated by the circadian clock (Deery et al., 2009; Eckel-Mahan et al., 2012; Reddy et al., 2006). Transcriptome studies of several tissues such as liver, heart, muscle, retina, adipose tissue, and adrenal gland revealed that a variety of functions are regulated in a circadian manner (McCarthy et al., 2007; Miller et al., 2007; Oster et al., 2006a; Panda et al., 2002; Storch et al., 2002; Storch et al., 2007; Zvonic et al., 2006). In vitro experiments with tissue explants show that the presence of the tissue clock is sufficient to maintain the circadian rhythm of physiological functions such as detoxification in the liver, melatonin secretion from the retina, secretion of glucocorticoids from the adrenal gland, secretion of insulin from the pancreatic islets, and secretion of AVP from the SCN (Jansen et al., 1999; Jansen et al., 2000; Lee et al., 2011; Muhlbauer et al., 2009; Oster

et al., 2006b; Tosini and Menaker, 1996). SCN-explants also maintain a circadian rhythm in neuronal firing (reviewed by Brown and Piggins, 2007; Inouye and Kawamura, 1979).

For clear-cut conclusions and translation to human pathologies, the impact of the individual tissue clocks on physiologic or behavioral rhythms in the living animal needs to be assessed. Transplantation studies of wild type adrenal to clock-mutant mice or vice versa showed that the tissue clock of the adrenal is more than a slave oscillator and actively gates the response to ACTH (Oster et al., 2006b). Genetic approaches generally target *Bmal1* because it is the only clock gene that is indispensible for clock oscillation (Partch et al., 2013). Brain specific expression of *Bmal1* in *Bmal1*$^{-/-}$ mice restored circadian behavioral rhythms whereas other phenotypes were not rescued (McDearmon et al., 2006). At that time, the lack of rescue of other functions in this mouse line was interpreted as consequence of non-circadian functions of *Bmal1* in peripheral tissues. However, tissue-specific deletion of *Bmal1* in liver severely impaired rhythms in blood glucose levels showing that the intrinsic peripheral clocks are of importance in the circadian regulation of physiologic processes (Lamia et al., 2008). Taken together, the regulation of circadian rhythms depends on the interplay of cell-intrinsic circadian cues with neuronal and humoral factors.

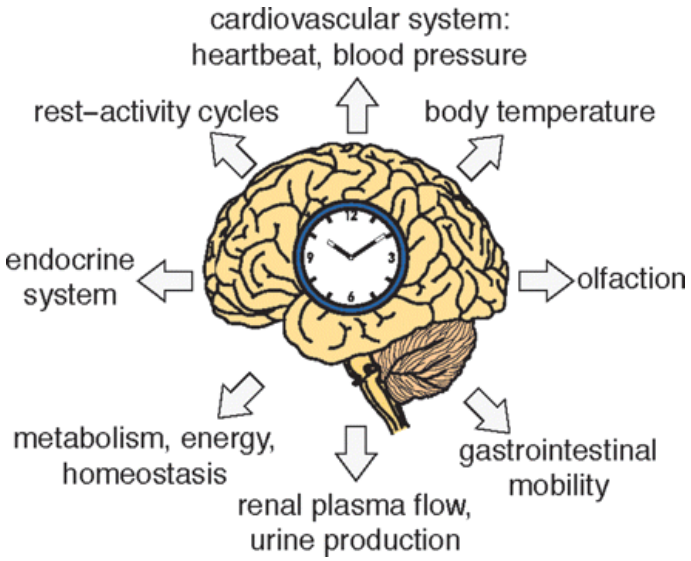

Fig.1.1.4 Mammalian physiology undergoes daily oscillations. The interplay between the master clock in the brain's suprachiasmatic nuclei and daily recurrent environmental factors sets the individual clocks of mammalian organs and tissues such as liver, heart, pancreas, adrenal, adipose tissue, blood vessels, and muscle and is supposed to regulate optimal timing of rest–activity cycles, body temperature, cardiovascular and endocrine processes, renal activity, intestinal motility, and metabolism, specifically the metabolism of xenobiotics (e.g., toxins ingested with food, medical drugs) in liver, kidney, and small intestine is also highly circadian (Modified from Saini et al., 2011).

1.2 Solute transport in the brain

1.2.1 Anatomy and function of the brain compartments and their barriers

Studying intravenous injection of dyes, Paul Ehrlich observed that brain and spinal canal were not stained (Ehrlich, 1885). In 1913, his colleague Edwin Goldmann successfully demonstrated that brain parenchyma (brain parenchyma consists of neurons and glia cells), the spinal canal, and cerebrospinal fluid (CSF) form a compartment that is separated from the periphery by tight barriers. Electron-microscopic observation revealed that tight junctions seal the cells to form these barriers and impede the passage of substances between these cells (Brightman and Reese, 1969; Reese and Karnovsky, 1967). Nonetheless, exchange of substances between compartments has to take place and therefore selective transport proteins have evolved that are located in the plasma membrane of barrier cells (Saunders et al., 2013; Segal, 2000). As a result of this gating function, the brain is embedded in a homeostatic, protective, and nutritive milieu (Cserr and Bundgaard, 1984).

1.2.1.1 Tight barriers gating the entry to the brain

The characteristic location, anatomy, and histology of the barriers reflect their specialized functions. The choroid plexus (ChPx) is distinguished from other barriers in that the surface is fully immersed in CSF, has a lobulated structure, and mediates diverse physiological processes (reviewed by Redzic, 2004). The ChPx produces CSF by active secretion of electrolytes and water across it`s epithelium. This CSF-production, about 500 ml/day in humans, results in a net flow of CSF (bulk-flow) through the brain that promotes dispersion of solutes (Johanson et al., 2005; Knopf et al., 1995; Praetorius, 2007).

There are three types of ChPx located in each of the four ventricles (Fig.1.2.1.1). The barrier function rests chiefly on the tightly sealed, polarized epithelial layer (Vorbrodt and Dobrogowska, 2003). Beneath the epithelial layer, a network of choroidal blood vessels is embedded in a loose connective tissue matrix. Since choroidal blood vessels lack tight junctions the basal side of the epithelial layer has direct access to the blood, whereas, at the same time, the apical side is in direct contact to CSF. To maximize the exchange of molecules the surface of the ChPx is very large and additionally has a microvillae brushborder that facilitates exchange of molecules (Redzic and Segal, 2004).

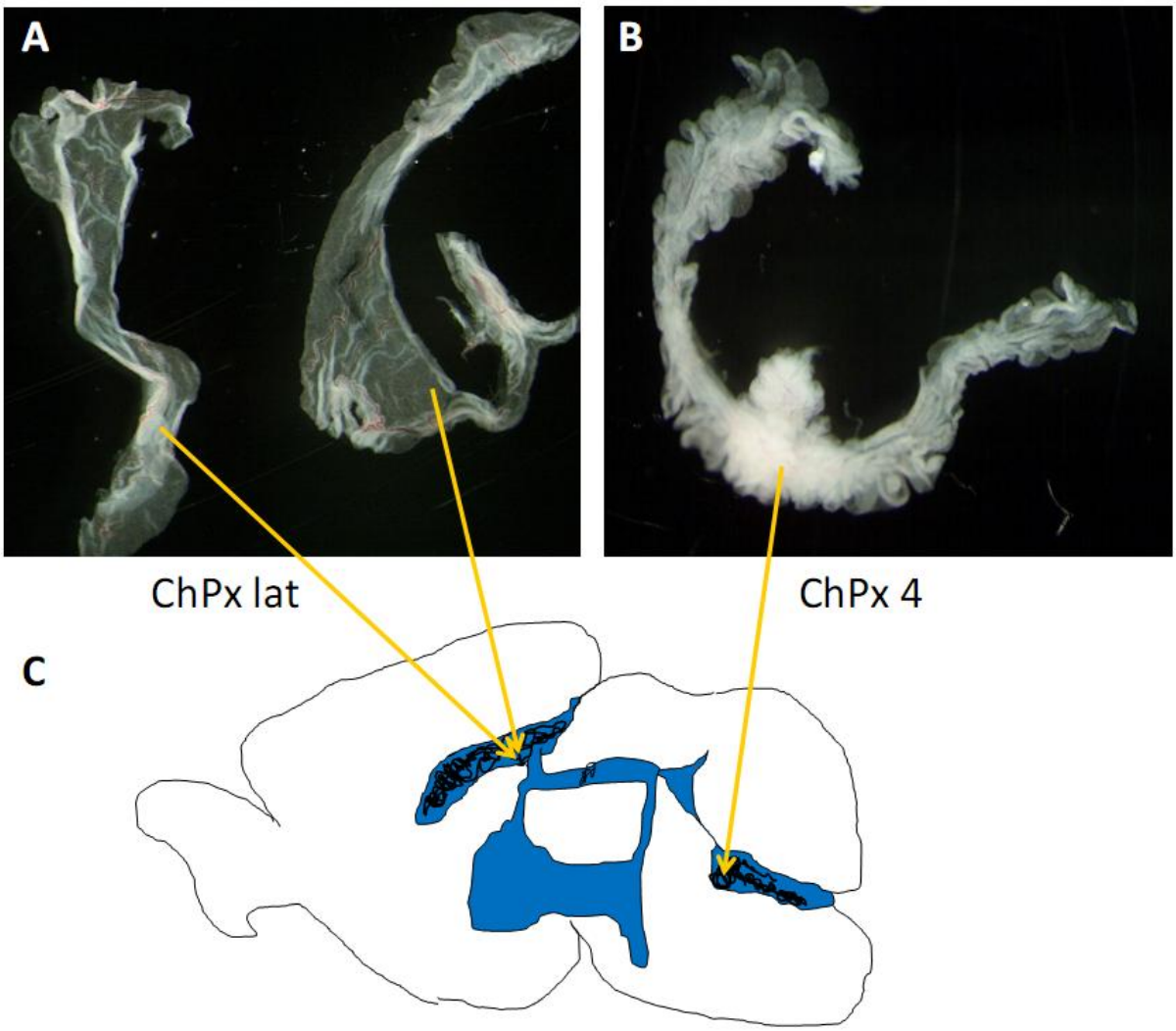

Fig.1.2.1.1 Anatomy of the cerebrospinal-fluid system. (**A**) Blood vessels in the ChPx from both lateral ventricles are covered by a transparent, epithelial monolayer. (**B**) ChPx from the fourth ventricle, however, has a cauliflower-like structure. (**C**) ChPx epithelia are the main production sites of CSF. CSF is secreted into the ventricles and drains via the fourth ventricle into the subarachnoid space that surrounds the brain parenchyma and is reabsorbed by the arachnoid membrane. Continuous secretion of CSF causes a bulk-flow in antero to posterior direction through the ventricular system. The yellow arrows on the left side point to the anterior lateral ventricle containing the ChPx, the arrow on the right side points towards the posterior, fourth ventricle.

The ChPx also contains an extended vesicle system that mediates transepithelial transport and storage of glycogen and hormones such as leptin, serotonin, and thyretin (Nilsson et al., 1990; Schreiber et al., 1990; Smith et al., 2004; Thomas et al., 2001; Zlokovic et al., 2000). The ChPx is an endocrine tissue that regulates a variety of peptides and cytokines with high importance for development, maintenance, and repair of nerve cells (Emerich et al., 2005;

Johanson et al., 2011a; Thanos et al., 2010). Furthermore, a range of hormone-processing enzymes participate in activation or degradation of hormones that are present in the CSF (Chodobski and Szmydynger-Chodobska, 2001; Skipor and Thiery, 2008).

In addition to the ChPx, the blood-brain-barrier (BBB) and the arachnoid membrane shield the brain from the periphery. The BBB consists of a branched network of vessels that transverse the brain parenchyma (Fig.1.2.1.2). The vessels are tightly sealed by intercellular junctions. Glial cells surround the endothelia and shield the sensitive neurons and interstitial fluid (ISF) from noxious substances. A characteristic of the BBB is the fast reactivity to changing requirements that allows for fast delivery of substances to the neurons located in proximity to the widespread network of blood vessels (Hawkins and Davis, 2005; Zlokovic, 2008). Specifically the blood brain barrier functions as the main entry site for sugar and oxygen that provide energy to the brain (Saunders et al., 2008).

The arachnoid membranes contact the outer surface of the cortex and the CSF in the spacing between brain parenchyma and the meninges, the so called subarachnoid space. It serves as a reabsorption site of CSF (Davson et al., 1970; Grzybowski et al., 2006).

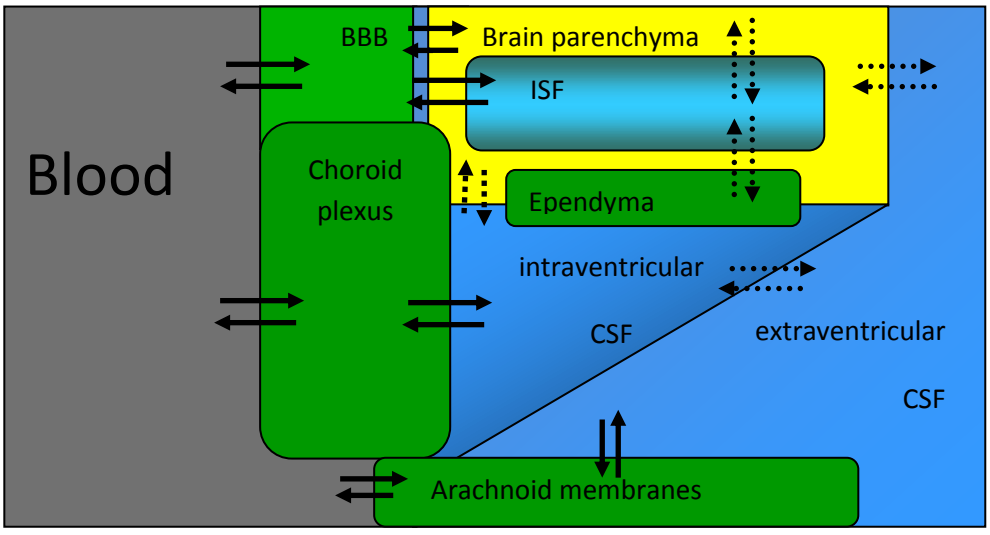

Fig.1.2.1.2: Brain compartments. Shown are paths for exchange (arrows) of molecules between blood and the brain compartments. Solid arrows indicate selective transport over tight barriers whereas dashed arrows symbolize paracellular passage of molecules. Once released to ISF or CSF, molecules can easily traffic through the compartments whereas the exchange between blood and CSF is tightly regulated by the barrier (modified from Johanson et al., 2005).

1.2.1.2 The brain ventricular system

The ventricular system of the brain is a system of interconnected cavities located inside the brain parenchyma (Fig.1.2.1.1). It consists of two lateral ventricles each located in one hemisphere, the third ventricle, and fourth ventricle with the latter one connected via the medial apperture and foramina Luschka to the cisterna magna and the subarachnoid space. The ventricular system is lined by ependyma and filled with CSF. The ependyma shields the brain parenchyma from CSF flow inside the ventricles and often is considered as barrier between the ventricular system and brain parenchyma (Del Bigio, 2010). However, Goldmann´s intraventricular injection studies showed that dyes and other solutes cross the ependyma by simple diffusion.

The ChPx is a specialized extension of the ependymal and protrudes into the ventricular lumen. Secretion of CSF into the ventricles and reabsorption from the subarachnoid space and spinal canal promote a continuous stream of CSF through the ventricular system, the so-called bulk-flow. The CSF flows from the lateral ventricles in caudal direction towards the fourth ventricle, where it leaves the brain parenchyma, enters the cisterna magna, and finally circulates in the subarachnoid space. On its way through the ventricular system, the CSF composition is changing due to continuous uptake and release of solutes by adjacent structures of the brain. Once it arrives in the subarachnoid space, substances carried by the CSF are diluted and circulate in the subarachnoid space around the brain parenchyma (Davson et al., 1970). Notably, a fraction of the CSF flows down along the spinal cord or penetrates the lymphatic system presumably via prelymphatic flow along the BBB (Johnston et al., 2004; Knopf et al., 1995; Zakharov et al., 2004).

1.2.1.3 Interfaces between CSF and brain parenchyma

The brain parenchyma is embedded in extracellular matrix and interstitial fluid (ISF). Extracellular matrix forms a far-reaching channel system and thus provides pathways for directed flow of ISF, namely short-distance and long-distance volume transmission (Agnati et al., 2010) and transport along paravascular pathways (Rennels, 1990; Iliff et al., 2012). Such directional transport through the parenchyma is involved in signal transmission between brain regions as shown for central monoamine signaling (Fuxe et al., 2010) or clearance of solutes from ISF towards CSF (Cserr et al., 1986; Iliff et al., 2013). The dispersion of tracers significantly differs between different areas of the brain and depends on ISF content in these

areas (Hrabetova and Nicholson, 2007). From that one can conclude that, areas of the brain differ in the composition of ISF and the exchange of substances is restricted.

Some neurons send processes across the ependymal lining into the ventricles and are thus in direct contact with the CSF where neuronal extensions form ciliated terminals that mediate neurosecretory functions via the CSF (Mathew, 1998; Vigh-Teichmann and Vigh, 1983; Vigh et al., 2004). In addition, astrocytes, a type of glia cells, are believed to mediate communication between CSF-derived signals and neurons (Rodriguez et al., 2005; Vigh and Vigh-Teichmann, 1998; Wittkowski, 1998). Astrocytes intercalate the ependymal lining, reinforce its barrier function, and mediate perception and release of signals such as retinoic acid (Shearer et al., 2012) and ATP (Frayling et al., 2011; Marpegan et al., 2011). Tanycytes are specialized ependymal cells that reach from the ventricle into the hypothalamus. There is evidence for a major participation of tanycytes in physiologic processes, in particular the regulation of body weight and energy balance (Bolborea and Dale, 2013).

1.2.1.4 Humoral communication via CSF

A range of physiological or behavioral functions such as sleep/wakefulness, appetite, and repair of the brain are regulated by humoral signaling via CSF (Zappaterra and Lehtinen, 2012). In the ventricular system, regional abundance of substances arises from bulk-flow that flushes solutes once arrived in the ventricles in a rostro-caudal direction through the ventricular system (Cserr and Bundgaard, 1984).

The site of release of these signals and molecules determines the response as illustrated by transplantation studies of the SCN (LeSauter et al., 1997). Furthermore, the effect of intraventricular orexin administration locally depends on the site of injection (Espana et al., 2001). The migration of neuronal precursor cells along the rostral migratory stream depends on a gradient of chemokines that are released by the ChPx into the lateral ventricle. Ependymal flow gives direction to the antero-posterior gradient. Inversion of this gradient by transplanting ChPx to an ectopic site greatly impairs cell migration (Sawamoto et al., 2006). This shows that imposition of distinct milieus and directed flow of CSF significantly affects brain functions.

1.2.2 Cilia in the ventricular system

1.2.2.1 Structure of cilia

Cilia are tiny, rod-shaped organelles that protrude from the surface of the cell. Ependymal motile cilia are about 10-14 µm in length and have a diameter of 0.2 µm. Monocilia are shorter and function as platforms for the presentation of receptors whereas motile cilia are mostly found in bundles and exert a lash-like movement. The two types of cilia can be distinguished by their structural organization (Zariwala et al., 2007). The basic structure of cilia is a pair-wise arrangement of microtubules running longitudinally from the base to the tip of the cilium (named axoneme) that produce a specific pattern with 9 outer microtubule doublets in primary cilia (9x2+0) and an extra pair of microtubule at the centre of the axoneme of motile cilia (9x2+2). Monocilia can exert a rotational movement in a developmental context (Cartwright et al., 2008; Drummond, 2012) whereas motile ependymal cilia exert a directed lash-like movement (Purkinje, 1836) and in addition have chemosensory functions (Shah et al., 2009). Each microtubule doublet of motile cilia is decorated with an outer dynein arm and an inner dynein arm that interact to generate the ciliary movement. Genetic mutation of these dyneins impairs motility (Ibanez-Tallon et al., 2003). Hydin is an additional component of motile cilia that has an essential role in the anchoring of dynein arms to microtubules (Lechtreck and Witman, 2007).

The ciliary membrane is a continuum of the plasma membrane. It arises at the transition zone and encloses the axoneme and associated structures. At the transition zone, the axoneme is attached to the basal body that anchors the cilium to the plasma membrane. The basal body is composed of transition fibers, a mother centriole, basal foot caps, and striated rootlets (Seeley and Nachury, 2010). Transition fibers are the main site of attachment of cilia to the plasma membrane and form a ciliary gate. Septins and a range of other proteins are part of the ciliary gate also called ciliary partitioning system. They form a diffusion barrier and at the same time enable exchange between the ciliary compartment and the cytoplasm (Reiter et al., 2012). The striated rootlets together with actin filaments and microtubules connect the cilia within the cell, they serve to propagate mechanical forces and coordinate the beating of individual cilia within a cell to a metachronal wave (Werner et al., 2011).

1.2.2.2 Cilia assembly and disassembly via intracellular transport systems

Intracellular transport of proteins and lipids is mediated by a fast, selective shuttling mechanism between vesicular structures of the cell (Kirchhausen, 2000). Vesicles shuttling between cytoplasmic vesicles and the ciliary base consist of highly specific proteins termed BBSome. Mutations in BBSome-associated proteins result in severe congenital diseases as observed in patients suffering Bardet-Biedel syndrome (Bennouna-Greene et al., 2011; Imhoff et al., 2011; Jin and Nachury, 2009; Marion et al., 2009). The BBSome assembles enzymatic and structural proteins to vesicles (Jin et al., 2010). Proteins that are required for ciliary functions have to be specifically targeted to these vesicles to be delivered to their final destination (Westlake et al., 2011). The delivery and removal of cargo is regulated by the ciliary pore or ciliary partitioning system located at the base of the cilium (Lee, 2011; Ounjai et al., 2013). Transport of ciliary proteins along the axoneme is regulated by intraflagellar transport (IFT). Kinesin-II is a motor protein responsible for anterograde IFT while cytoplasmic dyneins are required for retrograde transport (Pedersen and Christensen, 2012). Assembly and disassembly of the microtubule doublets occurs at the tip of the cilium. Balanced action between anterograde and retrograde IFT maintains the ciliary length (Avasthi and Marshall, 2012).

In addition to structural proteins and components that are required for transport, the cilium also contains a variety of receptors that are localized to the ciliary membrane. Protruding from the surface of the cell, the cilium is more exposed to extracellular signaling molecules and serves as antenna and signal transducer for perception. A few examples are light detection at the retina, odorant perception at olfactory sensory neurons, and activation of the hedgehog- and Wnt-signaling pathways. In all of these cases, localization of receptors to the ciliary membrane is essential (Berbari et al., 2009) and though critically depends on the BBSome- and IFT-mediated transport to the ciliary tip.

1.2.2.3 Cilia-related pathologies

Whereas in flagellatae motile cilia are the motor of autonomous movement, mammalian motile cilia induce fluid dynamics in body secretions. Such flow directs the transport of solutes (Yamadori et al., 1975; Ibanez-Tallon et al., 2004). Ciliary disfunction results in many severe pathologies such as obesity and mental retardation, kidney failure, and pulmonary obstruction (Afzelius, 2004; Zariwala et al., 2007). A very prominent phenotype is the

development of hydrocephalus, a disease characterized by swelling of the ventricles and the brain parenchyma to several dimensions of the original size. The swelling is caused by an accumulation of CSF in the ventricles and the extracellular space.

The dispersion of CSF in the ventricular system is facilitated by ependymal flow, a directional flow that is induced by motile cilia of ependymal cells. Impairment of ependymal flow by genetic disruption of Mdnah5, an axonemal dynein which is essential for ciliary motility causes closure of the cerebral aqueduct that connects the third to the fourth ventricle. As consequence, CSF drainage is abolished and accumulation of excess liquid leads to hydrocephalus (Ibanez-Tallon et al., 2004). It is not yet resolved whether closure of the cerebral aqueduct originates from lack of

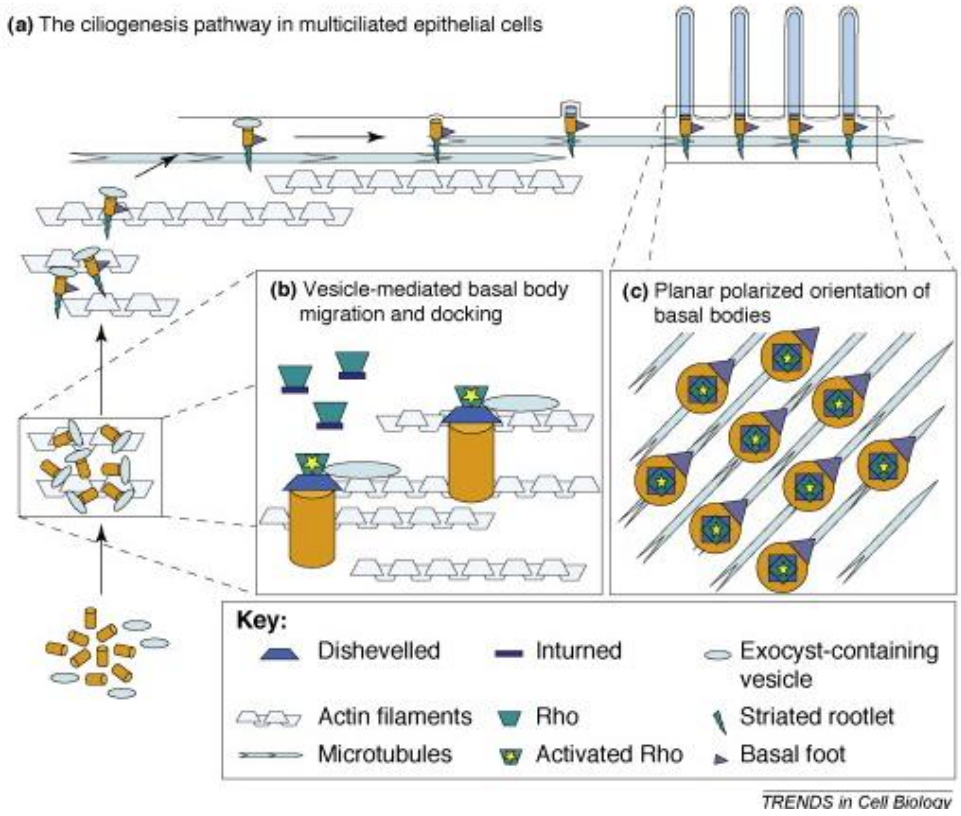

Fig.1.2.2.4 Polarization of cilia bundles. (a) Following their generation, basal bodies (orange cylinders) are associated to vesicles (light blue ovals) and directed towards the apical membrane, presumably along actin filaments (light blue textured lines). During this process of trafficking, basal feet (purple triangles) and striated rootlets (thin green triangles) assemble onto the basal bodies. By vesicular fusion, basal bodies are delivered to the cell surface where they attach to the plasma membrane. Following attachment, the ciliary axoneme (long blue cylinders) starts elongating from the basal body thereby forming a protrusion of the cell that is ensheated by the ciliary membrane. The cilia orient in a planar polarized manner that is determined by physical interactions between its basal feet with a hypothetical, planar polarized microtubule network (blue textured lines). **(b,c)**

Planar polarized orientation of basal bodies depends on Dvl and Rho, two components of the PCP, although the mechanism of polarized orientation and a possible link to PCP remains to be uncovered (from Vladar et al., 2012).

mechanical cues of ependymal flow or rather from impaired transport of morphogens or growth factors.

Another mechanism of hydrocephalus pathogenesis is based on increased production of CSF that cannot be removed. Several peptide hormones are present in CSF that may regulate the secretion of CSF from ChPx (Johanson et al., 2008). Mouse lines with impaired ciliogenesis as seen in the mouse line $Tg737^{orpk}$ show increased concentrations of chloride in CSF and ChPx indicating that cilia are involved in the regulation of electrolyte transport in ChPx (Banizs et al., 2005). Fluid transcytosis in cultured ChPx is inhibited by the GPR-receptor neuropeptide FF receptor 2 located at the cilium (Narita et al., 2010).

Taken together, directional ependymal flow and cilia-driven fluid mixing greatly affect brain physiology by mediating dispersion of solutes, facilitating CSF outflow, and directing transport of solutes to specific target sites.

1.2.2.4 Planar organization of cilia

Coordination of cilia movement within one cell is believed to happen via connections to the cytoskeleton (Vladar et al., 2012). But how does the individual cell get information about the orientation from the surrounding ependyma? Cilia are organized on the cell surface by rotational polarity orienting the basal bodies within one cell and by translational polarity orienting them along the tissue axis (Fig.1.2.2.4). Planar polarity of cilia refers to the coupling of rotational and translational polarity between ependymal cells (Kishimoto and Sawamoto, 2012; Marshall and Kintner, 2008; Mirzadeh et al., 2010). Coupling the orientation within cells along the ventricle produces the stereotypical flow of ventricular CSF (Breunig et al., 2010).

The conserved planar cell polarity (PCP) pathway organizes the polarization of epithelia across the tissue and produces precise pattern formations e.g. the regular arrangement of Drosophila wing hairs (non-cell autonomous PCP). Mice with defective inducibility of the PCP pathway lack antero-posterior orientation of fur hairs (Fig.1.2.2.5) and

misorientation of stereocilia in cochlea besides a range of other phenotypes (Simons and Mlodzik, 2008). Paracrine cues such as Wnt-signals are involved in the tissue-wide establishment of PCP. They transmit the information about directionality across tissues (Gordon and Nusse, 2006; Huang and Klein, 2004). Even though the exact cellular and molecular mechanisms remain to be unraveled it seems that PCP, cilia, and polarized ciliary beating are linked to each other, at least to a certain extent (Kishimoto and Sawamoto, 2012; Marshall and Kintner, 2008; Wallingford, 2010; Wallingford and Mitchell, 2011).

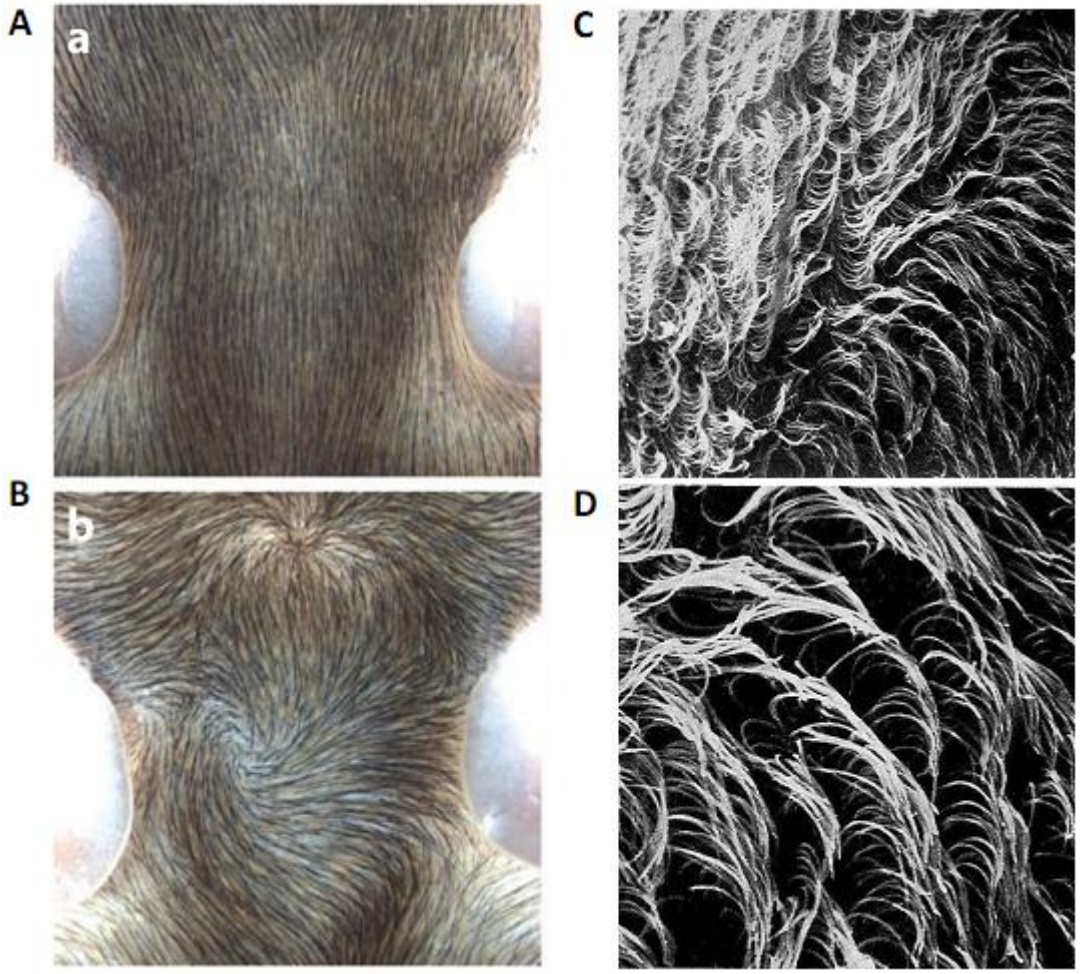

Fig.1.2.2.5 Planar cell polarity (PCP). (**A,B**) The most obvious defect in PCP is the hair orientation in mouse fur. (**A**) Whereas in wild type mice, the neck fur is aligned, (**B**) the fur in *fz3* mutant mice is randomly arranged forming a swirl pattern with whorls and waves. Taken from (Simons and Mlodzik, 2008).

(**C,D**) Scanning electron microscopy of planar polarized cilia in the ventricular system. Ependymal cilia are shown that point in a common direction (Yamadori and Yagihashi, 1975).

2 Material and methods

2.1 Animals

2.1.1 Animal housing and breeding

All animal experiments were carried out in compliance with the German Law on Animal Welfare and were approved by the Office for Consumer Protection and Food Safety of the State of Lower Saxony. Mice were housed in transparent individually ventilated cages with filter tops in specific pathogen free conditions. Room temperature and humidity were kept constant at 21°C and 55%. Animals were kept in a cycle of alternating phases of light and darkness (12 h light: 12 h darkness). Standard chew and water was provided *ad libitum*. Breeding was after the animals reached the age of 8 weeks in pairs or triples. Pups were weaned until they reached the age of three weeks. The mutant animals were distinguished by an ear mark and 0.4 cm tail biopsies were used for genotyping.

For circadian experiments, animals at the age of 10 weeks were housed in a separated, vibration protected room, entrained to a 12 h light: 12 h dark cycle (L:D 12:12) for 10 days, and subsequently released into darkness. On the second day of constant darkness (DD), animals were sacrificed in duplicates in time intervals of four hours starting at subjective circadian time 2 (CT2) which is after 38 hours in darkness.

All other adult animals of the strain C57Bl/6N were entrained at the same conditions and processed at the indicated Zeitgeber time (ZT) whereas ZT0 is set to the onset of the light. Animals of the other strains were housed under L:D 12:12 conditions in the animal facility.

Mouse-line	**Mutation**	**Short description**	**Reference:**
C57Bl/6N	-	Wildtype strain	NIH
129/SV	-	Wildtype strain	(Threadgill et al., 1997)
Per2:Luc	Per2:Luc	Luciferase expression coupled to Per2-expression	(Yoo et al., 2004)
Bmal1$^{-/-}$	Bmal1$^{-/-}$	Global deletion of Bmal1 results in disruption of the circadian clock	(Bunger et al., 2000)
Emx1:CrexEsco2$^{fl/fl}$	Emx1::Cre Esco2$^{fl/fl}$	Mouse-line with opened ventricular system	(Whelan et al., 2012)

Tab.2.1.1 Mouse lines.

2.2 Colorimetric in-situ Hybridization

2.2.1 Probe design

Probe design was performed as described in (Yaylaoglu et al., 2005).

The probes were chosen as follows: FoxJ1 bp 1200-2123 (NM008240.2)

Bmal1	bp 1257-1893 (NM007489.2)	
Slc23a3	bp 28-558	(NM018824)
Atp1b2	bp 1-4191	(NM013415)
ACE	bp 13-4191	(NM 207624)
Per2	bp 1132-2027 (NM011066.3)	

2.2.2 Tissue preparation and procedure

Following isolation from the animal, brains were washed in PBS and preincubated in OCT® (Tissue TEK) for 5 minutes at room temperature. Brains were transferred to freezing chambers filled with OCT®. These were brought to -20°C until frozen, then stored at -80°C until sectioning was done. For sectioning, specimen were mounted on holders in a cryostat CM3050 (Leica) and kept at temperatures of -14°C, the cryochamber kept at -18°C. Sections were mounted on microscope slides (SUPERFROST® PLUS, Thermo Scientific) and stored in tightly sealed boxes in the presence of silica gel (Silica gel Rubin drying bags, Sigma-Aldrich) at -20°C. Before use, the boxes were brought to room temperature and slides were fixed in 4% PFA for 20 min, acetylated, and dehydrated as described (Yaylaoglu et al., 2005). The slides were assembled in flow through hybridization chambers and processed according to the protocol as described by (Yaylaoglu et al., 2005).

2.3 Molecular methods

2.3.1 RNA-isolation from tissue

The tissue was stored at -80°C in RNAlater® (Life Technologies). For processing, the tissue was transferred into fresh tubes (Safe-Lock Tubes 2.0 mL, Eppendorf), 2 mL TRI Reagent® Solution (Ambion) were added and tissue was disrupted by vigourous pipetting through a 29G syringe (BD Medical U-100 Insulin, Becton, Dickinson and Company). The solution was kept at room temperature for 5 min, 200 µL chloroform were added and vigorously mixed by shaking followed by an additional incubation time of 5 min at room temperature. Subsequently, the probe was centrifuged at 4°, 12000 rpm for 30 min. The supernatant was transferred to 1mL isopropanol with 1 µL coprecipitant (GlycoBlue®, Life Technologies), vigorously vortexed and centrifuged again at 4°C, 12000 rpm for 10 min. The pellet was washed in three steps with 100% ethanol and 2 times in 75 % ethanol. Subsequently, the pellet was dried at 37°C, and 15 µL water were added. RNA-concentration was determined by using a spectrophotometer (NanoDrop1000, Thermo Scientific) and the solution was stored at -80°C.

2.3.2 RNA integrity

The integrity of the isolated RNA was determined by using the Bioanalyzer (Agilent). Before usage, the electrodes were cleaned with RNaseZAP (Sigma) for 1 min and cleaned with pure water (Millipore). RNA 6000 Nano Reagent Kits (Agilent) were used according to the manufacturers protocol. RNA Nano Dye concentrate was vortexed and centrifuged. 0.5 µL of the concentrate were added to 32.5 µL gel, vortexed and centrifuged for 10 min at 8000 rpm. 1.2 µL RNA probe were pipette in a fresh tube (Eppendorf) denaturated at 70°C for 5 min. Same procedure for 1.2 µL ladder. A Nano Chip (Agilent) was loaded with 9 µL of the centrifuged gel. The probe and ladder were loaded at volumes of 1 µL onto the cip, subsequently vortexed and run in the Bioanalyzer. 2100 Expert (Agilent) was used to calculate the RNA Intergrity Number (Schroeder et al., 2006).

2.3.3 Reverse transcription

For each probe, 1 µg of RNA was used in a kit for first-strand cDNA synthesis (Thermoscript™, life Technologies) according to the protocol of the manufacturer. The

reverse transcription PCR was run at 42°C for 70 min and the reaction was subsequently denatured at 70°C for 2 min. cDNA was stored at -20°C.

2.3.4 qRT-PCR

The qPCR was performed using iQ SYBR GreenSupermix on a Thermocycler (iCycler, Bio-rad) as described (Oster et al., 2006a). Duplicate probes were pipetted in triplicates.

Primer name	**Sequence (5´->3´)**
Eefa for	AATTCACCAACACCAGCAGCAA
Eefa rev	TGCCCCAGGACACAGAGACTTCA
Nr1d1 for	AGCTCAACTCCCTGGCACTTAC
Nr1d1 rev	CTTCTCGGAATGCATGTTGTTC
Bmal1 for	CCTAATTCTCAGGGCAGCAGAT
Bmal1 rev	TCCAGTCTTGGCATCAATGAGT
Per1 for	AGTTCCTGACCAAGCCTCGTTAG
Per1 rev	ATTGCCCTCTGCTTGTCATC
Cry2 for	GCGAAGGTGTCGGCTATGA
Cry2 rev	GTCCTCCACGGAGAAATTCAAG

Tab.2.3.4 Primer sequences.

2.3.3 Microarray

The Microarray analysis was performed in the transcriptome analysis lab (TAL) at the University of Göttingen according to their protocol (http:www.microarrays.med.uni-goettingen.de). Exon 1.0ST arrays for whole transcript expression analysis (Affymetrix) were performed. 1 µg of RNA was processed with RNA-integrity numbers higher than 9.

For annotation of the results, the Bioconductor database was used (Okoniewski and Miller, 2008).

2.4 Experiments with tissue in culture

2.4.1 Isolation of choroid plexus

Freshly isolated brains were transferred to medium M171 (GIBCO, Invitrogen) supplemented with MEGS (GIBCO, Invitrogen). Two forceps were used to cut the cerebellum off and divide the remaining brain into two halves along the midline. The proximal entry to the lateral ventricles was further opened. Choroid plexus was excised by cutting the ventral attachment. A bilateral cut was perfomed to remove the dorsal half of the cerebellum and lay open the underneath positioned choroid plexus. This choroid plexus of cauliflower-like appearance is attached to the cerebellum at three positions: in the middle and at the outer ends of both arms. Following their detachment, the choroid plexi were transferred to fresh medium.

2.4.2 Preparation of the "open pouch"

Brains were freshly isolated, washed in Dulbecco`s modified eagle medium (DMEM 21063, Gibco, Invitrogen) and subsequently placed in a coronal matrix (S92, PLANO). Razor blades were placed anterior to the transition from midbrain to the cerebellum and anterior to the entry site of the optic nerve. By smoothly pushing down the blades at these positions, coronal sections of 3 mm thickness were performed. The sections were placed into a fresh, medium-filled dish placing the posterior part of the section at the bottom. A piece of tungsten wire (Alfa Aesar) was electrolytically sharpened in 1M NaOH-solution (Merck). The tungsten wire was positioned at the ventral side of the third ventricle and slightly moved up and down until the ventral connection between both walls of the ventricle was cut. Where preserved, connections between the two hemispheres were separated at the anterior and posterior side of the ventricle. The ventricular lining was cropped in approximately 100 µm distance to the ventricular cleft with the cutting plane in parallel to the midline. A final cut along the proximal/distal axis conducted at the dorsal end of the third ventricle was performed. The sections were transferred to the incubation chamber and carefully separated with forceps. The ependyma was not touched, only the surrounding brain parenchyma.

2.4.3 Microscopy and recording of the open pouch

For microscopy of bead movement, fluorescent latex-beads (Fluoresbrite™ Multifluorescent 1.0 micron Microspheres, Polysciences) were added to 2 mL of DMEM 21063 and homogenously dispersed with a pipette tip. The open pouch was placed onto a Millicell® cell culture insert (Millipore). For microscopy of cilia at high resolution, specific chambers were fabricated**.** Culture dishes (Nunc®, VWR) were cut to the size of microscope slide (25x75 mm) with a 1 cm whole in the middle. Cover glass (Marienfeld) was glued on top of the microscope slide. Teflon rings were positioned around the whole and used as spacers for a second cover glass that serves as lid of the chamber.

An inverted DMR microscope (Leica) was used for all microscopy of fresh tissue preparations using 5x, 10x or 63x objectives. Movies were recorded using a Cascade II high-speed camera (Photometrix) and MultiRecorder software (Johannes Schröder-Schetlig, MPI for dynamics and self-organization, Göttingen).

2.4.4 Luciferase-reporter assay

2.4.4.1 Time-course recording of luciferase activity

Freshly isolated brains were either transferred to medium M171 (GIBCO, Invitrogen) supplemented with MEGS (GIBCO, Invitrogen) or DMEM 21063 (GIBCO, Invitrogen). Either ChPx or the open pouch were dissected as described above (sections 2.4.1 and 2.4.2). The tissue was washed 3 times in fresh medium, then transferred into the corresponding medium containing luciferin and placed in the luminometer for recording of the luminescence.

2.4.4.2 Spatial resolution of luciferase-activity recordings

Luminescence recording was performed using the LV200 LUMINOVIEW microscope (Olympus). The light-protected incubation chamber of the microscope was conditioned to 5% CO_2-concentration, a temperature of 37°C, and humidity was controlled by a water bath set to 37°C. The specimen was conveyed to a glass bottom culture dish (MatTek). The samples were incubated for up to 1 week.

For observation of the ependyma, the dish was placed into the dark chamber and the specimen was recorded for several days.

2.5 Software and analysis

R2009a (MathWorks)

Microsoft Office (Microsoft)

CircWave Batch V3.4

2.5.1 Circular statistics

Circular statistic was applied using Circstat (Berens, 2009).

2.5.2 Particle tracking

A particle tracking script was implemented [(C)2003 Nicholas Darnton, Jacob D. Jaffe, and the President and Fellows of Harvard University; http://www.rowland.harvard.edu/labs/bacteria/software/index.php]. This software was designed by Nicholas Darnton with the purpose of tracking small fluorescent beads in a microscope field over time. It does so by using a "nearest neighbor" approach comparing adjacent frames in a movie file.

The script was optimized according to our experimental conditions. Additionally, automatized read-out and visualization were implemented (see below for Matlab-script: Beadtrack Datareader; Beadtrack Datacompare).

A supplemental script was written by Christian Westendorf for color-coding of direction and averaging of tracks (Beadtrack Vectorplot). This program automatically generates overlay pictures of color-coded tracks or averaged arrows with the corresponding brightfield picture.

```
function Beadtrack_Datreader(date,x5,x10,x20)

% Reads in and eveluates data sampled with the Photometrics Cascade II 512
% (c) Christian Westendorf
% Parameters

loadpath1 = ['/ /',date,'/'];
A = dir([loadpath1,'*.dat']);
sIA = size(A);
savepath1 = ['/ /'];
for m = 1:sIA(1)
   name = A(m).name;
   C1 = name(15:17);
   C2 = name(22:24);
   Ct1 = str2double(C1);
   Ct2 = str2double(C2);
   H = opheader([loadpath1,name]);
   B = H.frames;
   bin =  H.binX;
   if ~isempty(x5)
      x5f = [(x5(:,1) == Ct1) (x5(:,2) == Ct2)];
      x5f = sum(x5f,2);
      x5f = x5f > 1;
   else
      x5f = 0;
   end
   if ~isempty(x10)
      x10f = [(x10(:,1) == Ct1) (x10(:,2) == Ct2)];
      x10f = sum(x10f,2);
      x10f = x10f > 1;
   else
      x10f = 0;
   end
   if ~isempty(x20)
      x20f = [(x20(:,1) == Ct1) (x20(:,2) == Ct2)];
      x20f = sum(x20f,2);
      x20f = x20f > 1;
   else
```

```
    x20f = 0;
end
if sum(x5f) + sum(x10f) + sum(x20f) == 0
    Skip = 1;
else
    Skip = 0;
end
if Skip < 1
        if sum(x5f) > 0
      if bin == 1
          Beadsize = [1 24];
      else
          Beadsize = [1 12];
      end
      Maxdist = 15;
      Calib = 2.538;
      lim = 5;
      Spacing = 3;
    elseif sum(x10f) > 0
      if bin == 1
          Beadsize = [3 20];
      else
          Beadsize = [2 16];
      end
      Maxdist = 12;
      Calib = 1.279;
      lim = 8;
      Spacing = 3;
    elseif sum(x20f) > 0
      Beadsize = [5 30];
      Maxdist = 5;
      Calib = 0.64;
      lim = 5;
      Spacing = 3;
    end
    T_large = {};
    V_large = {};
    if H.sizeX  == 512
      cut = 100;
```

```
else
   cut = 500;
end
if B > 30
   if B > cut
      K = floor(B/cut);
   else
      K = 1;
   end
   Nrstacks = K;
   for j = 1:K
      savestats = [];
      X = cut*(j-1)+1;
      Y = cut*(j-1) + cut;
      if X == 1
         X = 2;
      end
      if Y > B
         Y = B;
      end
      clear options
      options = struct;
      options.fromFrame = X;
      options.toFrame = Y;
      [M,H,T] = opread([loadpath1,name],options);
      if j == 1
         Framerate = H.acquisitionFrequency * 10;
         Framerate = Framerate/1000;
      end
      T = double(T);
      T = T -T(1);
      I = M(:,:,2);
      I2 = bpass(I,1,3);
      if exist([savepath1,'/',C1,'_',C2,'.mat'],'file') == 0
         figure
         imagesc(I2)
         colormap gray
         thresh = 1000;
         save([savepath1,'/',C1,'_',C2,'.mat'],'thresh')
```

```
else
    load([savepath1,'/',C1,'_',C2,'.mat'])
end
sIM = size(M);
nrimg = sIM(3);
for h = 1:nrimg
    if j == 1 && h == 1
        P = 0;
    else
        P = 1;
    end
    if P == 1
        display(h)
        I = M(:,:,h);
        I2 = bpass(I,1,3);
        I2 = double(I2);
        mask = I2 > thresh;
        bw = mask;
        bw2  = bwlabel(bw);
        D = regionprops(bw,'area');
        D2 = find([D.Area] > Beadsize(1) & [D.Area] < Beadsize(2));
        BW2 = ismember(bw2,D2);
        L = logical(BW2);
        stats = regionprops(L,'area','centroid');
        if ~isempty(stats)
            [stats(1:length(stats)).Frame] = deal(h);
            savestats = [savestats; stats];
        end
    end
end
tracks = trackbeads(savestats,Maxdist,1/Calib);
sIt = size(tracks);
F = zeros(sIt(2),1);
for i = 1:sIt(2)
    if length(tracks(i).frame) > 5
        F(i) = 1;
    end
end
F = logical(F);
```

```
        tracks2 = tracks(F);
        sIt2 = size(tracks2);
        F1 = zeros(sIt2(2),1);
        for i = 1:sIt2(2)
            X1 = [tracks2(i).x(1) tracks2(i).y(1)];
            X2 = [tracks2(i).x(end) tracks2(i).y(end)];
            V = sqrt((X1(1)-X2(1))^2+(X1(2)-X2(2))^2);
            if V > (lim*Calib)
                F1(i) = 1;
            end
        end
        F1 = logical(F1);
        F2 = ~F1;
        tracks_moving = tracks2(F1);
        tracks_stat = tracks2(F2);
        T_large{j} = tracks_moving;
        sIm = size(tracks_moving);
        V_all = struct('total',{},'x',{},'y',{});
        for i=1:sIm(2)
            Time = 0:Framerate:(length(tracks_moving(i).frame)-1)*Framerate;
            T = Time(1:Spacing:end);
            R_x = tracks_moving(i).x(1:Spacing:end)';
            R_y = tracks_moving(i).y(1:Spacing:end)';
            R = [R_x R_y];
            V_x = diff(R_x)./diff(T(1:2));
            V_y = diff(R_y)./diff(T(1:2));
            V = [V_x V_y];
            V_tot = (V(:,1).^2 + V(:,1).^2).^(1/2);
            V_all(i).total = V_tot;
            V_all(i).x = R(:,1);
            V_all(i).y = R(:,2);
        end
        V_large{j} = V_all;
        if exist([savepath1,C1,'_',C2],'dir') == 0
            mkdir([savepath1,C1,'_',C2])
        end
save([savepath1,C1,'_',C2,'/',C1,'_',C2,'_Tracks_',sprintf('%.2d',j),'.mat'],'tracks_moving','tracks_stat','V_all','Calib','Maxdist','Beadsize','Framerate','date','Spacing')
        close all
```

```
        end
      end
    end
  end
```

```
function Beadtrack_Datacompare_angle_improved(arglist)
```

Reads in and compares beadtrack data sampled with the Photometrics Cascade II 512

(c) Christian Westendorf , Regina Faubel

```
date = arglist{1};
Pair = arglist{2};
C1 = arglist{3};
Calib = arglist{4};
date2 = date;
F = date == '_';
date2(F) = '-';
loadpath1 = ['/ /',date,'/'];
loadpath2 = ['/ /',date,'/Auswertung_2/'];
savepath1 = ['/ /',date,'/'];
if exist(savepath1,'dir') == 0
   mkdir(savepath1)
end
Param = {'Fontsize',12,'Fontweight','bold'};
Base = dir([loadpath1,'*.dat']);
Base = Base(1).name;
Base1 = Base(1:10);
Base2 = Base(25:end);
sIP = size(Pair);
TL = 5;
Maxnr = 2000;
for m = 1:sIP(1)
   C3 = sprintf('%.3d',Pair(m,1));
   C2 = sprintf('%.3d',Pair(m,2));
   BFname = [Base1,'_Exp',C1,'_Rec',C3,Base2];
   M = opread([loadpath1,BFname]);
   I = M(:,:,2);
   figure
   set(gca,'YDir','reverse')
   xlim([0 512])
   ylim([0 512])
   hold all
   imagesc(I)
```

```
colormap gray
B = dir([loadpath2,'/',C1,'_',C2,'/*.mat']);
k2 = str2double(B(end).name(end-5:end-4));
Tracknr = 0;
while Tracknr <= Maxnr
  for k = 1:k2
    Base3 = sprintf(['_Tracks_','%.2d','.mat'],k);
    Trackname = ['/',C1,'_',C2,Base3];
    load([loadpath2,C1,'_',C2,Trackname])
    Vec1 = 0:10:180;
    Vec2 = 180:10:360;
    J2 = pink(length(Vec1)+1);
    J3 = flipud(hot(length(Vec2)+1));
    J1 = [J2(1:end-1,:);J3(2:end,:)];
    sIm = size(tracks_moving);
    for i = 1:sIm(2)
      L = length(tracks_moving(i).x);
      Tracknr = Tracknr + 1;
      if Tracknr > Maxnr
        break
      end
      if L > TL
        L2 = floor(L/TL);
        LVec = round(linspace(1,L,TL));
        for j = 1:TL-1
          a = [tracks_moving(i).x(LVec(j))/Calib,tracks_moving(i).x(LVec(j+1))/Calib];
          b = [tracks_moving(i).y(LVec(j))/Calib,tracks_moving(i).y(LVec(j+1))/Calib];
          x2 = a(2) -a(1);
          y2 = b(2) -b(1);
          f = [x2,y2];
          g = [1,0];
          if f(2) < 0
            ang = 360 -acosd(dot(f,g)/(norm(f)*norm(g)));
          else
            ang = acosd(dot(f,g)/(norm(f)*norm(g)));
          end
          if sum(f) == 0
            ang = 0;
          end
```

```
                if ang > 180
                    Vec = Vec2;
                    J = J1(1:length(Vec1),:);
                else
                    Vec = Vec1;
                    J = J1(length(Vec1):2*length(Vec1),:);
                end
                F = find(Vec >= ang,1);
                plot(a,b,'-','Color',J(F,:),'Linewidth',1);


              end
            end
            if Tracknr > Maxnr
              break
            end
          end
          if Tracknr > Maxnr
            break
          end
        end
        if k == k2
          break
        end
    end
    xlabel('x (Pixel)',Param{1},Param{2},Param{3},Param{4})
    ylabel('y (Pixel)',Param{1},Param{2},Param{3},Param{4})
    title({date2,...
    ['C1 ',C1,' /C2 Data ',C2,' /C2 BF image',C3,'-Angle (Tracks  total number = ',num2str(Tracknr-1),')']},...
      Param{1},Param{2},Param{3},Param{4})
    set(gca,Param{1},Param{2},Param{3},Param{4})
    box on
    name = [C1,'_',C3,'+',C2,'_Angle'];
    prepexport2(30,30,0,0,name,savepath1);
    close all
end
```

```
function Beadtrack_Vectorplot_improved(arglist

% Reads in and compares beadtrack data sampled with the Photometrics Cascade II 512
% (c) Christian Westendorf, Regina Faubel

date = arglist{1};
Pair = arglist{2};
C1 = arglist{3};
Calib = arglist{4};
loadpath1 = ['/ /',date,'/'];
loadpath2 = ['/ /',date,'/Auswertung_2/'];
savepath1 = ['/ /',date,'/'];
Param = {'Fontsize',12,'Fontweight','bold'};
Nr = 12;
if exist(savepath1,'dir') == 0
   mkdir(savepath1)
end
Base = dir([loadpath1,'*.dat']);
Base = Base(1).name;
Base1 = Base(1:10);
Base2 = Base(25:end);
sIP = size(Pair);
Boxsize = 32;
setlength = 30;
histvec = 0:10:250;
histvec_xy = -200:20:200;
Colormap = hot(length(histvec)+1);
Colormap = Colormap(1:end-1,:);
for m = 1:sIP(1)
   C3 = sprintf('%.3d',Pair(m,1));
   C2 = sprintf('%.3d',Pair(m,2));
   BFname = [Base1,'_Exp',C1,'_Rec',C3,Base2];
   M = opread([loadpath1,BFname]);
   I = M(:,:,2);
   sI = size(I);
   Boxvec = 1:Boxsize:sI(1);
   Rest = sI(1) -Boxvec(end);
   Boxvec = Boxvec + Rest -mod(Rest,2);
```

```
Boxvec = Boxvec * Calib;
Iname = [Base1,'_Exp',C1,'_Rec',C2,Base2];
H = opheader([loadpath1,Iname]);
f = H.acquisitionFrequency*10;
dt = 1/f;
loadpath3 = [loadpath2,C1,'_',C2,'/'];
D = dir([loadpath3,'*.mat']);
Number_mat = zeros(length(Boxvec),length(Boxvec));
Velocity_mat = zeros(length(Boxvec),length(Boxvec));
Vx_mat = zeros(length(Boxvec),length(Boxvec));
Vy_mat = zeros(length(Boxvec),length(Boxvec));
V_vec = [];
Vx_vec = [];
Vy_vec = [];
ang_vec = [];
for k = 1:length(D)
   Trackname = D(k).name;
   display(Trackname(1:end-4))
   load([loadpath3,Trackname])
   sIm = size(tracks_moving);
   for i = 1:sIm(2)
      X = tracks_moving(i).x;
      Y = tracks_moving(i).y;
      if length(X) > 2
         for j = 2:length(X)-1
            Point1 = [X(j-1) Y(j-1)];
            Point2 = [X(j+1) Y(j+1)];
            V = sqrt((Point1(1)-Point2(1))^2+(Point1(2)-Point2(2))^2)/(2*dt);
            Vx =  sign(X(j+1)-X(j-1)) * sqrt((Point2(1)-Point1(1))^2)/(2*dt);
            Vy =  sign(Y(j+1)-Y(j-1)) * sqrt((Point2(2)-Point1(2))^2)/(2*dt);
            V_vec = [V_vec;V];
            Vx_vec = [Vx_vec;Vx];
            Vy_vec = [Vy_vec;Vy];
            BoxX = find(Boxvec>X(j),1,'first');
            BoxY = find(Boxvec>Y(j),1,'first');
            Velocity_mat(BoxX,BoxY) = Velocity_mat(BoxX,BoxY) + V;
            Vx_mat(BoxX,BoxY) = Vx_mat(BoxX,BoxY) + Vx;
            Vy_mat(BoxX,BoxY) = Vy_mat(BoxX,BoxY) + Vy;
            Number_mat(BoxX,BoxY) = Number_mat(BoxX,BoxY) + 1;
```

```
                a = [Point1(1),Point2(1)];
                b = [Point1(2),Point2(2)];
                x2 = a(2) -a(1);
                y2 = b(2) -b(1);
                l = [x2,y2];
                g = [1,0];
                if l(2) < 0
                   ang = 360 -acosd(dot(l,g)/(norm(l)*norm(g)));
                else
                   ang = acosd(dot(l,g)/(norm(l)*norm(g)));
                end
                if l(1) == 0 && l(2) == 0
                   ang = 0;
                end
                ang_vec = [ang_vec;ang];
             end
          end
       end
    end
    figure
    subplot(4,4,[2 5])
    imagesc(I)
    colormap gray
    freezeColors
    set(gca,'YDir','reverse')
    hold on
    F = Number_mat == 0;
    Number_mat(F) = 0.1;
  Velocity_avg = Velocity_mat./Number_mat;
    Vx_avg = Vx_mat./Number_mat;
    Vy_avg = Vy_mat./Number_mat;
    Velocity_avg(F) = 0;
    Vx_avg(F) = 0;
    Vy_avg(F) = 0;
    Number_mat(F) = 0;
 sIv = size(Number_mat);
    for f = 1:sIv(1)
       for h = 1:sIv(2)
          if Number_mat(f,h) >= 10
```

```
    P = 1;
else
    P = 0;
end
    if f < slv(1)
    X1 = (Boxvec(f+1) -Boxvec(f))/2+Boxvec(f);
else
    X1 = (Boxvec(f)+1 -Boxvec(f))/2+Boxvec(f);
end
if h < slv(2)
    Y1 = (Boxvec(h+1) -Boxvec(h))/2+Boxvec(h);
else
    Y1 = (Boxvec(h) + 1 -Boxvec(h))/2+Boxvec(h);
end
xlim([-10 522])
ylim([-10 522])
if P == 1
    X2 = X1 + Vx_avg(f,h);
    Y2 = Y1 + Vy_avg(f,h);
    P1 = [X1,Y1];
    P2 = [X2,Y2];
    Vel = Velocity_avg(f,h);
    A = ceil(Vel/5);
    if A > length(histvec)
        A = length(histvec);
    elseif A == 0
        A = 1;
    end
    Cmap = Colormap(A,:);
     a = [P1(1) P2(1)];
    b = [P1(2) P2(2)];
    x2 = a(2) -a(1);
    y2 = b(2) -b(1);
    p = [x2,y2];
    g = [1,0];
    if p(2) < 0
        ang = 360 -acosd(dot(p,g)/(norm(p)*norm(g)));
    else
        ang = acosd(dot(p,g)/(norm(p)*norm(g)));
```

```
        end
        if sum(p) == 0
           ang = 0;
        end
        X2 = X1 + cosd(ang)*setlength*Calib;
        Y2 = Y1 + sind(ang)*setlength*Calib;
        P2 = [X2,Y2];
        arrow(P1./Calib,P2./Calib,'EdgeColor',Cmap,'FaceColor',Cmap,'Length',4,'Width',1)
     else
  end
  end
end
Tickvector = 0:50:500;
Tickvector = Tickvector*Calib;
set(gca,'XTick',Tickvector)
set(gca,'YTick',Tickvector)
set(gca,'XTicklabel',0:50:500)
set(gca,'YTicklabel',0:50:500)
xlabel('x [\mum]',Param{1},Param{2},Param{3},Param{4})
ylabel('y [\mum]',Param{1},Param{2},Param{3},Param{4})
title({['C1 = ',C1,' /C2 (Data) = ',C2,' /C2 (BF image) = ',C3],'Averaged flow profile'},...
   Param{1},Param{2},Param{3},Param{4})
set(gca,Param{1},Param{2},Param{3},Param{4})
box on
 subplot(4,4,[3 8])
[X1,Y1] = meshgrid(1:sIv(1),1:sIv(2));
pcolor(X1,Y1,transpose(Number_mat))
shading flat
set(gca,'YDir','reverse')
colormap(flipud(pink))
expdate = date;
V = date == '_';
expdate(V) = '-';
xlabel('Boxnr',Param{1},Param{2},Param{3},Param{4})
ylabel('Boxnr',Param{1},Param{2},Param{3},Param{4})
title({['Date = ',expdate],'Number of tracks per box'},Param{1},Param{2},Param{3},Param{4})
cb = colorbar('Location','South');
zlab = get(cb,'ylabel');
set(zlab,'String','Nr of tracks',Param{1},Param{2},Param{3},Param{4});
```

```
set(gca,Param{1},Param{2},Param{3},Param{4})
box on
 [Y,histvec_xy] = hist(nonzeros(Vx_vec),histvec_xy);
subplot(4,4,[9 10])
bar(histvec_xy,Y./(sum(Y)),'Edgecolor',[1 1 1],'Facecolor',[0 0.4 0.7])
hold on
xlim([-210 210])
ylim([0 0.4])
V = get(gca,'Ylim');
stem(0,V(2),'--r','Linewidth',1.5,'Marker','none')
xlabel('v_{x} [\mum/s]',Param{1},Param{2},Param{3},Param{4})
ylabel('Nr of counts',Param{1},Param{2},Param{3},Param{4})
title('v_{x} Histogram',Param{1},Param{2},Param{3},Param{4})
set(gca,Param{1},Param{2},Param{3},Param{4})
box on
[Y,histvec_xy] = hist(nonzeros(Vy_vec),histvec_xy);
subplot(4,4,[11 12])
bar(histvec_xy,Y./(sum(Y)),'Edgecolor',[1 1 1],'Facecolor',[0 0.4 0.7])
hold on
xlim([-210 210])
ylim([0 0.4])
V = get(gca,'Ylim');
stem(0,V(2),'--r','Linewidth',1.5,'Marker','none')
xlabel('v_{y} [\mum/s]',Param{1},Param{2},Param{3},Param{4})
ylabel('Nr of counts',Param{1},Param{2},Param{3},Param{4})
title('v_{y} Histogram',Param{1},Param{2},Param{3},Param{4})
set(gca,Param{1},Param{2},Param{3},Param{4})
box on
[Y,histvec] = hist(nonzeros(V_vec),histvec);
subplot(4,4,[13 14])
bar(histvec,Y./(sum(Y)),'Edgecolor',[1 1 1],'Facecolor',[0 0.4 0.7])
xlim([-10 210])
ylim([0 0.4])
xlabel('v_{tot} [\mum/s]',Param{1},Param{2},Param{3},Param{4})
ylabel('Nr of counts',Param{1},Param{2},Param{3},Param{4})
title('v_{tot} Histogram',Param{1},Param{2},Param{3},Param{4})
text('Parent',subplot(4,4,[13 14]),'Interpreter','latex',...
'String',['Total number = : ',num2str(sum(Y))],...
'Position',[0 0.3],...
```

```
    'FontWeight','bold',...
    'FontSize',14);
    set(gca,Param{1},Param{2},Param{3},Param{4})
    box on
    [A1,A2] = rose(ang_vec,Nr);
    A2 = A2./(sum(A2)/2);
    rMax = 0.2;
    subplot(4,4,[15 16])
    h = polar(0, rMax);
    delete(h)
    set(gca, 'Nextplot','add')
    [B1,B2] = pol2cart(A1,A2);
    h = patch(reshape(B1,4,[]), reshape(B2,4,[]), 'b');
    set(h,'Edgecolor',[1 1 1],'Facecolor',[0 0.4 0.7])
    xlabel('Angle [^o]',Param{1},Param{2},Param{3},Param{4})
    title('Angle Histogram',Param{1},Param{2},Param{3},Param{4})
    set(gca,Param{1},Param{2},Param{3},Param{4})
    box off
name = [C1,'_',C2,'_Box',num2str(Boxsize)];
    prepexport2(40,40,0,0,name,savepath1);
    close all
end
toc
```

2.5.3 Cilia beat pattern

```
function Cilia_directions(arglist)
% Semiautomatic Cilia directions
% (c) Christian Westendorf, Regina Faubel
% Parameters
date = arglist{1};
C1 = arglist{2};
Columns = arglist{3};
Imsize = arglist{4};
loadpath1 = ['/ /',date,'/'];
savepath1 = ['/ /',date,'/'];
savename = [C1,'_combined.jpeg'];
if exist(savepath1,'dir') == 0
   mkdir(savepath1)
end
LVec = zeros(1,numel(Columns));
for j = 1:numel(Columns)
   LVec(j) = length(Columns{j});
end
 Imagespercol = max(LVec);
Firstcolumn = Columns{1}(~isnan(Columns{1}));
C2 = sprintf('%.3d',Firstcolumn(1));
switch Imsize
   case 'constant'
      A = dir([loadpath1,'*Exp',C1,'_Rec',C2,'*.dat']);
      M = opread([loadpath1,A.name]);
      sI = size(M(:,:,1));
   case 'changing'
      sI = [512,512];
end
I_large = nan(Imagespercol*sI(1),numel(Columns)*sI(2));
I_BF = nan(Imagespercol*sI(1),numel(Columns)*sI(2));
C = 0;
for d = 1:numel(Columns)
   display(d)
   Colvec = Columns{d};
   for h = 1:length(Colvec)
      if isnan(Colvec(h)) == 0
```

```
C2 = sprintf('%.3d',Colvec(h));
A = dir([loadpath1,'*Exp',C1,'_Rec',C2,'*.dat']);
[M,H,T] = opread([loadpath1,A.name]);
Nrframes = H.frames;
BFimg = M(:,:,2);
   k = 1;
for j = 2:Nrframes-1
   I1 = M(:,:,j);
   I2 = M(:,:,j+1);
   I = I2 -I1;
  Thresh = mean(nonzeros(double(I)));
   F = I > Thresh;
   I = I.*uint16(F);
   I = double(I);
   if j == 2
      I_avg = I;
      sInew = size(I);
   else
      I_avg = I_avg + I;
   end
   k = k + 1;
end
I_avg = uint16(I_avg./k);


I_med = medfilt2(I_avg,[4 4]);
   C = C + 1;
if C == 1
   Setmean = mean2(I_med);
   I_med_adj = I_med;
else
   Offmean = mean2(I_med);
   I_med_adj = I_med + (Setmean-Offmean);
end
   y1 = (d-1)*sInew(2)+1;
y2 = d*sInew(2);
x1 = sum(I_large(:,y1)>0)+1;
x2 = sum(I_large(:,y1)>0)+sInew(1);
```

```
            I_large(x1:x2,y1:y2) = I_med_adj;
            I_BF(x1:x2,y1:y2) = BFimg;
        end
    end
end
sI = size(I_large);
for j = 1:sI(1)
    if sum(isnan(I_large(j,:))) == sI(2)
        Stopline = j;
        break
    end
end
I_final = I_large(1:Stopline-1,:);
I_BF_final = I_BF(1:Stopline-1,:);
F = isnan(I_final);
I_final(F) = 0;
I_BF_final(F) = 0;
figure
imagesc(I_final)
axis tight
colormap jet
imwrite(uint16(I_final),[savepath1,savename],'tif')
imwrite(uint16(I_BF_final),[savepath1,savename,'_BF'],'tif')
```

2.5.4 3D visualization

For the three dimensional visualization of the ventricle, serial brain sections were stained for *FoxJ1* and scanned. The boundaries were manually aligned and aligned by two dimensional crosscorrelation (MATLAB xcorr2.m function) on top of each other. An isosurface was created and rendered using isosurface.m function.

3 Results

3.1 Circadian clock and the choroid plexus

3.1.1 Cultured Choroid plexus has an autonomous circadian clock

For monitoring the amplitude and period of circadian clocks, mice are commonly used that express a Per2-luciferase fusion protein (Welsh et al., 2004). Explants from the ChPx of the fourth ventricle (ChPx4) maintained in luciferin-containing DMEM medium showed a robust change in luciferase activity over a 24 h period that is essentially uniform across the entire ChPx4 (Fig.3.1.1 A). The temporal profile in luminescence generated by the ChPx4 *in vitro* was quantified in a lumicycler and showed pronounced oscillations with a period of 24.4±0.5 h (n = 3) that began to dampen after about 4 days (Fig.3.1.1 B). We compared the phase relationship between the circadian clocks of the ChPx of the lateral ventricle and the ChPx4 *in vivo* by determining the *Nr1d2* expression profiles of freshly dissected ChPx. These two ChPx tissues are separated by a sizable distance. In both cases, this clock gene showed peak expression at circadian time 6 (CT6) (Fig.3.1.1 C). We conclude that the ChPx houses a circadian clock and that this clock is in phase for both ChPx analyzed.

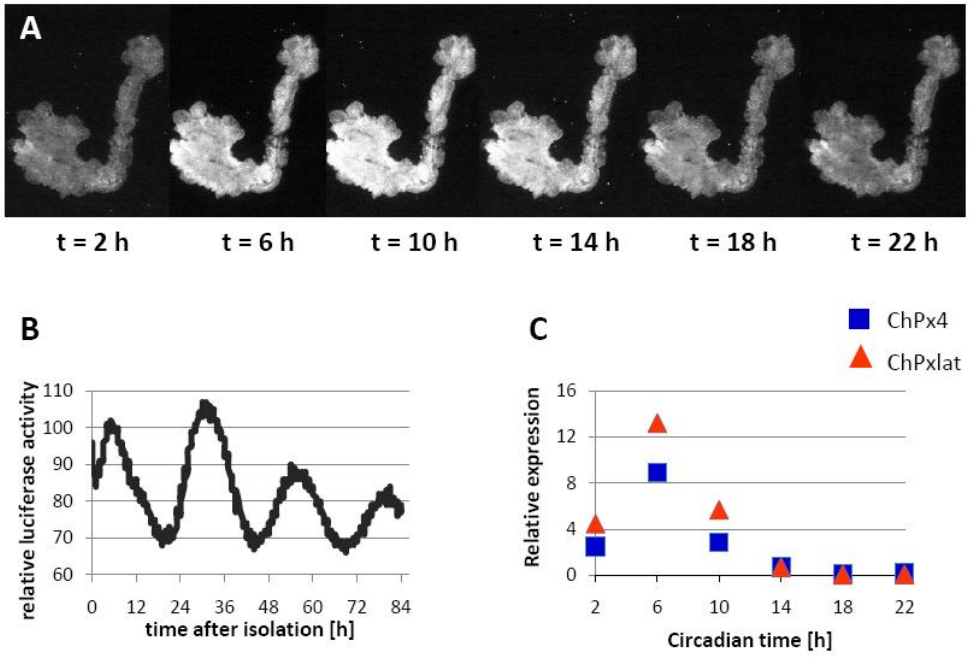

Fig.3.1.1 A circadian clock resides in ChPx. (**A**) Per2:luciferase activity is homogenously oscillating in ChPx4 derived from reporter mice. (**B**) The activity of Per2:luciferase in ChPx4 is subjected to a circadian rhythm that dampens after few days. (**C**) Expression of the clock gene Nr1d2 in ChPx4 is in phase with expression in ChPx derived from the lateral ventricle (ChPxlat).

3.1.2 Characterization of the circadian transcriptome of the choroid plexus

In the light of these results, we collected the medially located, very voluminous ChPx4 from mice at 12 time points spaced 4 h apart. We then determined the circadian transcriptome using Affymetrix GeneChip Exon 1.0 ST arrays. These arrays have on the average 40 individual probes covering the exons of each gene (Clark et al., 2007). Annotation included exon probes for ~38,000 transcripts, 61% of which were expressed in the ChPx4 at least at one of the 12 time points of the circadian profile. Circadian analysis using CircWave (Batch V3.4; see also Oster et al., 2006a) revealed that 1551 transcripts (~7% of the total) were regulated in a circadian manner ($p \leq 0.025$, $pANOVA \leq 0.075$).

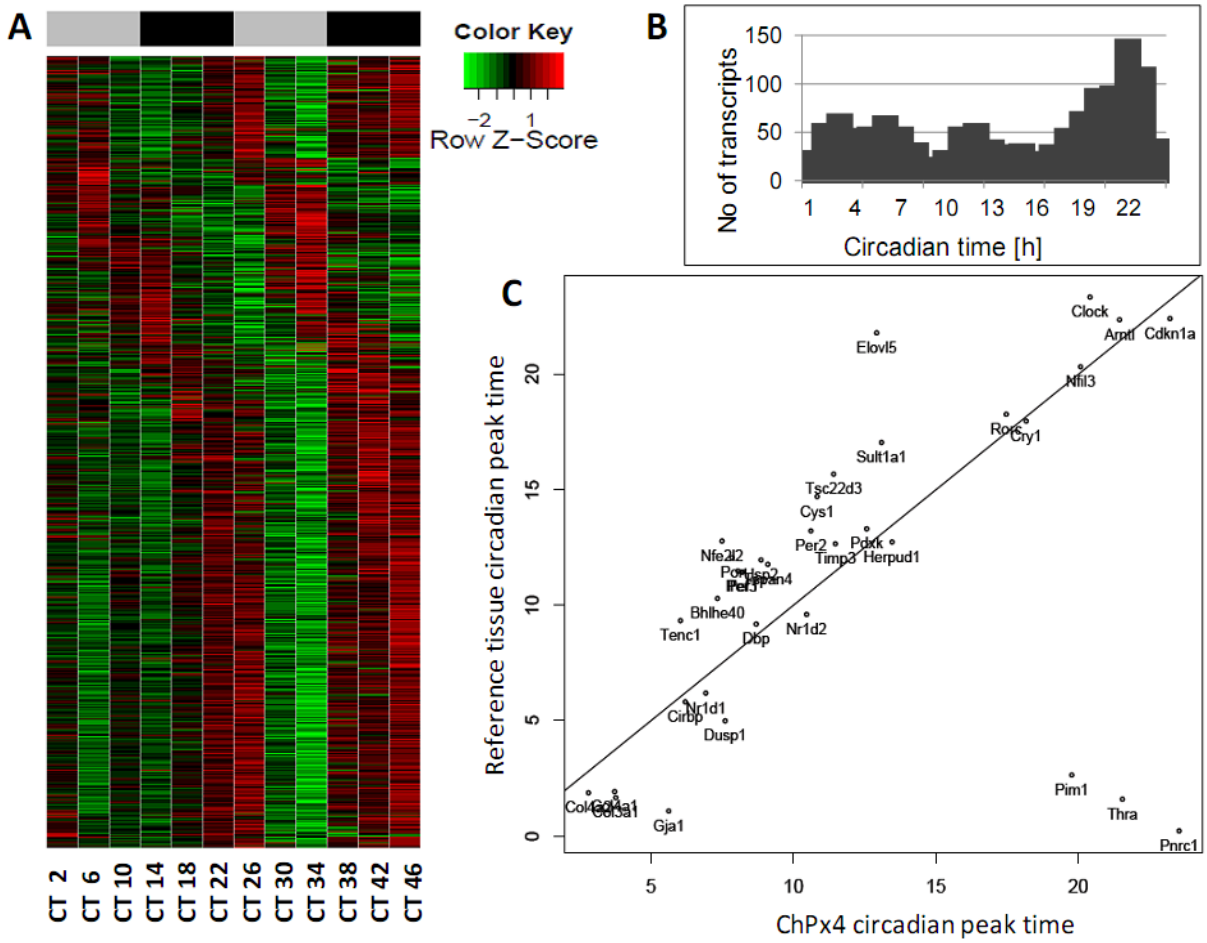

Fig.3.1.2.1 Transcriptome analysis reveals circadian regulation in ChPx4. (**A**) Heat map showing circadian expression for about 1300 genes in ChPx4. (**B**) A cluster of transcripts is upregulated just prior the transition from the active phase to the resting phase (CT22). (**C**) Correlation plot of the phase of common circadian transcripts expressed in ChPx4 with their mean phase in other peripheral tissues (see Yan et al., 2008). The expression of these common circadian transcripts shows similar phase relationship between ChPx4 and other tissues.

These transcripts correspond to 1281 unique genes. A heat map (Fig.3.1.2.1 A) and an associated histogram of peak expression time (Fig.3.1.2.1 B) show both a major peak around CT22 and a minor peak at CT6. ~550 clock-controlled genes appear involved in processes occurring around the onset of the resting phase.

Yan and coworkers have identified a cohort of circadian transcripts that show similar phases in a number of tissues such as liver, kidney, and adrenal gland (Yan et al., 2008). We found that 35 of these genes are also circadian in the ChPx4 and with the exception of *Elovl5*, fall on a diagonal indicating similar phase relationship (Fig.3.1.2.1 C).

Canonical clock genes show a marked circadian profile in both the microarray data set and in a qPCR analysis (Fig.3.1.2.2). Results from microarrays, *in situ* hybridization and qPCR are also consistent and show that e.g. *Bmal1* expression peaks at the end of the night (Figs. 3.1.2.3 A1-4, E). *Ace*, the gene encoding angiotensin converting enzyme and the ascorbic acid transporter gene *Slc23a2* both exhibit a robust circadian rhythm by ISH and in microarrays (Fig.3.1.2.3 B1-C4,F,G). Even low amplitude oscillations exemplified by the gene encoding an ATPase subunit (*Atp1b2*) showed consistency between the two data modalities (Figs.3.1.2.3 D1-4,H).

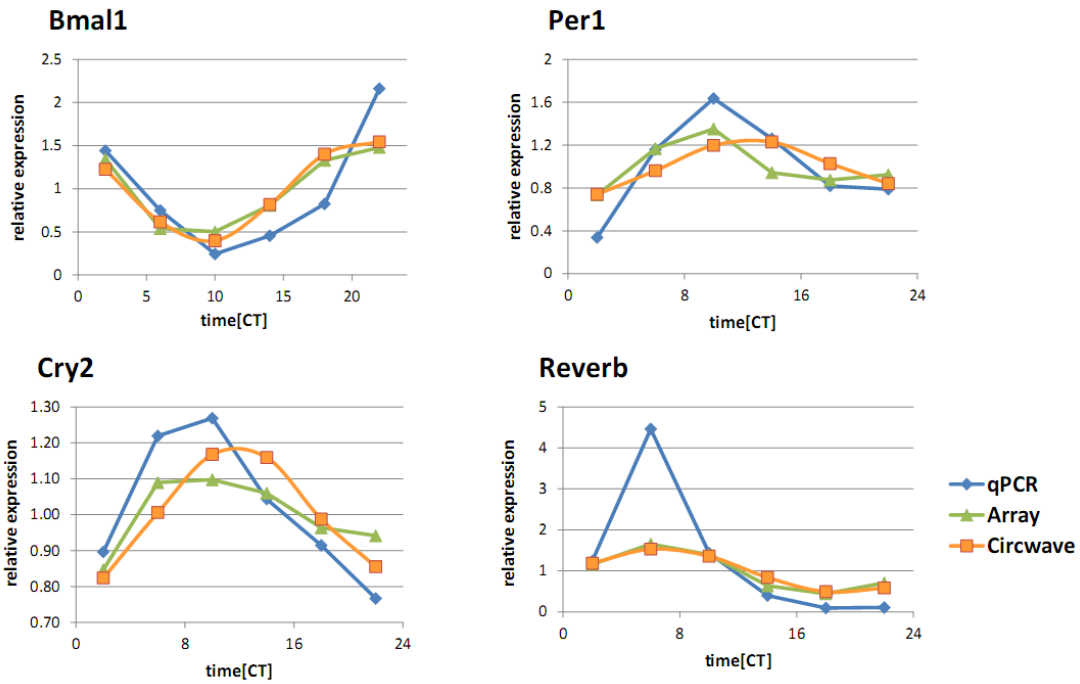

Fig.3.1.2.2 Confirmation of circadian oscillation by qRT-PCR. Significant oscillation and consistent peak expression times were obtained from the microarray data, sinus-fitting on the microarray data (CircWave BatchV3.4), and qRT-PCR.

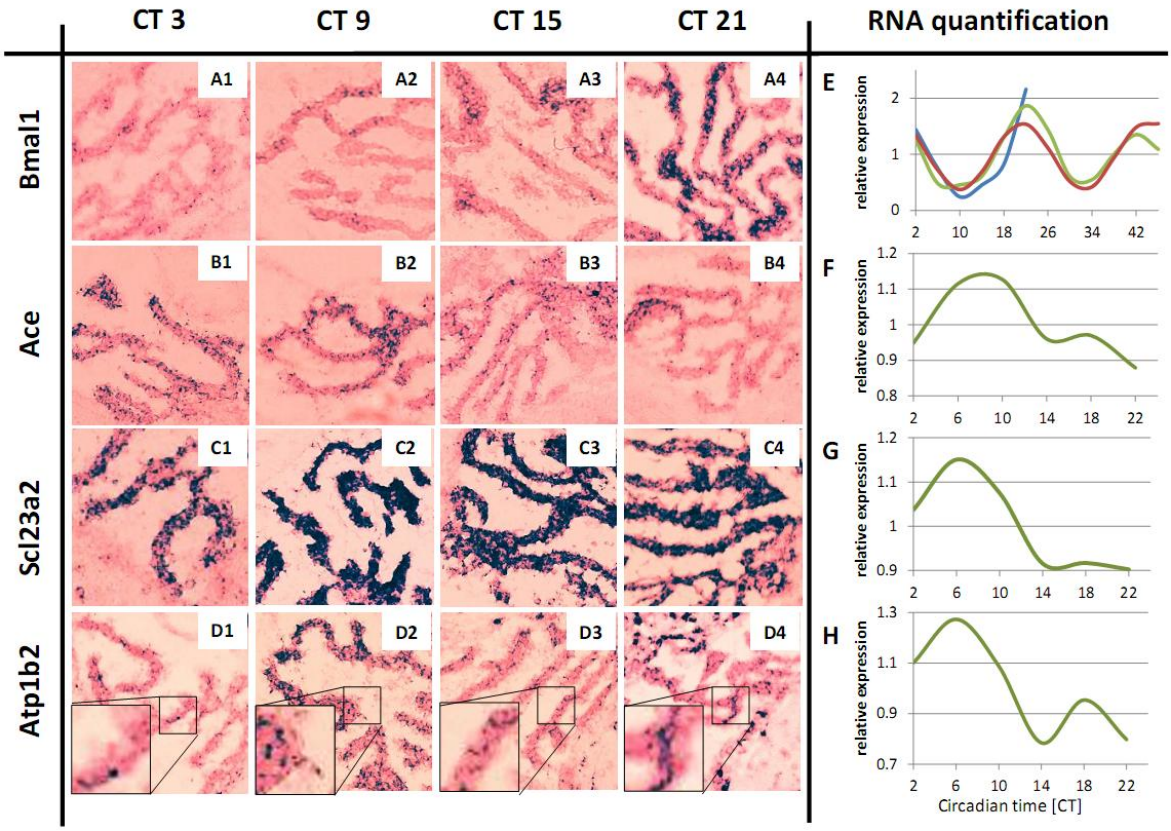

Fig.3.1.2.3 *In situ* hybridization of circadian transcripts in ChPx. A1-D4 *In situ* hybridization (ISH) showing gene expression in ChPx4 at four circadian time points. *Bmal1* staining is maximal at CT21 (**A1-A4**) consistent with the findings obtained by array (green), curve-fitting on array data (red), and qPCR (blue) (**E**). Comparison of data obtained from *in situ* hybridization of three additional genes in ChPx4 showed similarity: minimal expression of angiotensin converting enzyme (*Ace*) is found at CT0 (**B1-B4** and **F**) and maximal intensity was observed at CT9 (**C2**); maximal expression of *Slc23a2* is determined to be at CT6 from the array data (**G**). From the array data we calculated a peak at CT5 for *Atpase1b2* expression. Plotting of the data shows a major peak at CT6 and a minor peak around CT19. *In situ* hybridization shows round-shaped staining of epithelial cells around the time of the major peak (**D2**) whereas at CT21 staining resembles rather the rod-shaped endothelial cells of ChPx4 (**D4**).

Taken together, nearly 1,300 genes expressed in the ChPx4 exhibit a circadian profile. Moreover, ChPx4 explants exhibit a robust circadian rhythm of Per2-luciferase activity suggesting the presence of a self-sustained clock in this organ. In what follows we will address the circadian transcriptome for several ChPx-typical functions: production of CSF, transport of solutes, detoxification, production of secreted signaling factors, and cilial physiology.

3.1.3 Circadian regulation of CSF-production

The ChPx releases Na^+, Cl^-, HCO_3^- and takes up K^+ thereby giving rise to a concentration gradient which results in a recruitment of water into the ventricular volume (Fig.3.1.3). Additionally, the ChPx releases numerous nutrients and proteins that, together with water and brain metabolites, constitute the CSF. A variety of transporters are known to act in a concerted fashion to generate the ion gradient. A major player is a Na,K-ATPase (Johanson et al., 2008) that extrudes sodium and consists of two alpha and two beta subunits. There are four genes encoding an alpha subunit and four genes encoding a beta subunit. Our data show that three of the alpha subunits and three of the beta subunits are expressed in the ChPx4, and the beta 2 subunit exhibits a robust circadian rhythmicity in the epithelium (Figs.3.1.2.3 D1-4, H). To replenish the K^+ extruded by the Na,K-ATPase from the ChPx epithelium, three K^+ inwardly-rectifying channels (Damkier et al., 2010; Millar et al., 2007) are highly expressed in ChPx with *KCNJ13* showing a very pronounced circadian oscillation.

Carbonic anhydrases (CAR) produce HCO_3^- and protons which are used by basally located solute carriers (Slc12a6,4a2,4a7) and apically located solute carriers (Slc9a1,4a5,12a7) to promote transport of Na^+ and Cl^-across the ChPx (see Fig.3.1.3). While the transporters and channels do not show significant circadian oscillation, *Car14*, one of the three *Car* genes expressed in ChPx4, exhibits circadian expression.

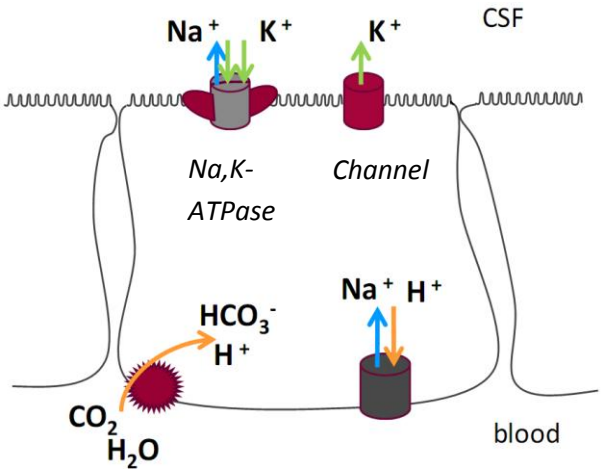

Fig.3.1.3 Circadian components of CSF-production. Schematic drawing of CSF-secretion by a ChPx epithelium cell. Circadian regulated components of transport are in red. The membrane bound carbonic anhydrase (CAR14) and Na, K-ATPase are driving forces of CSF-production.

Of note, carbonic anhydrase activity in ChPx of rat had previously been characterized as circadian (Quay, 1972). Our data raise the possibility that transcriptional changes in *Car14* underly this rhythm. It is interesting to note that the gene encoding the beta 2 subunit of Na,K-ATPase, *KCNJ13,* and *Car14* show peak expression between CT5 and CT11, that is within a relatively narrow time window supporting the idea of circadian regulation of CSF production. Nilsson and colleagues (Nilsson et al., 1992) report a day-time dependency of CSF-flow speed in the human aqueduct with maximal speed around 2 a.m. in the middle of the resting phase. Our finding that genes encoding key CSF-producing enzymes are upregulated in the middle of the resting phase supports the idea that CSF-flow is modulated by the circadian clock residing in the ChPx.

3.1.4 Organization of solute delivery and clearance

The circadian transcriptome of the ChPx4 comprises approximately 50 genes encoding transporters from the Solute Carrier (Slc)-family, as well as channels and ABC transporters. The phase distribution of these transcripts shows two peaks, a minor one towards the end of the active phase and a major peak in the middle of the resting phase (Fig.3.1.4). Transported solutes are primarily not required by ChPx itself but enter the brain ventricles via transcytosis across the ChPx epithelium.

The major peak around CT6 includes transcripts for Slc-proteins that facilitate transport of amino acids, vitamin C and inorganic ions. Slc23a2, a Na^+-dependent ascorbic acid transporter is expressed in ChPx but not in the capillaries of the BBB. Hence such localized *Slc23a2* expression provides a selective entry site of ascorbic acid into the brain (Spector and Johanson, 2006). The peak expression of *Slc23a2* at CT6 coincides with that of amino acid transporters *Slc7a1*, *Slc7a5*, *Slc38a1*, *Slc38a3*, and *Slc38a5,* all of them located in the plasma membrane. ChPx expresses additional Slcs with a similar solute profile that are not rhythmically expressed but provide alternative amino acid transport pathways. Apparently, solute transport has both, a circadian and a non-circadian component, suggesting that the circadian clock helps in fine-tuning of transport at specific times of the day.

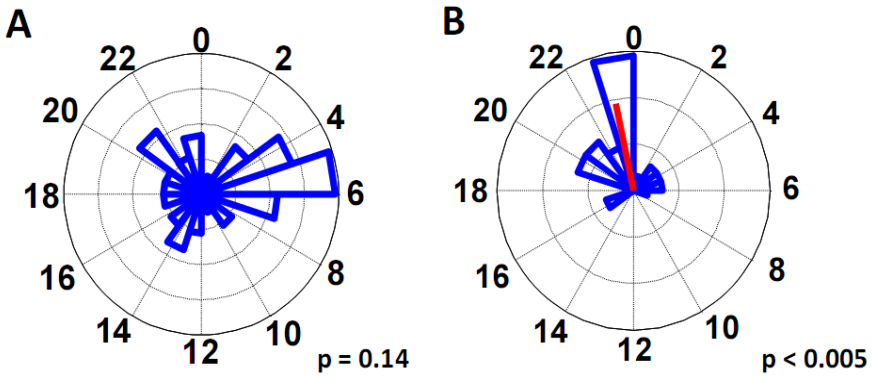

Fig.3.1.4 Phase distribution of transporters and endocrine signaling. (**A**) Circular histogram shows a biphasic distribution of transcripts encoding transporters and (**B**) phase clustering of endocrine factors and their receptors preceding the onset of the resting phase. The p-value results from Rayleigh-testing for uniform distribution. The red bar is the mean resultant vector that indicates peak phase clustering.

The minor peak group includes transporters for zinc, iron, and xenobiotics. In contrast to, e.g., amino acid transport, general upregulation of these Slcs is not restricted to a specific time window during the day. Abcc8 (peak expression at CT0) encodes a multidrug resistance-related protein, Slc15a4 (peak at CT13) is a peptide transporter, Slc16a4/a6 (CT9/18) are monocarboxylate transporters, Slc13A4 (CT7) and members of the Slc22a1/a15/a23 (CT23/21/4) encoding major facilitators of detoxification. These transporters are thought to be involved in the clearance of several toxins and neuroactive signals from CSF (de Lange, 2004; Hediger et al., 2004; Koepsell and Endou, 2004; Alebouyeh et al., 2003). The spread of peak time over the day might reflect an adaptation of individual transport systems to day-time dependent variation in the presence of specific toxins.

3.1.5 Detoxification Pathways

After toxic solutes have entered the ChPx from CSF, the ChPx epithelium is capable to process them through the detoxification machinery (Fig.3.1.5). ChPx harbors a general detoxification pathway that processes substrates via at least two enzymatic phases (Ghersi-Egea et al., 2006). Phase I-enzymes are a group of oxido-reductases that initiate the process of degradation by functionally activating the substrate. In the ChPx, ferredoxin–monooxygenases (FMO) and P450 cytochrome oxidoreductase (POR) are reported to be major phase I-enzymes but several other members of the Cyp450 family are also expressed in the ChPx (Strazielle et al., 2004). Deleterious byproducts of POR-activity are processed by

several forms of the epoxide hydroxylase. We find robust oscillation of *Fmo1* (CT10), *Fmo2* (CT13), *Por* (CT8), and *epoxide hydrolase 2* (CT12) indicating a circadian regulation of toxin processing.

Phase I products are mostly reactive intermediates that are conjugated by phase II-enzymes. Most of these enzymes are transferases. Our data show significant oscillation for *sulforyl-transferase-1a1* and *-1c2* (CT13, CT13) but not of genes encoding glucorono-or glutathione-transferases. We attribute this constitutive expression to their role in buffering of the CSF and in scavenging of radicals produced by non-phase I processes (Strazielle et al., 2004).

In liver, several Phase I and Phase II enzymes are regulated by the PAR-domain basic leucine zipper transcription factors that are encoded by *Dbp*, *Lef*, and *Hlf* (Gachon et al., 2006). Interestingly, expression of these clock output genes in the ChPx is circadian regulated and in synchrony (CT9, CT8, CT8) with the circadian regulated Phase I and Phase II genes. This suggests that the transcriptional mechanism by which the circadian clock imposes rhythm to processes of detoxification is conserved between liver and ChPx.

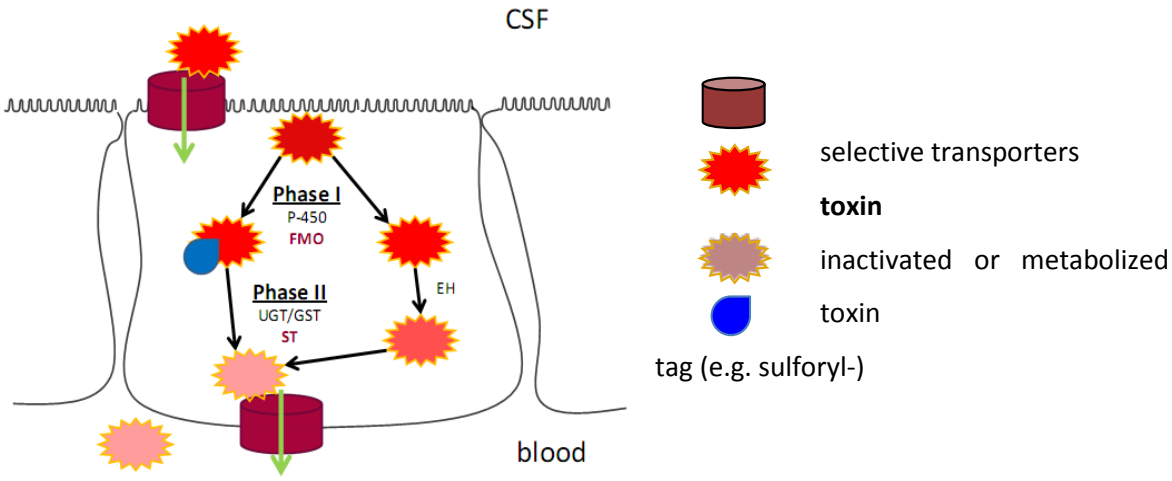

Fig.3.1.5 Circadian regulation of detoxification in ChPx. Schematic drawing of the detoxification pathway in the ChPx. Toxic agents are taken up by selective transporters located at the CSF-facing membrane. Subsequently they are processed and inactivated or metabolized and finally released to blood by selective transporters. Circadian regulated phase I genes are *Por, Fmo1, Fmo2,* and *Ephx2* (CT8, CT10, CT13, CT12). Oscillating Phase II genes are encoding sulforyltransferases (all with peak expression at CT13). Uptake of toxins from the CSF and extrusion of conjugates to the blood requires a variety of selective transporters that are non-circadian or oscillating with unspecific phase preference.

The ChPx expresses several degrading enzymes that are not part of the Phase I and Phase II mechanism. However, these enzymes target neurotransmitters. Examples are *Faah* (CT0), which is involved in processing of anandamides, *L-amino acid oxidase* (CT4) that promotes serotonin degradation, and the amine oxidase *Aoc2* (CT22) that promotes degradation of phenylethylamines. Taken together, we found good evidence that detoxification and degradation of toxic and/or neuroactive substances in the ChPx is regulated in a circadian manner.

3.1.6 Circadian regulation of endocrine functions

Since ChPx is also an endocrine tissue, it secretes a variety of signaling molecules and also expresses cognate receptors. We found that many secreted and membrane-bound signaling molecules are subjected to circadian regulation and cluster in phase. These are *Slit1*, *Sema4C*, *Sema4D*, *Gdnf*, *Noggin*, *Notch2*, *Efnb1*, *Wnt7a*, *Dkk1*, *Dkk2*, *Dhh*, *Ihh*, *Sfrp5*, and diverse members of the growth factor family. Also these transcripts are significantly upregulated around CT22 (Fig.3.1.4). In addition, peak expression around CT22 is observed for several transcripts encoding metallopeptidases and retinol dehydrogenases that mediate functional modification of signaling molecules.

Several of these signaling molecules exert neuroprotective functions (Chodobski and Szmydynger-Chodobska, 2001; Johanson et al., 2011a; Thanos et al., 2010; Zappaterra and Lehtinen, 2012). However, angiotensin-converting enzyme (*Ace*, CT10) exerts a regulatory effect on directed water and electrolyte transport (Lee et al., 2013; Riquier-Brison et al., 2010). The functional difference might explain why *Ace* is in antiphase to other circadian signaling molecules. Apparently, the ChPx transcriptome prepares an overall upregulation of the endocrine machinery in terms of neuroprotection at the onset of the subjective light phase but this functional cluster is most prominent in antiphase to CSF-production and detoxification.

3.1.7 Cilia components exhibit circadian oscillation

ChPx has sparse multiciliated cells (O'Connor et al., 2013; Yamadori, 1972) with short and only few cilia per bundle. Whereas the motile function of these cilia is debated (O'Connor et al., 2013; Roth et al., 1985), the function of these cilia as signaling center is well established. Since *hydin* (CT7), a gene that is necessary for motility of cilia (Lechtreck et al., 2007) is

expressed in ChPx4, it is most likely that motile cilia are present. Assuming that the circadian oscillation of the transcript affects the protein, one would expect increased cilia motility around the transition from the resting phase to the active phase.

Further ciliary genes have been identified in the circadian transcriptome, including structural components of cilia. One example is *Crocc* (CT2), which is located to the ciliary rootlet. *Crocc* has a crucial role for axoneme stability and for anchoring the cilia to cellular components (Gilliam et al., 2012). *Dnahc17* (CT23) encodes for an axonemal dynein and *Tuba3a* (CT23) affects the ciliary length (Sharma et al., 2011). A broad effect on the composition of ciliary components is expected from changes in the transport mechanism locating proteins to the base of the cilium. This transport involves the BBSome and the ciliary pore at the partitioning barrier, and the IFT bringing proteins towards the tip of the cilium. Pronounced circadian oscillation was found for several components that regulate these three steps of transport: *BBS10* (CT2) (Marion et al., 2009) and *IFT80* (CT13) as well as axonemal motors *Kif17* (CT22) and *Kif3* (CT18) and components of the ciliary partitioning system, namely, *RanGap1* (CT23) and *Sept3* (CT18).

Interestingly, most of these circadian transcripts show peak expression between CT18 and CT2, a 6 hours time window in which also receptors that are targeted to cilia are upregulated e.g. *Ptch2* (CT19), a receptor that is required to mediate the response to the cytokines *Dhh* (CT24) and *Ihh* (CT23). Both these particles are part of the hedgehog signal transduction pathway (Berbari et al., 2009). Taken together, the circadian components of the ciliary transport systems are upregulated simultaneously with their cargo, the ciliary components and ciliary receptors, and with circadian ligands of ciliary receptors. In view of this temporal coregulation it is likely that structural appearance and sensory functions of cilia are upregulated at the end of the resting phase.

3.2 A novel methodological approach towards assessment of cilia dynamics

3.2.1 Visualization of beat orientation across the ependyma

Already in 1835, Purkinje was able to describe the lash-like movement of cilia from fetal mammalian ependyma that distinguishes from the movement of cilia in the lung (Purkinje 1936). Almost 100 years later, a more detailed assessment of ciliary beat parameters was possible using cinematography in combination with stroboscopes (Gray et al., 1930). Today, the usage of high-speed cameras and differential interference contrast (DIC) allows a much more detailed and time-resolved analysis of the parameters of the ciliary stroke. Mammalian tissues are commonly prepared for such observations by sectioning the tissue into thin stripes to observe cilia from a lateral aspect. Shinohara et al. showed that observation of cilia on a whole mount is also possible. They recorded mouse node (a signaling center in the early mouse embryo) orthogonally to the tissue plane of the node and identified both position and rotational movement of the nodal monocilia. These analyses included but a few cilia and were performed manually by marking cilia using ImageJ (Shinohara et al., 2012).

These methods of observation and analysis are not directly applicable to the ciliated ependyma for two main reasons. First, prior to application of DIC the brain tissue needs to be sectioned to very thin layers in parallel to the cilia carpet. Second, since the ependyma is covered by thousands of cilia bundles forming a carpet of cilia, a manual analysis of cilia beating is impossible. To overcome these difficulties, we developed a novel slicing technique and, additionally, an automated analysis of ciliary movement from movies taken from ependymal cilia carpets.

A freshly isolated mouse brain was placed into DMEM and cut into thick coronal sections (1mm) using a brain matrix device. Next, neuronal tissue underneath the ependyma was dissected away using a sharpened tungsten needle. The ventricle was opened from its ventral side and the resulting ependymal patch (from here on “open book”) was placed into an incubation chamber that was specifically constructed for this purpose. The ciliated surface of the ependyma facing the objective was recorded through a 60x magnification DIC objective at 50 frames per second (fps), which is about twice the beating frequency of cilia (Fig.3.2.1 A-F). Subsequently, the movies were processed by averaging the change in pixel intensity over time. By averaging ciliary movement over a total of 500 frames (10s), the directionality of the ciliary stroke was revealed (Fig.3.2.1 G). To cover the entire surface of the third ventricle (approximately 3 x 2 mm), the tissue was laterally translocated with the

microscope stage and in this way the entire surface was captured in individual tiles that were subsequently combined to generate an overall view of the ventricular ependyma (see Fig.3.3.2 below).

Fig.3.2.1 Visualization of cilia beating patterns. A-F Cilia above the wall of the third ventricle were recorded using DIC. Cilia are tiny and transparent with a length around 14 µm. Bundles of cilia can be recognized by comparing the surface at different time points during the beating cycle. Time intervals between the consecutive pictures are 20 µsec. Note that cilia bundles can be characterized by phase and direction. **G-J** White color indicates the averaged change in pixel intensity. (**G**) The pattern is consistent with the movement observed in the time-series. (**H**) Cilia beat pattern forming a whirl. (**I,J**) Mosaic of cilia beat pattern covering a larger area of the ciliated ependymal wall of the third ventricle. Note that the scale bars indicate the length of 20 µm.

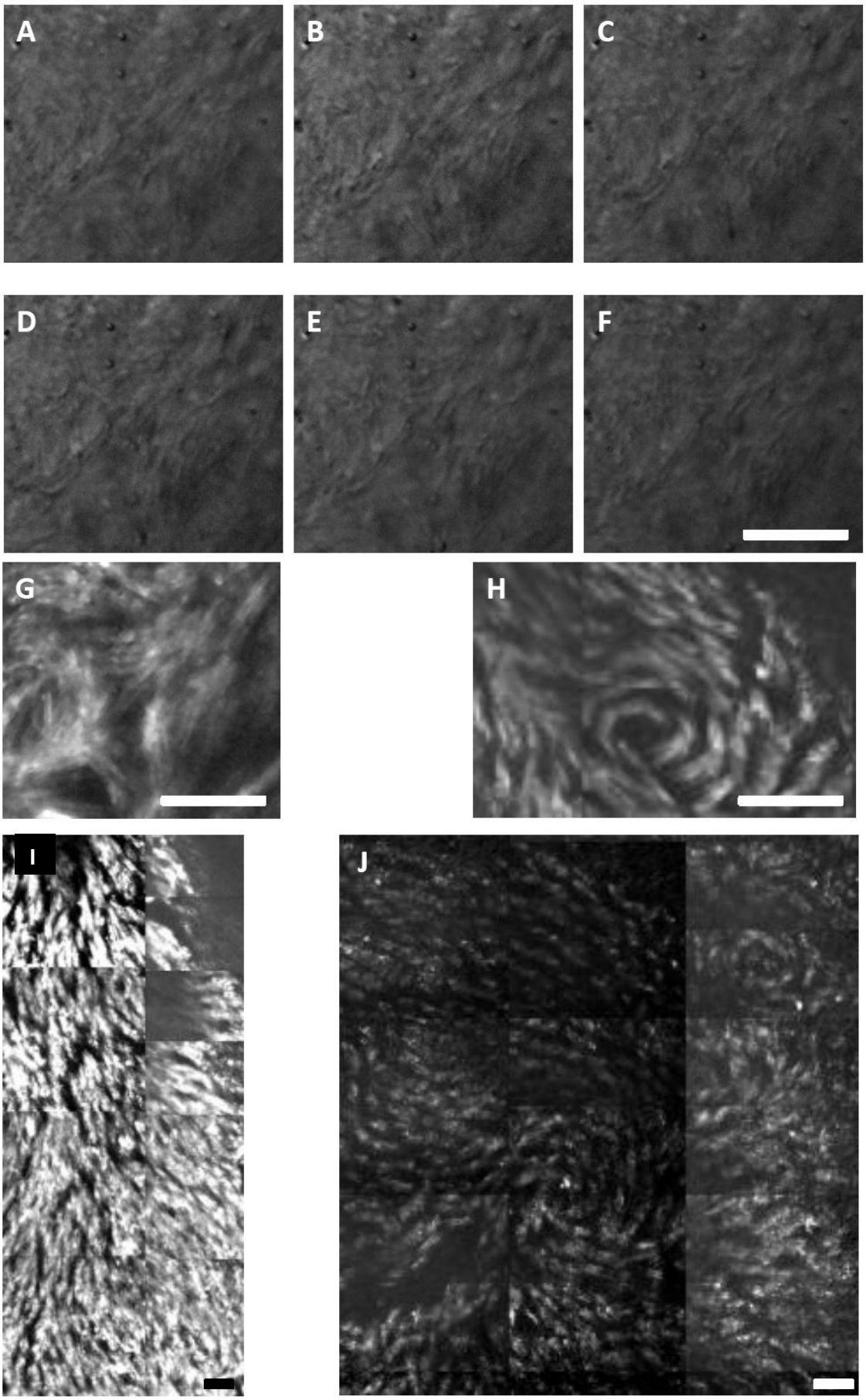
A
B
C
D
E
F
G
H
I
J

3.2.2 Assessment of cilia-dependent fluid dynamics

Ibanez-Tallon et al. were the first to apply computational particle tracking to analysis of fluid dynamics that is induced by ependymal cilia (Ibanez-Tallon et al., 2004). They prepared ependyma from the lateral ventricle, placed fluorescent beads in close proximity to the preparation, and determined the velocity of cilia-induced propagation of the particles. Some years later, Sawamoto et al. extended this method by injection of particles onto whole mount preparations of the lateral ventricle and observed a unidirectional propagation above the ependyma (Sawamoto et al., 2006). An advantage of this preparation is that the tissue of interest is analyzed under most natural and intact conditions and the influence of neighboring microenvironments is preserved. The “open book” preparation fulfills the requirements as best as possible for the third ventricle. However, higher spatial resolution is needed and the visualization of flow should not be limited by the application site of beads. Therefore, the beads were dispersed in the medium and global fluid dynamics were assessed above the cilia carpet of the “open book” preparations.

For visualization of cilia induced streams in the third ventricle, fluorescent beads with 1 µm of diameter were first added to DMEM and then homogenously dispersed. “Open book“ ependyma was placed onto a membrane in an incubation chamber filled with 2 mL DMEM containing fluorescent beads and recorded from top view. The beads and medium were propelled by the cilia thereby generating a flow in the volume above the cilia carpet. The movement of beads was recorded at 29 fps for a time period of 1 min through a 5x and a 10x objectives yielding a ROI of 1.2mm x 1.2mm and 610µm x 610µm, respectively. A corresponding bright field picture was also taken to document the exact position of the ROI within the ventricle.

For computational analysis of bead movement, a matlab tracking code (Jake Jaffe, see Material and Methods 2.5.3) was used to identify the beads in the focal plane and to determine their propagation over time. From this data, information about the speed and direction of the flow was visualized. This code was extended in cooperation with Christian Westendorf so as to overlay color coded tracks with the bright field picture of the tissue. The color coding was for either direction of flow or bead velocity.

Recordings were performed at 5x/10x magnification above the ependyma. The plane of the tissue was identified using those fluorescent beads that were immobilized between the cilia. At the plane of cilia, the beads were moved in mainly two directions as indicated by

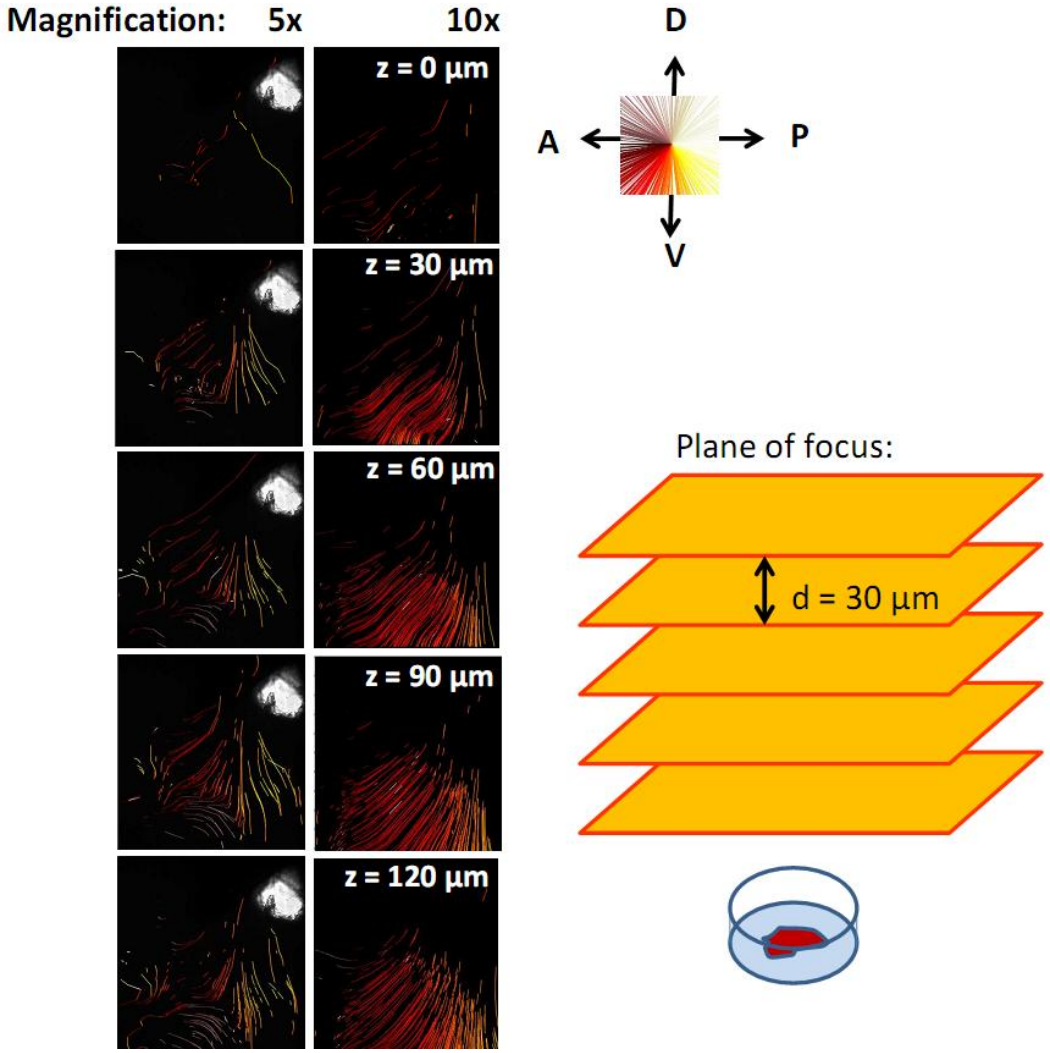

Fig.3.2.2 Particle tracking of beads above the ependyma. Overlay of a brightfield picture and tracks at their original position. Removal of the anterior commissure during the sectioning procedure leaves a whole that becomes apparent in the brightfield picture. The color-code indicates the direction of the tracks. Flow direction was assessed at the cilia carpet (z= 0) and at several distances above as illustrated schematically. Flow direction in this specific region is conserved from z= 0 to z= 120µm.

yellow and red tracks (Fig.3.2.2). 30µm above, tracks were found in most regions of the ventricle and with conserved direction compared to the previous plane. Even at a height of 120µm above the ventricle wall, the direction of the flow pattern is similar to that observed at z = 0. Obviously, the cilia in the third ventricle generate a fast and directed flow. However,

at a region that is close to the boundaries of the ventricle and highly uneven the flow direction at a distance of 120µm from the tissue surface is very different to the flow direction in the volume up to 90µm (Fig.3.2.3). Such regions are found e.g. anterior to the entrance of the ventral part of the third ventricle.

How can bead flow patterns be assessed including those regions of the third ventricle that are buckled? Beads occasionally trapped at the ependyma define the plane of the cilia carpet. First a 1 min recording was carried out in this plane (z = 0µm; Fig.3.2.3). Using the stage micrometer, a next imaging plane z = 30µm higher up was recorded. This was repeated several times at successive planes above the marker bead. Similar directions of flow were observed up to a distance of 60-90µm from the marker bead (Fig.3.2.3). If the recordings are evaluated for bead velocity, the resulting mean of color coded tracks shows higher velocities in close proximity to the cilia and thus can be used for identification of the flow along the wall (Fig.3.2.3 B, D). As our investigation shows, determination of bead flow above buckled ciliated epithelia requires special care in the recording process. When the flow patterns across larger segments of the lateral wall are determined, one needs to pay special attention to regions of unevenness.

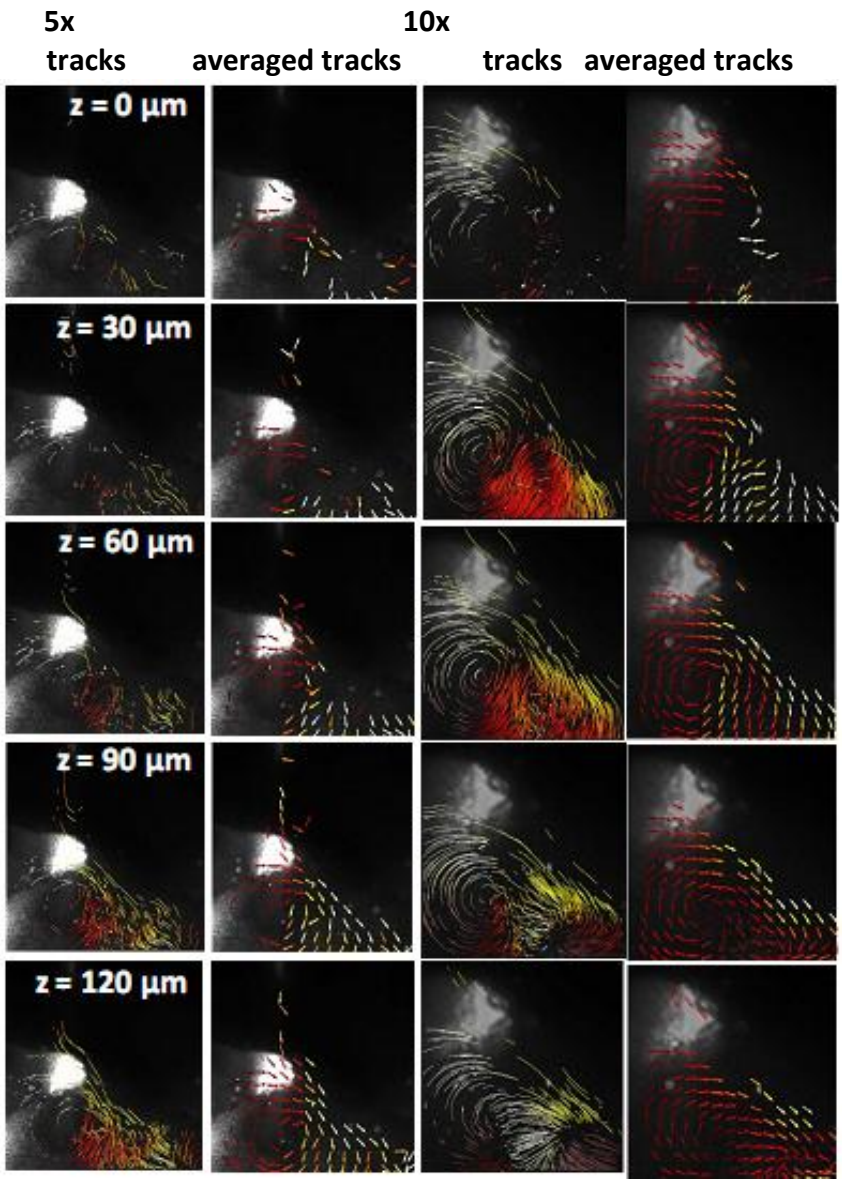

Fig.3.2.3 Flow pattern at buckled regions is more difficult to assess. The overlay of tracks with the brightfield picture shows that in certain regions the flow above the cilia carpet is not directional. The majority of tracks in at a distance from z=0 to z=60µm is directed towards the bottom as indicated by red and yellow color. However, at a distance of z=120µm tracks differ in direction. Color-coding of the averaged tracks according to velocity (relatively low in red and high in white) shows that those tracks with the highest velocity can be used as reliable measure of flow direction along the wall.

3.3 Spatial resolution of cilia activity above ependyma

3.3.1 A closer look to the cilia carpet that covers the third ventricle

The third ventricle is bounded by the thalamus and hypothalamus on both, the left and right, sides. Of particular importance is the fact that numerous hypothalamic nuclei including the suprachiasmatic, the arcuate, and the paraventricular nuclei are located in close apposition to the ventricle and therefore may send or receive signals directly from the CSF. It should be recalled that the width of the third ventricle is in the range of 50 micrometers, and hence the distribution and localization of such signals may be determined, at least in part, by a cilia-mediated CSF-flux and not by bulk-flow or heart-beat induced contractions and expansions.

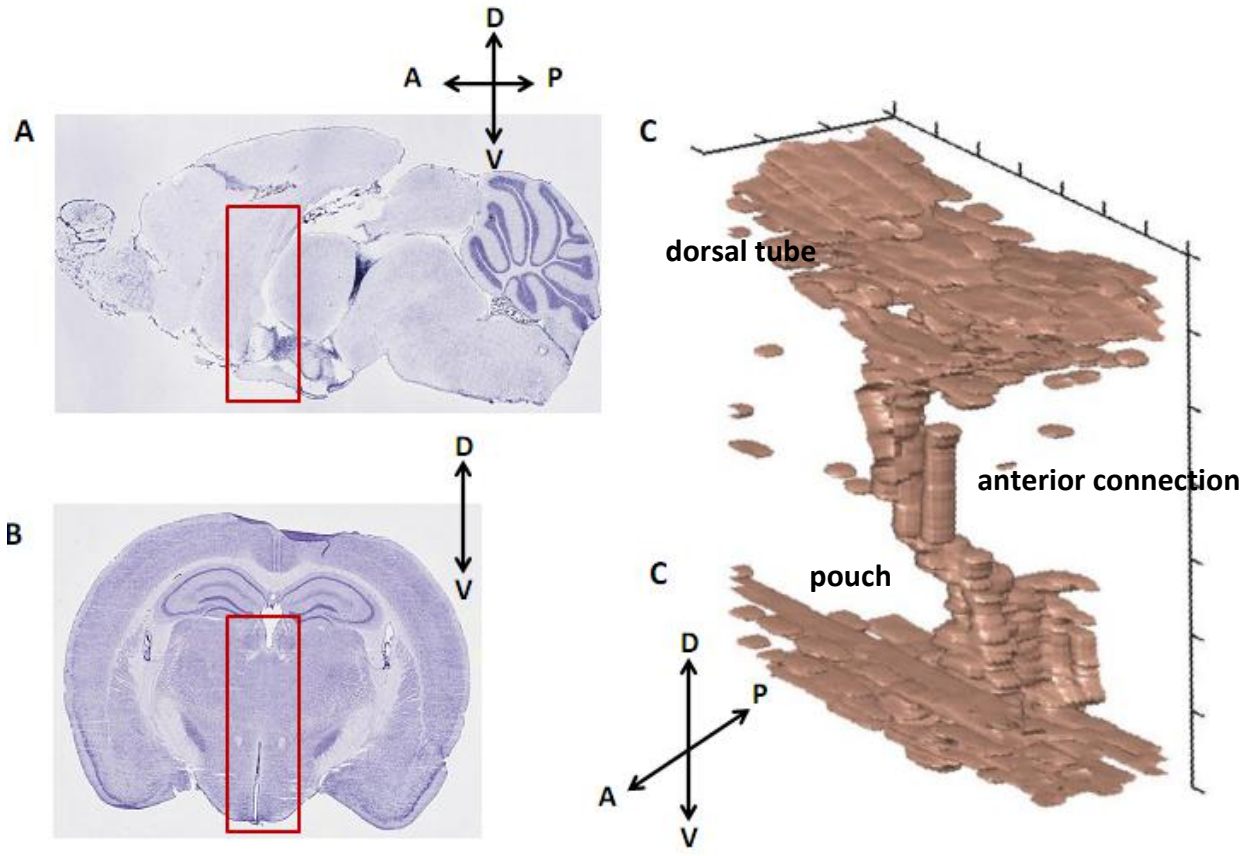

Fig.3.3.1 Three-dimensional structure of the third ventricle. (**A,B**) *In-situ* hybridization of *FoxJ1*. Extensive staining is observed for ependyma. (**A**) A sagittal section shows the third ventricle in full length. (**B**) In a coronal section, the ventral part of the ventricle appears as thin line. (**C**) A 3D reconstruction of FoxJ1-staining in the anterior part of the third ventricle shows that the ventricle is divided into a dorsal part (tube) and a ventral part (pouch). The position is indicated by the red boxes in the sections on the left side (A,B). Arrows indicate the antero-(A) posterior(P) axis and the dorso-(D) ventral (V) axis.

In order to get a detailed overview on the anatomy of the third ventricle, serial mouse brain sections were stained for *FoxJ1* expression (Fig.3.3.1 A, B) which is a marker for multi-ciliated epithelia (Ostrowski et al., 2003). Consecutive sections were aligned and the surface of the ventricle was reconstructed from the stain (Fig.3.3.1 C). The reconstruction shows the bipartitioning of the third ventricle. A dorsal tube is oriented straight along the antero-posterior axis and a very narrow pouch is located ventrally. A narrow passage leads from the dorsal tube to the anterior part of the pouch (Fig.3.3.1 C). A second, posteriorly located passage reunites the two parts of the third ventricle around bregma -2.4 at the midline (data not shown). On the surface of both ventricular cavities *FoxJ1* is persistently expressed suggesting that the ependymal lining is uniformly decorated with bundles of cilia.

3.3.2 Mapping the cilia orientation at the walls of the third ventricle

In order to gain insight into the functionality of these cilia bundles, live imaging of their movement was analyzed as described above (Fig.3.3.2). The cilia throughout the third ventricle are constantly moving and the pattern of ciliary beat orientation is the same between animals (n= 3) subjected to analysis at a particular time of the day.

We can distinguish two types of ciliary beating pattern.

(1) There are extended regions where cilia bundles beat with a common orientation. E.g. at the anterior access and posterior exit of the ventral "pouch" of the 3rd ventricle (henceforth referred to as "pouch"), all cilia bundles beat in parallel to the long axis of the connecting channels (Fig.3.2.1 I).

(2) Cilia bundles may show complex beating patterns such as intercalation of cilia from neighboring bundles or cilia bundles from clusters that generate a swirl pattern or spiral pattern (Fig.3.2.1 H,J).

Microdomains of ciliary beat directions measure anywhere from 60 to 1000 microns in length. Since the pouch dimension is in the millimeter range multiple microdomains are combined and aligned in a puzzle-like fashion as indicated by dotted lines in Fig.3.3.3 C. Such complex beating patterns raise the possibility that cilia do not just promote the flow and

mixing of the CSF but orchestrate a targeting of CSF components to particular locations within the pouch.

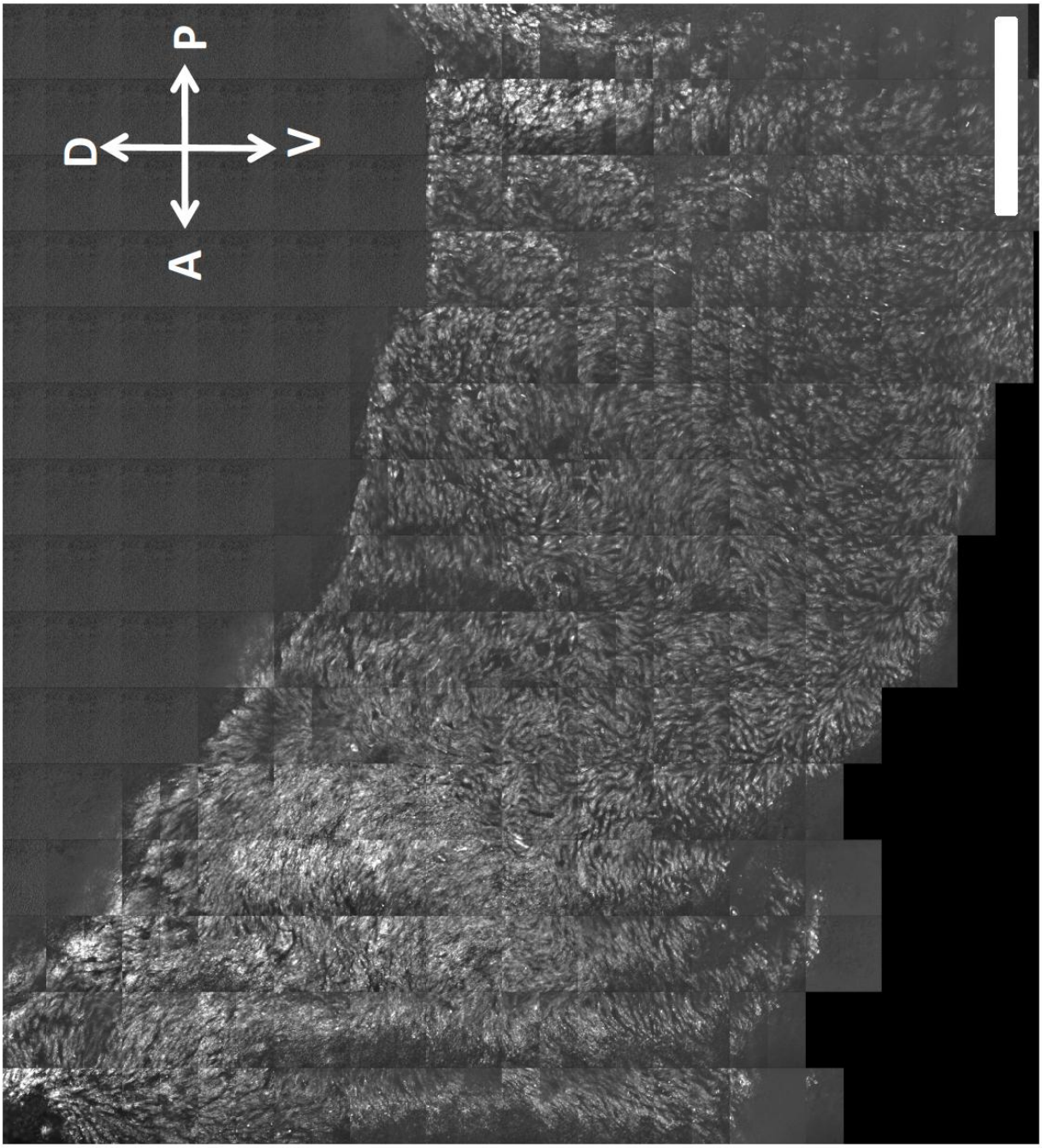

Fig.3.3.2 *In situ* beating of ependymal cilia. The mosaic picture of beating pattern obtained from 300-400 individual movies shows cilia orientation in the 3rd ventricle pouch. Cilia beating of neighboring cells is synchronized across microdomains. The arrangement of these microdomains throughout the pouch results in a characteristic pattern. The bar indicates 270µm.

3.3.3 Flow pattern along the third ventricle lining

The flow direction above the cilia carpet of the pouch was determined immediately after the preparation of the pouch (Fig.3.3.3 A). Comparison to the flow pattern obtained five hours later shows that the cilia-induced flow is stable during this time window (Fig.3.3.3 A,B). From that we conclude that the flow pattern along the wall is not changed during the isolation and culturing and in consequence the recordings of the flow direction reflect cilia activity in the ventricle of the living animal.

As previously observed for the cilia beat direction, fluid dynamics above the cilia carpet are consistent between animals at a certain time of the day. Furthermore, the flow patterns above the left wall and above the right wall show mirror image symmetry (Fig.3.3.3 E, F).

The bead flow is tightly correlated with the beating pattern of the cilia and reflects their organization to microdomains (Fig.3.3.3 C,D). At the anterodorsal entry, a broad flow is directed towards the bottom of the pouch. This flow then bifurcates into two domains. Domain 1 turns towards the anterior wall of the pouch whereas domain 2 turns towards the region adjacent to the SCN. At the anteroventral end of the pouch, a stream arises from the preoptic area (domain 3) that flows in dorsal direction until it integrates in the domain 2 flow. Domain 4 evolves below the roof of the pouch at the level of the PVN. In this domain, particles are transported in parallel to the roof in a posterior to anterior direction, collide with and integrate into the main ventrally directed stream formed by domain 2. Domain 4 has exactly defined borders. Starting from it`s ventral border, particle tracks point towards the bottom of the pouch referred to as domain 5. Behind the PVN, a wide field evolves from the roof of the pouch and straightly flows ventrally until it reaches the bottom and then disappears. This flow-field is domain 6 that completes the anteromedial part of the pouch and the remaining posterior part is referred to as domain 7. Domain 7 comprises only regions with strictly dorsally directed flow.

Comparison between the flow domains (Fig.3.3.3 C) and cilia beating orientation (Fig.3.3.3 D) shows a strict correlation. This implicates that the architecture of the ciliary carpet lining the pouch of the third ventricle produces very specific CSF flow patterns that are capable of targeting solutes to specific regions within the pouch.

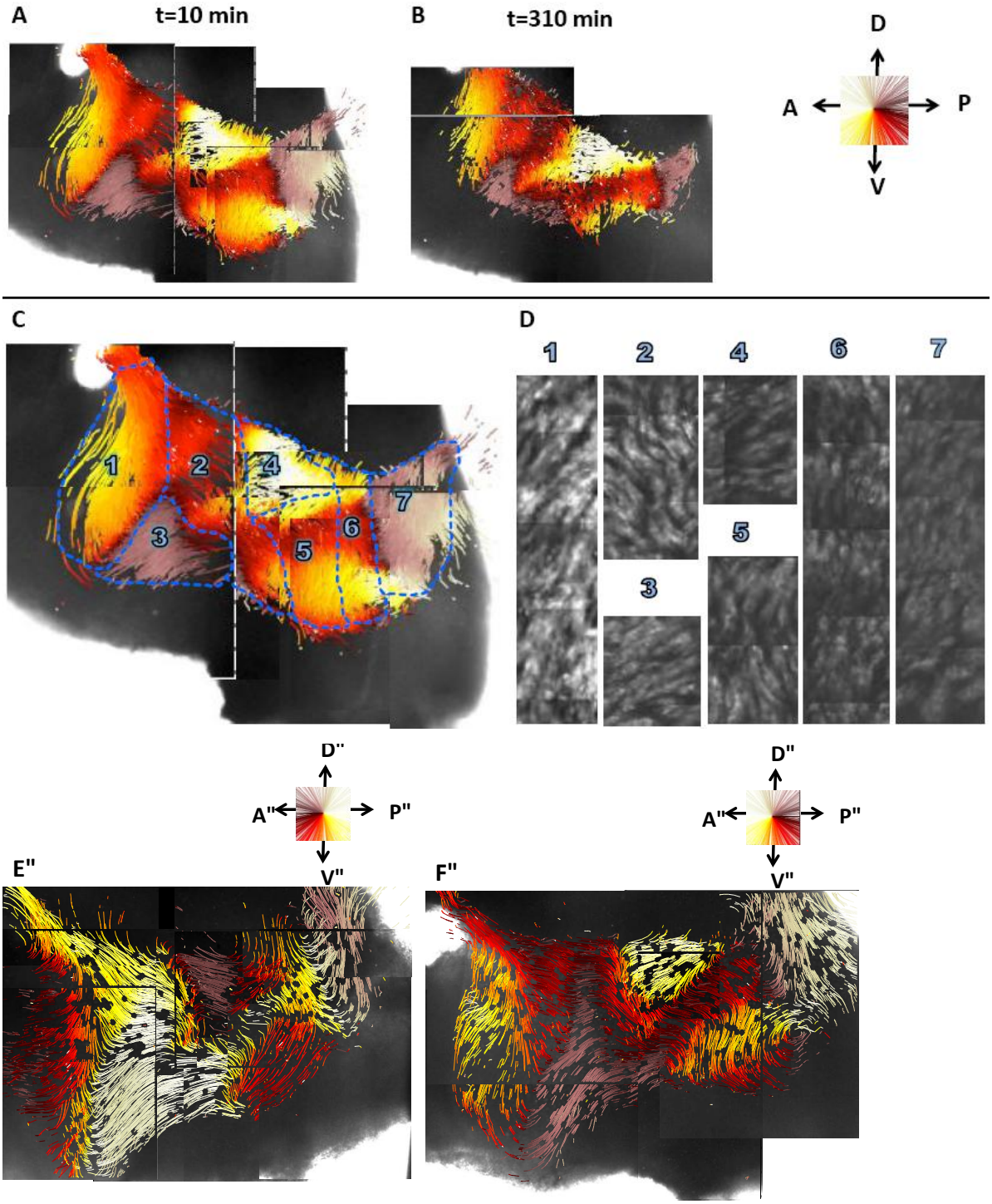

Fig.3.3.3 Cilia beat produces a characteristic flow pattern above the ependymal lining. (**A**),(**B**) The flow direction in the pouch of the 3rd ventricle shows little change in the time interval of 10 min to 310 min after sacrificing the mouse. (**C**) With respect to the flow directions the pouch can be subdivided into 7 domains. (**D**) Bead flow correlates with cilia beat orientation. Cilia orientation in domain 1 is aligned with flow along the preoptic area, in domain 2 from the paraventricular nucleus in direction of the SCN, and in domain 7 from arcuate nucleus and median eminence to the posterior exit of the pouch. (E) Ependymal flow on the left side of the ventricle and (F) ependymal flow on the right side of the ventricle (mirrored) show symmetry.

3.3.4 Conserved cilia orientation

The Emx1:Cre x Esco2$^{loxP/loxP}$ mouse line is characterized by an impairment of corticogenesis (Whelan et al., 2012). The lateral ventricle and the tube of the 3rd ventricle of these mice are not covered by brain tissue but are open towards the subarachnoid space. As consequence, CSF secreted from ChPx of the lateral ventricles is in direct contact with the subarachnoid membrane and, in contrast to the normal situation, not drained through the ventricular system into the subarachnoid space. Assuming that bulk-flow of CSF affects the orientation of cilia, one would expect marked differences of cilia orientation and resulting changes in the flow pattern of these mutant animals. However, the cilia orientation (Fig.3.3.4.2) and resulting flow pattern of these animals (Fig.3.3.4.1) are virtually indistinguishable between mutant and wildtype mice (n= 10). This result challenges the idea of CSF bulk-flow as orienting cue for cilia beat organization.

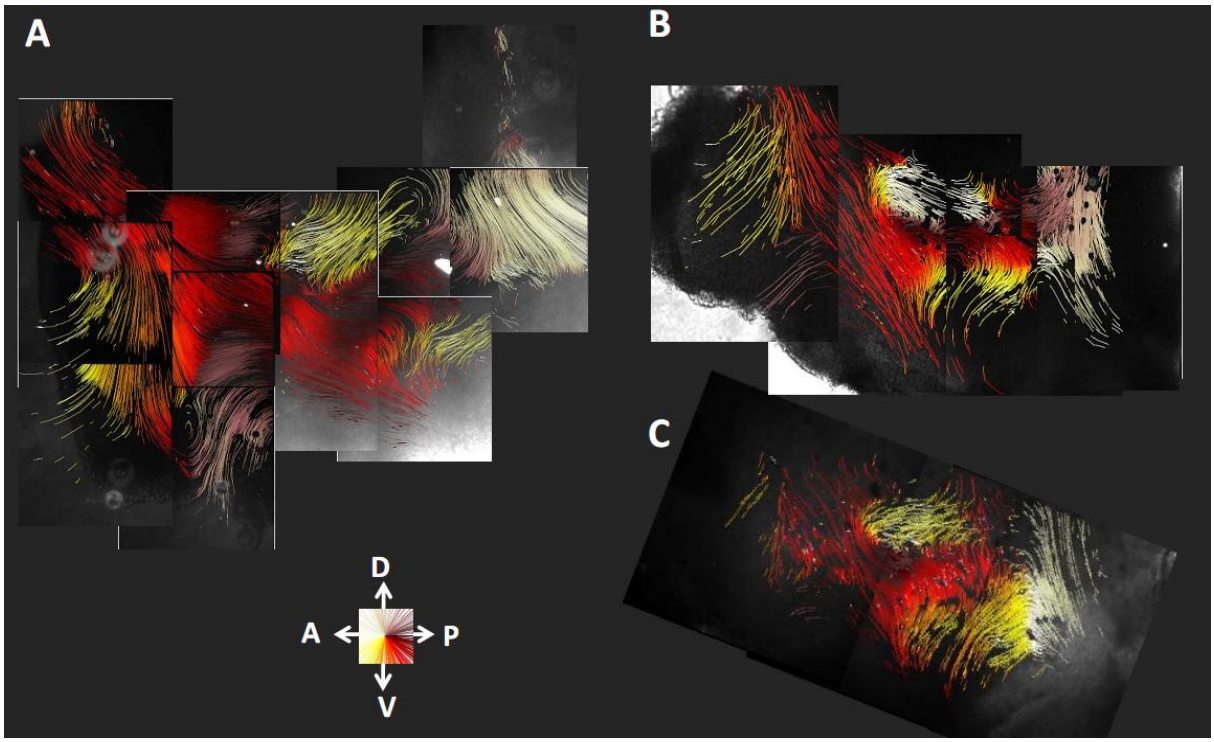

Fig.3.3.4.1 Flow pattern in mice with impaired CSF bulk-flow. (A) Above the pouch of Emx1:Cre x Esco2$^{loxP/loxP}$ mice, the cilia-induced flow pattern shows subdivision to the 7 domains as previously described for wildtype mice. (**B**) 129/SVJ mice show the same regional organization as C57Bl/6N mice. (**C**) At the age of two weeks, the characteristic pattern is already determined.

The high degree of cilia regulation suggests that the direction of flow is important for physiologic functions. We assessed the flow in a different mouse strain in order to see if the flow pattern is conserved. The flow in the pouch of the 3rd ventricle of 129/SVJ mice is organized to the same domains (Fig.3.3.4.1 B). During the development of mice, most ependymal cells are not ciliated before birth. During the first postnatal week, cilia formation increases and cilia are supposed to be fully developed two weeks after birth (Guirao et al., 2010; Spassky et al., 2005). The flow pattern in the pouch of 129/SVJ at this age is indistinguishable from the flow of adult mice (Fig.3.3.4.1 C). Obviously, the organization of cilia is already fully established at this stage.

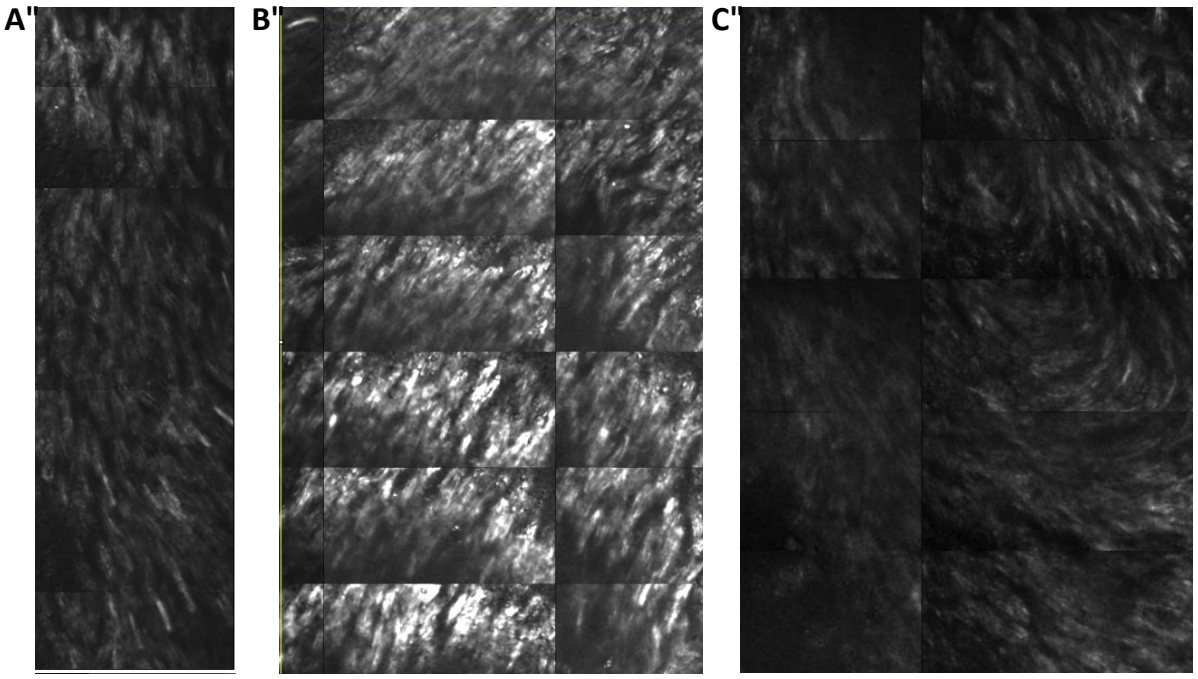

Fig.3.3.4.2 Cilia beat pattern evolves independently of bulk-flow. The cilia beating in the pouch of Emx1:Cre x Esco2$^{loxP/loxP}$ mice is organized to the same domains as in WT mice. (**A**) Cilia in domain are oriented along a dorso-ventral axis.. (**B**) Cilia beating in domain 3 is directed iin parallel to the flow in domain 3 and corresponding cilia in wildtype mice. .(**C)** At the transition from domain 6 to domain 7, cilia beating changes orientation to the inverted direction. There are no indications for less synchronization of cilia beating within one domain. Error bar is 300 µm.

It seems that cilia are oriented with high precision to generate a characteristic flow pattern that specifically connects certain regions of the ventricle. Consistency among different animals and strains implicates an integral function of these flows. The results obtained with the Emx1:Cre x Esco2$^{loxP/loxP}$ mouse line and young animals showed that changes in bulk-flow direction or size of the ventricle do not show any effect on the flow pattern.

3.4 Temporal regulation of transport along the ependymal lining

3.4.1 Ependymal cells harbor circadian clock oscillation

As previously done for the choroid plexus, we investigated in circadian clock gene oscillation in cells of the ependymal lining. The pouch was dissected from freshly isolated brains of Per2:Luc mice and transferred to tissue culture. Recordings of luciferase activity revealed a circadian rhythm of *Per2* expression over several days (Fig.3.4.1 A). Apparently, clock oscillation occurs autonomously but synchronized between cells under our culture conditions.

In order to exclude that synchronization between cells is caused by resetting effects during cultivation, the Per2-expression was assessed in freshly isolated brains. Therefore, mice were entrained to an LD-cycle of 12:12 hours and released into constant darkness. On the second day in darkness, brains were collected in triplicates at two different time points, sectioned to 14 µm of thickness, and in-situ hybridization was performed on every third section. At CT 10, high expression of Per2 was observed in ependymal cells whereas at CT 22, only sparse cells along the lining of the ventricle were stained (Fig.3.4.1 B).

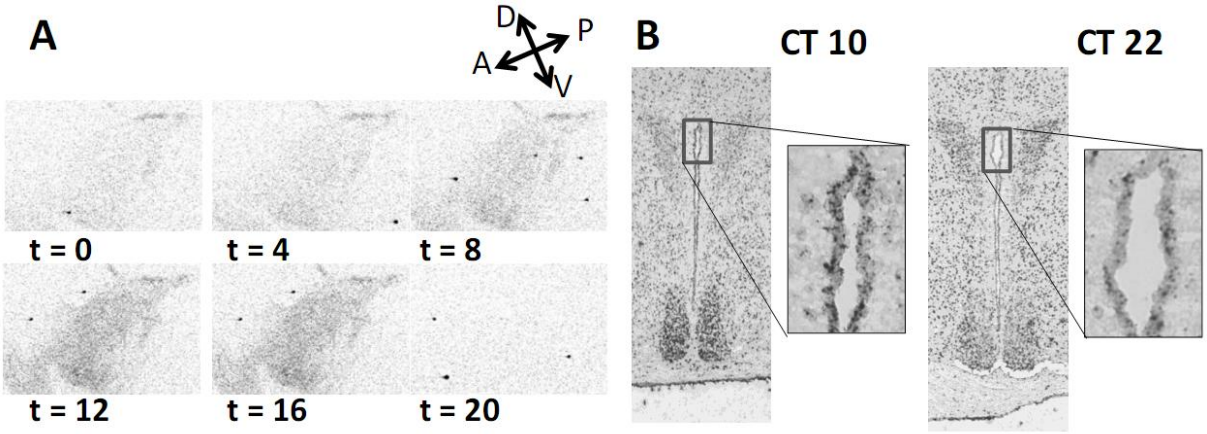

Fig.3.4.1 Circadian rhythm of PER2 in the third ventricle. (A) Per2:Luc activity of ventricle-explants shows a robust oscillation at the second day in culture. (**B**) ISH reveals that Per2 is highly expressed in ependymal cells of the third ventricle at CT10 whereas at the same position only few cells are stained twelve hours later.

3.4.2 Daily recurrent transport paths along the ventricular wall

The presence of a circadian clock in the ependyma raises the question whether cilia activity is subjected to circadian regulation. Open book preparations of the pouch where freshly prepared at a range of different times during the LD-cycle and flow patterns were analyzed.

At different times of the LD-cycle, the flow in domains 1 and 7 has consistent orientation. However, in the medial region of the ventricle, different flow patterns are observed that depend on the time of the day. Prepared at a time window spanning Zeitgeber time 7 (ZT7) to ZT13, flow patterns are consistent (n = 8) between the animals and resemble the ZT10 pattern described previously (Fig.3.4.2 A, B).

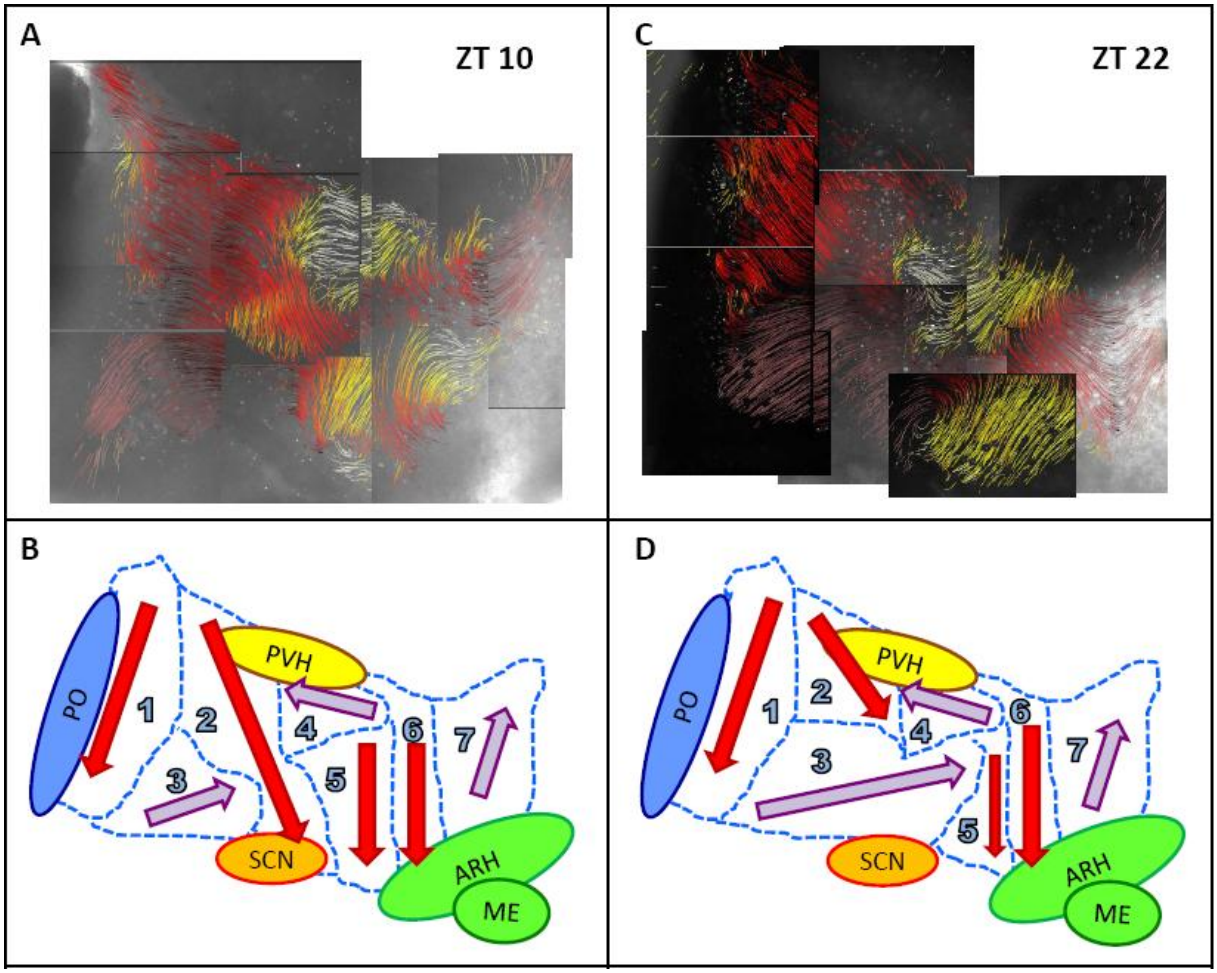

Fig.3.4.2 Changes in flow pattern at opposite times of the day. (**A**), (**B**) Particle tracking reveals that around ZT10 domains 2 and 5 separate domains 3 and 4 and flow is directed from the level of the paraventricular nucleus (PVH) to the level of the suprachiasmatic nucleus (SCN). (**C**), (**D**) At ZT22.5, domain 3 expands over domains 2 and 5 that are seen to shrink. Due to this expansion, domains 3 and 4 share common borders and flow arising above the SCN is directed towards the PVN. (**B**), (**D**) Schemes of the flow patterns include domains 1 and 7 that show consistent flow patterns between ZT10 and ZT22.5. No significant difference is observed in the flow in domain 1 that is adjacent to the preoptic area (PO) and in domain 7 that arises adjacent to the median eminence (ME) and arcuate nucleus (ARH).

At ZT22.5, a flow pattern (n = 12) was obtained that differs from the ZT10 pattern (Fig.3.4.2 C,D) but is consistent with the flow pattern at ZT23.5 (n = 4). Whereas at ZT10 particles above the PVN were pushed from domains 2 and 4 towards the SCN, expansion of domain 3 around ZT23 deflects this flow to posterior regions. Unlike at ZT10, domains 3 and 4 share a common border. As a result of this particles can transverse the 3/4 boundary in either direction which gives rise to a whirl that can readily be seen in the flow diagram (Fig.3.4.2 C). One way to exit the whirl is that particles end up in the posterior part of domains 5 or 6 and from there are directed towards the ventricle`s bottom.

Preparations taken during the interval between ZT0 and ZT6 did not show a consistent pattern. In some of the animals, the patterns of flow from the left and the right walls of the pouch were not symmetric, and flow patterns similar to those described for either the late day (ZT10) or the late night phase (ZT22.5) are detected during this time window (see Fig. 3.4.2).

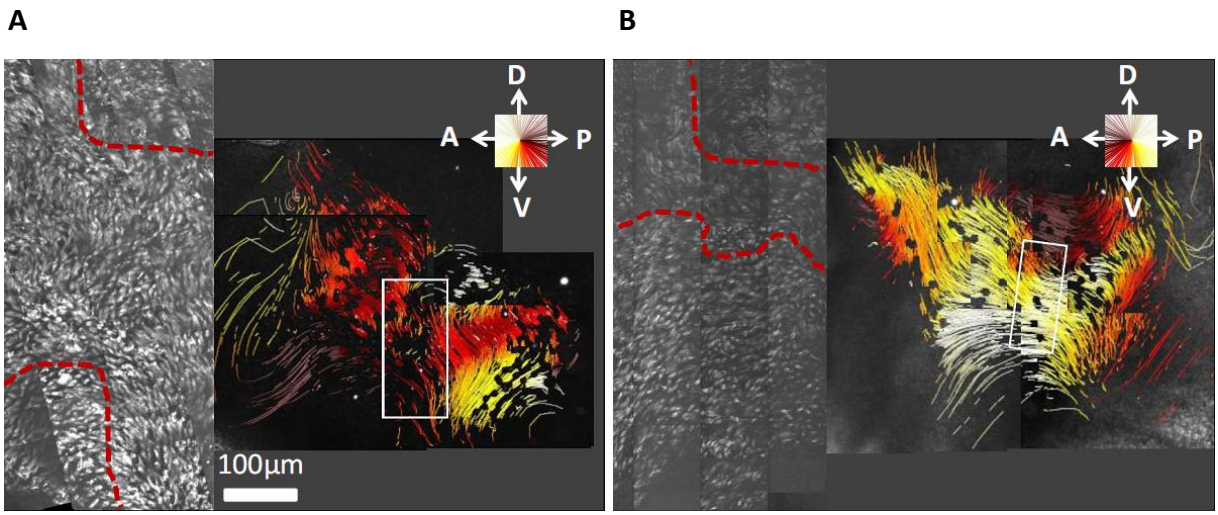

Fig.3.4.3 Different orientation of cilia underlies changes in flow pattern. (**A**) At ZT10, cilia in domain 2 are oriented along the dorso-ventral axis and reach to the bottom of the ventricle. The white marking indicates the region of the ventricle where cilia were recorded. (**B**) Cilia beat orientation has changed at ZT23.5 in a section with flow pattern of type ZT23. Domains 3 and 4 are no more separated by cilia from domain 2. The circle in domain 4 marks an extended swirl flow pattern.

The schematic characteristics of the flow pattern at ZT10 and ZT23 illustrate changes of the flow pattern. In keeping with the results discussed above (Section 3.3.3), the changes in flow at different times of the day are likely to result from changes in the orientation of the cilia

beat. To begin to address this question, we compared the cilia beat orientation underlying the different patterns (Fig.3.4.3). In 12 sections analyzed we were able to draw back the differences in the flow pattern to changes in the beat orientation.

The changes in flow and cilia beat direction between ZT10 and ZT23 are mostly concentrated to the middle of the third ventricle. Intriguingly, this zone is in proximity to the SCN, the site of the master clock of the mammalian brain. The main flow direction in domain 2 at ZT10 is towards the SCN while 13 hours later, the flow is away from the SCN. One can speculate that in the former case substances are targeted to the SCN, while at ZT23 they would be washed away.

3.4.3 Fluid pattern in circadian clock deficient mice

The circadian clock can impose a circadian rhythm on the expression of genes which are then referred to as clock-controlled genes (CCGs). In the absence of a circadian clock CCGs lack a circadian profile, but may, nonetheless, still be expressed e.g. at a constant level. Genetic ablation of *Bmal1*, a clock gene, causes a loss of the circadian rhythm of CCGs. Thus if the above-observed variation of flow direction is dependent on a circadian clock, one would predict that such changes should disappear in Bmal1-deficient mice. In other words, genetic deletion of the clock gene *Bmal1* would be expected to cause changes in the flow pattern if the cilia orientation was regulated by the circadian clock.

The flow pattern of Bmal1-mutant (*Bmal1*$^{-/-}$) mice (Fig.3.4.4) reveals flow directions similar to the wild type in anterior and posterior located regions. In the middle of the pouch, the flow pattern is different in *Bmal1*$^{-/-}$ mice when compared to wildtype mice. Flow of domain 3 expands into domain 4. In some animals the upwards directed flow eliminates domain 5 completely and reaches the roof of the pouch. In other animals, this upwards movement is less pronounced. In all cases, particles above the SCN are transported in direction of the roof of the pouch where the PVN resides but in none of the mutants a flow in direction to the SCN was observed. Even though an external rhythm was superimposed by keeping the animals under light-dark conditions expansion of domain 3 was not reversed to a pattern seen in wildtype mice at ZT10 (Fig.3.3.3). These findings point out that cues for orientation of cilia in the center region of the 3rd ventricle are regulated by *Bmal1*. This observation raises the possibility that the circadian clock regulates the flow in the third ventricle and this way the delivery and removal of solutes.

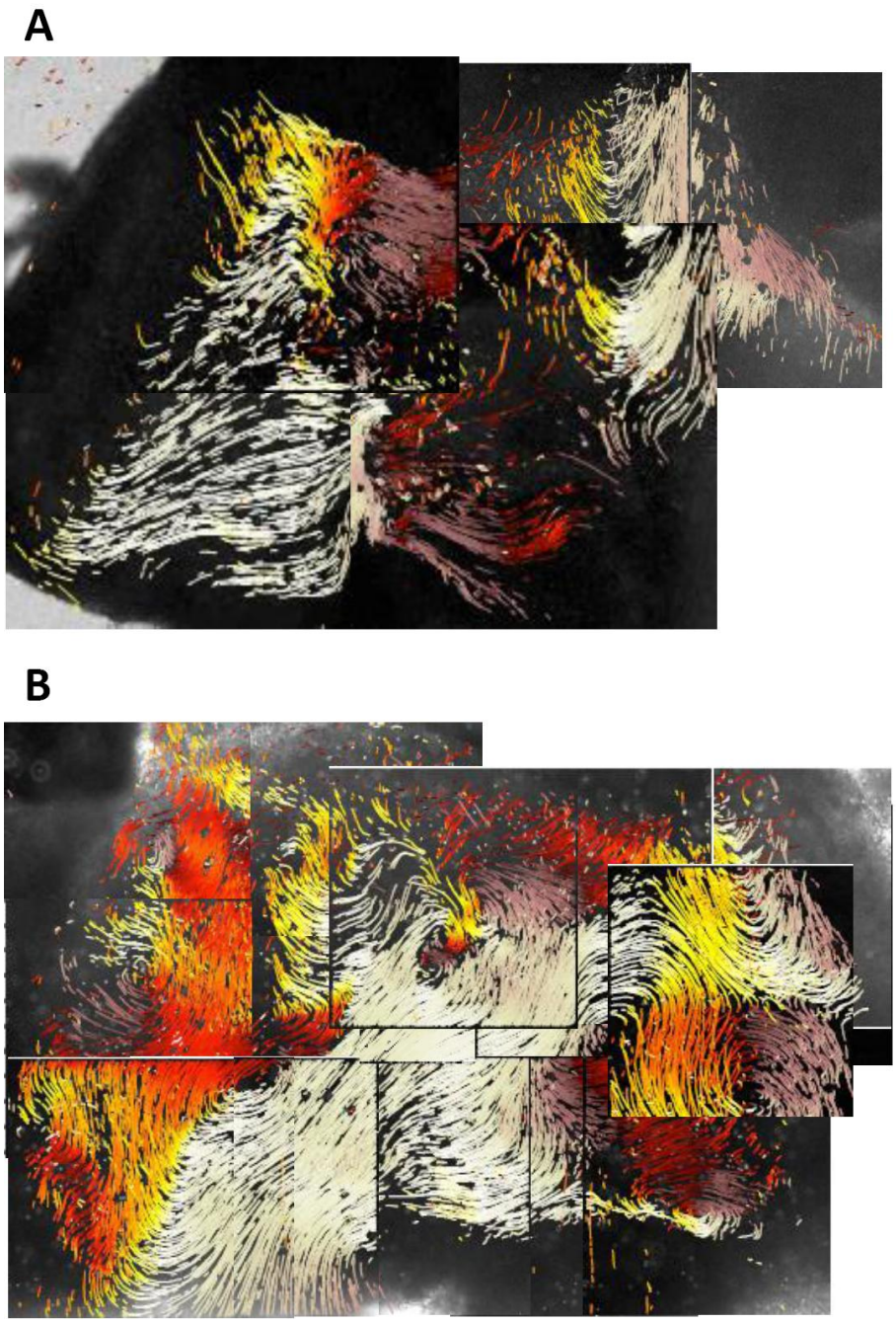

Fig.3.4.4 Flow pattern of Bmal1$^{-/-}$ mice. (**A,B**)The flow pattern shows ventral flow in domains 1 and 6 and flow towards the exit in domain 7. Domain 3 is contacting domain 4 or even domain 6. In several cases domain 3 abolishes any bottom-directed flow between domain 1 and 6.

4 Discussion

4.1 The circadian clock in ChPx4

Our data show that the ChPx4 has a tissue-autonomous circadian clock and ~7% of the ChPx4 transcriptome exhibits circadian oscillation. Such a percentage is reminiscent of what has been previously reported for other organs and tissues (Ramsey et al., 2006). We expect that the circadian functions of ChPx are fine tuned so as to optimally fulfill their role, e.g., in CSF-secretion and neuroprotection. A way to investigate this point is the generation of transgenic mice with a ChPx-specific genetic ablation of the circadian clock. So far, no tissue-specific genetic manipulation has been established in ChPx (Keep and Smith, 2011). However, a mouse line exists expressing an inducible Cre-recombinase (Cre^{ERT}) under the control of the FoxJ1-promoter that is active specifically in multiciliated cells (Ostrowski et al., 2003). At a certain embryonic stage, ChPx specifically and strongly expresses FoxJ1 (Jacquet et al., 2011) and induction of Cre-recombinase activity at this stage causes excision of LoxP-flanked genes from genomic DNA in the ChPx. Thus phenotypic analysis of FoxJ1-Cre^{ERT} animals crossed with the floxed Bmal1 mouse line is a promising tool to unravel the benefits of the ChPx clock and it`s integration into the hierarchically organized circadian regulation of processes in the brain.

Our data show that several enzymatic components of the detoxification machinery are upregulated at the end of the resting period whereas circadian transporters that are involved in extrusion of toxins show varying phases. This asynchrony indicates that uptake of specific toxins from CSF or release of metabolized conjugates to blood must not necessarily be coordinated with their enzymatic processing. However, clustering of circadian components of the enzymatic cascade including phase I and phase II enzymes might prevent the brain from damage by reactive intermediates and byproducts occurring during metabolic degradation.

Circadian regulation of detoxification has been well described from transcripts to physiologic functions of peripheral organs (Belanger et al., 1985; Claudel et al., 2007; Gachon and Firsov, 2011; Panda et al., 2002). Due to its location in the central nervous system, detoxification at the ChPx is an important aspect of neuroprotection (Johanson et al., 2011b). The ChPx should thus be considered when examining and interpreting chronopharmacological effects (Ohdo, 2007; Paschos et al., 2010) and the circadian regulation in assays addressing drug targeting of the brain (de Boer and Gaillard, 2007;

Dobson and Kell, 2008; Johanson et al., 2005; Spector, 2010). It seems that ChPx is the main entry site of neurotoxic factors (Bigotte and Olsson, 1989) and therefore drug treatment targeting tissues outside of the brain should be timed to their maximal extrusion from and minimal transport into the CSF. Moreover, circadian dynamics in the detoxifying capacities of the ChPx may regulate the concentration of drugs targeting the CSF in a circadian manner and thus should be considered when pharmacologically targeting the brain.

The presence and concentration of neurotoxins in CSF are also affected by the production rate of CSF. Circadian regulation of CSF production was first indicated by the observation of a circadian rhythm in CSF flow velocity in the ventricular aqueduct of humans (Nilsson et al., 1992) and circadian rhythmicity of carbonic anhydrase activity in ChPx (Quay, 1972). Our transcriptome study revealed that important components of the CSF production involve gene products that show a circadian expression pattern, but at the same time homologous gene products exist that are expressed at constant level. In other words, the circadian component of expression is superimposed to base level expression. This was to be expected since CSF-production must continuously refresh and replenish the ventricular volume. A risk of downregulation is accumulation of toxic metabolites and damage of neuronal tissue (Preston, 2001; Wostyn et al., 2013). Temporal regulation of detoxification might serve to scavenge toxins from CSF when the osmotic gradient across the ChPx is increased and as consequence crossing of toxins over the barrier is facilitated.

Although the wash-out function provided by the CSF bulk-flow is essential for CSF-homeostasis,, removal of hormones, cytokines, and neuropeptides can be of disadvantage. One example is secretion of Slit1 from ChPx, a chemokine that mediates the chemorepulsive effect on neuronal precursor cells along the rostral migratory stream (Sawamoto et al., 2006). *Slit1* transcript is oscillating in antiphase to circadian components involved in CSF-production. This temporal separation will support the generation of a Slit1-gradient from ChPx to the lateral horn of the ventricle i.e. in a direction opposite to bulk-flow direction. As most circadian components of endocrine functions show phase clustering with Slit1 we assume that at the end of the active phase the choroid plexus communicates via humoral pathways with periventricular regions. Obviously, the circadian clock in ChPx coordinates CSF-production and endocrine functions such that it allocates a time windows for humoral pathways and a time window for increased wash-out by CSF-flow.

4.2 The circadian clock in ependyma

Ependymal and ChPx epithelia both derive from radial glia cells (Spassky et al., 2005) and differentiate to ciliated epithelia that share anatomic and functional characteristics. Because a tissue-autonomous clock resides in ependymal cells of the third ventricle (Guilding et al., 2010) we assume that due to their close lineage relationship circadian regulation of common genes is preserved. It is interesting to note that the circadian ChPx4 transcriptome included components of cilia themselves as well as components of the BBSome and IFT that regulate the presence of cilia components by selective transport along the axoneme of the cilium and exchange with vesicular systems. The presence of such specific components is critical for cargo selectivity and direction of transport (Pedersen et al., 2008). Localization of the hormone oxytocin to ependymal cilia changes with the time of day and circadian restriction of light-Inducible localization of oxytocin to cilia (Devarajan et al., 2005) indicates circadian changes of cilia-specific transport systems. Our findings reveal that transcriptional regulation via the circadian clock underlies this circadian regulation of ciliary transport.

Such regulation and specifically the circadian rhythm found for *hydin*, *rootletin*, *Kif17*, and *Kif3* that regulate motility, orientation, and length of cilia raised the question of whether cilia activity is regulated by the clock. The flow pattern in the pouch of the third ventricle differs at two opposite times of the day and these changes were shown to be caused by different orientation of the cilia beat in these regions. The two types of flow patterns are temporally correlated to maximal transcriptional activation and inhibition of the E-box promoter elements of clock genes suggesting a direct regulation by the clock gene *Bmal1* and its antagonists such as *Per1 and Per2*. Indeed, in terms of flow pattern and cilia beat direction *Bmal1*-mutant mice strongly resemble wildtype animals sacrificed at the end of the active phase, a time of the day where E-box regulated genes show a through of expression.

It remains to be elucidated whether the length, motility, and frequency of the ciliary beat are also subjected to clock oscillation. As we found strong correlation between cilia orientation and flow pattern we would expect, if present, minor effects of changes in cilia length and motility on the direction of flow between the PVN and the SCN.

4.3 Organization of cilia in the ventricle

An advantaged of our cilia imaging method is the high degree of spatial and temporal resolution providing details about the organization of cilia beating and its effect on the flow above the cilia. Yamadori and colleagues pursued a similar objective when they performed electron microscopy of cilia orientation in the ventricle and visualized flow with erythrocytes. They concluded that beating pattern is consistent between individual mice and according to the approximate orientation of the cilia, different regions can be determined (Yamadori and Yagihashi, 1975). The regional differences were assumed to arise from flow of freshly secreted CSF and CSF that is conveyed by bulk-flow in the opposite direction until it drains from the ventricle via the two lateral openings into the subarachnoid space, namely, the foramina Luschka. Therefore, a close relationship between cilia orientation and anticipated bulk-flow direction was concluded. Application of our method revealed that, at least in the pouch of the third ventricle, cilia orientation is not oriented along bulk-flow direction but is organized to tightly regulated and highly complex patterns.

The movement of erythrocytes used in the above described studies has low sensitivity for fluid flow compared to our beads because the size is about 10-fold and the structure is platelet-like. This might explain the discrepancy to our results. Moreover, orientation of immobilized cilia is hard to recognize and not sensitive for small angle deviations that were found in *in-situ* recordings of beating cilia (Fig.1.2.2.5).

At least in the pouch of the third ventricle cilia orientation is independent of CSF bulk-flow direction. We found presence of domains with equally oriented cilia inducing a fast flow whereas differently oriented cilia in other regions retain solutes in fluid swirls. Especially in narrow regions of the ventricle the parallel oriented cilia are of advantage increasing flow speed and thus promoting the bulk-flow of CSF. As discussed above, the functions of CSF are broader than simply to flow through the ventricular system. Nutrients and hormones are transported to target regions of the brain. When they arrive at a fluid swirl, they are washed several times over the surface of the ventricle. This would increase the chance of binding to a cognate receptor. In domains where cilia are oriented in line with the bulk-flow, solutes are accelerated and the probability of interaction with the surface decreases. Orientation of cilia by the flow would be of disadvantage in other tissues as well. Mucus-flow in the lung directed by gravity would not remove particles from the lung. Our

findings that the flow pattern is preserved in two mouse strains, at different stages, and in the absence of directed bulk-flow strongly support the idea that the orienting cues are regionally determined.

In vitro studies revealed that external fluid flow over ependymal cells is an orienting cue for cilia during maturation (Guirao et al., 2010). The integration of this orienting cue requires cilia and Vangl2 and since both, cilia and Vangl2 are also required for polarization of basal bodies the authors concluded that CSF flow would be the orienting cue for ependymal cilia also in vivo. This hypothesis is not supported by the flow pattern of Emx:CrexEsco2$^{loxP/loxP}$ mice which is not distinguishable from flow patterns of wildtype mice. This result implicates that the orientation of cilia along the flow is an artifact of the in vitro system. *Vangl2* is a planar cell polarity (PCP) gene (Montcouquiol et al., 2003) and studies on planar cell polarity revealed conflicting results when cell culture or different tissues of the same organism were compared (Wallingford, 2010). Presumably, this is also the case for observations on rotational cilia orientation that depends on *Vangl2*. Two important features of ependymal cells are absent in vitro: the adherence between cells and to underlying tissue and the presence of non-cell-autonomous signals deriving from other cell types in the brain. Nevertheless, assuming that coupling between hydrodynamic forces and cilia orientation occurs in vivo it would have a minor effect compared to other cues. As components of the PCP pathway seem to be crucial for the rotational orientation of cilia (Guirao et al., 2010; Hirota et al., 2010; Tissir et al., 2010), candidates for such cues are signals that activate this pathway (Kishimoto and Sawamoto, 2012). Considering that cilia themselves (Guirao et al., 2010; Vladar et al., 2012) as well as localization of Vangl2 to the cilium (Hirota et al., 2010) mediate the integration of such signals, the search should be focused on molecules that directly bind to the cilium. In vitro, these other cues are apparently absent from mature ependymal cells because reorientation of cilia beating was not observed after maturation of cultured cells (Guirao et al., 2010).

4.4 Dynamics in the orientation of cilia

However, there seems to be no evidence from literature that cilia change their orientation after differentiation. Our observation that spirals and swirls form at certain times of the day strongly implicate changes in the PCP as mechanism of the regional changes since affected cilia patterns (Fig.3.2.1) strongly resemble the patterns in fur hair orientation of mice with

defective Wnt-mediated activation of the PCP pathway (Fig.1.2.2.5). A well accepted hypothesis is that once established, polarization via PCP is locked (Marshall and Kintner, 2008; Wallingford, 2010; Wallingford and Mitchell, 2011) and for patterning of certain tissues such as lung epithelia, cochlea, and skin hair this locking might be reasonable. If present in ependyma, such locking mechanism might be restricted to certain time windows and thus reflect a gating mechanism. Conflicting results about involvement of PCP in rotational and translational polarity in ependyma (Guirao et al., 2010; Mirzadeh et al., 2010; Vladar et al., 2012) might originate from regulation via the circadian clock.

Circadian dynamics in cilia are further indicated by the observation that forskolin treatment of ciliated cells increases the amount of soluble tubulin because it depolymerizes cell body microtubules and thus induces elongation of ciliary microtubules (Sharma et al., 2011). Another effect of forskolin treatment is resetting of the clock (Balsalobre et al., 2000). Of note, cytoskeletal assembly is subjected to the circadian clock (Gerber et al., 2013). Furthermore, serum-derived substances play a dual role: Treatment of cells with serum induces resetting of the circadian clock (Balsalobre et al., 1998) whereas serum-starvation induces the assembly of cilia in fibroblasts within a time window of less than 100 min (Westlake et al., 2011). Altogether, there is evidence for a coregulation of cilia formation and the circadian clock.

Finally, it remains to be shown whether the change in cilia orientation is caused by extracellular signals or by an intrinsic factor. Since rootletin is circadian regulated, it might be that the changes we observed derive from uncoupling of cilia from the cell body cytoskeleton but PCP would be unaffected. Immunohistochemistry will be helpful to solve this question. Moreover, application of our new method on PCP-mutant animals will reveal by what mechanism components of the PCP pathway affect the orientation of mature cilia in ependyma.

As pouch preparations can be kept as explants for several days, observation of cilia orientation might reveal whether reorientation is mediated by tissue-autonomous processes or depends on external cues.

In conclusion, the ciliary dynamics of continuous assembly and disassembly, the regulation of these dynamics by reaction of extracellular signals, and the circadian oscillation of ciliary genes and components establishing polarity are the starting point to unravel how the circadian clock regulates cilia orientation.

4.5 Targets for transport along the ventricular lining

The precise patterning of flow along the multiciliated ependyma could mean that endocrine signaling via the CSF is regulated by cilia orientation. Ciliary pathways arise from the organization to domains and might serve to mediate discrete communication between neurons and thus form a direct connection between the nuclei of the hypothalamus comparable to synaptic projections. However, synaptic signaling is physically restricted to neuronal projections whereas the ciliary pathways bear the potential to accumulate multiple factors from diverse sites on the way towards the target site. Moreover, the ciliary pathways form connections between different nuclei at a certain time of the day and by "flipping" the orientation of the beating between other nuclei at a different time of the day.

Hormonal signals from the periphery as well as synaptic spillover or active release of neuroendocrine substances have been convincingly shown to affect synaptic activity and therefore mammalian behavior. The finding of conserved organization of cilia beating might implicate that distribution of these solutes according to the flow direction in the individual domains affects brain physiology and behavior by precisely regulating delivery of these substances.

Since synchronization of cilia beat direction between neighboring cells increases the speed of the induced flow, we expect few interference between solute transport along the ventricular wall and CSF-bulk-flow. Therefore, transport along the ependyma provides routes for transmission of compounds to specific target sites of the brain. As result of directed trafficking, lower amounts of secretion are required to achieve a certain concentration of a signal in a distant target region.

Despite some approaches to trace the path of molecules it is still unclear how molecules find their way through the CSF towards their targets sites. A pioneering finding was the discovery that migration of neuronal precursor cells along the rostral migratory stream follows a gradient of chemokines and strongly depends on cilia beating (Sawamoto et al., 2006). The causal link between cilia beating and cell migration is induction of a directed fluid stream in the lateral ventricle transporting chemokines towards the rostral migratory stream that was observed after injection of ink. As neural progenitors also reside in the third

ventricle (Robins et al., 2013) the compartmentation of the flow to microdomains might serve to impose a similar regulation.

Signal transmission in the pouch is relevant in particular for chronobiology because the master clock SCN resides at the bottom of the third ventricle and regulates brain and non-neuronal peripheral oscillators via neuronal and humoral pathways. The observation that the clock-regulated change in flow direction is most pronounced in proximity of the SCN suggests that there may be consequences on humoral signaling of the SCN even though the exact path of these signals remains to be determined. Following disruption of the SCN, rhythm in locomotor activity can be restored by SCN transplantation to a certain degree but in dependence of the exact location of the graft (LeSauter et al., 1997). Grafts attached posterior to the SCN restored the circadian rhythm more efficiently when they were in proximity to the original SCN. Interestingly, for grafts located anterior to the SCN, the distance to the SCN did not affect the efficiency of restoration. Indeed the flow in the anterior region, namely, domain 3, transports solutes towards the original position of the SCN. Dependent on the distance to the SCN, secretions from posteriorly attached grafts would be transported by domain 5 or 6. Around ZT10, the flow in domain 3 is directed ventrally and so is the flow in domains 5 and 6. Around ZT22 the flow in domain 3 is directed from the SCN towards domain 4 unlike the flow in domain 5 and 6. We propose the changes in the flow as time-dependent regulatory mechanism for SCN-derived humoral factors.

Tracing the paths of endogenous factors i.e. by immunohistochemical staining on brain sections would reveal if the signals are transported along the ventricular wall or via interstitial fluid (ISF). If shuttling through the ventricle was the main path of transmission, the flow pattern would have a great impact on delivery to the target site. Since the ependymal cells allow unrestricted exchange between CSF and ISF, humoral communication via paracellular pathways would also be affected by CSF-flow. In future experiments, mice carrying ependyma-specific deletion of the clock gene *Bmal1* will be generated by using the FoxJ1:ERTCre line crossed with the Bmal1$^{fl/fl}$ line. During the first three weeks after birth, *FoxJ1* expression expands from ChPx to the ependyma. Temporal activation of the recombinase during this window will result in an ependymal-specific disruption of *Bmal1.* It is likely, that cilia beating orientation is determined by an ependymal-derived factor or at least the response to such a factor is gated by ependyma-specific genes that are regulated by *Bmal1*. If this is true, the cilia orientation will show the pattern of FoxJ1:ERTCre x Bmal1$^{fl/fl}$

mutant mice and the mouse line will serve as genetic tool to assess physiologic and behavioral consequences of cilia orientation and whether they affect clock synchronization by delivery of humoral signals.

References

Abe, M., Herzog, E.D., Yamazaki, S., Straume, M., Tei, H., Sakaki, Y., Menaker, M., and Block, G.D. (2002). Circadian rhythms in isolated brain regions. J Neurosci *22*, 350-356.

Afzelius, B.A. (2004). Cilia-related diseases. J Pathol *204*, 470-477.

Agnati, L.F., Guidolin, D., Guescini, M., Genedani, S., and Fuxe, K. (2010). Understanding wiring and volume transmission. Brain Res Rev *64*, 137-159.

Aguilar-Roblero, R., Garcia-Hernandez, F., Aguilar, R., Arankowsky-Sandoval, G., and Drucker-Colin, R. (1986). Suprachiasmatic nucleus transplants function as an endogenous oscillator only in constant darkness. Neurosci Lett *69*, 47-52.

Alebouyeh, M., Takeda, M., Onozato, M.L., Tojo, A., Noshiro, R., Hasannejad, H., Inatomi, J., Narikawa, S., Huang, X.L., Khamdang, S.*, et al.* (2003). Expression of human organic anion transporters in the choroid plexus and their interactions with neurotransmitter metabolites. J Pharmacol Sci *93*, 430-436.

Avasthi, P., and Marshall, W.F. (2012). Stages of ciliogenesis and regulation of ciliary length. Differentiation *83*, S30-42.

Balsalobre, A., Damiola, F., and Schibler, U. (1998). A serum shock induces circadian gene expression in mammalian tissue culture cells. Cell *93*, 929-937.

Balsalobre, A., Marcacci, L., and Schibler, U. (2000). Multiple signaling pathways elicit circadian gene expression in cultured Rat-1 fibroblasts. Curr Biol *10*, 1291-1294.

Banizs, B., Pike, M.M., Millican, C.L., Ferguson, W.B., Komlosi, P., Sheetz, J., Bell, P.D., Schwiebert, E.M., and Yoder, B.K. (2005). Dysfunctional cilia lead to altered ependyma and choroid plexus function, and result in the formation of hydrocephalus. Development *132*, 5329-5339.

Belanger, P.M., Lalande, M., Labrecque, G., and Dore, F.M. (1985). Diurnal variations in the transferases and hydrolases involved in glucuronide and sulfate conjugation of rat liver. Drug Metab Dispos *13*, 386-389.

Berens, P. (2009). CircStat: A MATLAB Toolbox for Circular Statistics. Journal of Statistical Software *31, issue 10.*

Bennouna-Greene, V., Kremer, S., Stoetzel, C., Christmann, D., Schuster, C., Durand, M., Verloes, A., Sigaudy, S., Holder-Espinasse, M., Godet, J.*, et al.* (2011). Hippocampal dysgenesis and variable

neuropsychiatric phenotypes in patients with Bardet-Biedl syndrome underline complex CNS impact of primary cilia. Clin Genet *80*, 523-531.

Berbari, N.F., O'Connor, A.K., Haycraft, C.J., and Yoder, B.K. (2009). The primary cilium as a complex signaling center. Curr Biol *19*, R526-535.

Bigotte, L., and Olsson, Y. (1989). Distribution and toxic effects of intravenously injected epirubicin on the central nervous system of the mouse. Brain *112 (Pt 2)*, 457-469.

Bobrzynska, K.J., and Mrosovsky, N. (1998). Phase shifting by novelty-induced running: activity dose-response curves at different circadian times. J Comp Physiol A *182*, 251-258.

Bolborea, M., and Dale, N. (2013). Hypothalamic tanycytes: potential roles in the control of feeding and energy balance. Trends Neurosci *36*, 91-100.

Breunig, J.J., Arellano, J.I., and Rakic, P. (2010). Cilia in the brain: going with the flow. Nat Neurosci *13*, 654-655.

Brightman, M.W., and Reese, T.S. (1969). Junctions between intimately apposed cell membranes in the vertebrate brain. J Cell Biol *40*, 648-677.

Brown, T.M., and Piggins, H.D. (2007). Electrophysiology of the suprachiasmatic circadian clock. Prog Neurobiol *82*, 229-255.

Buhr, E.D., and Takahashi, J.S. (2013). Molecular components of the Mammalian circadian clock. Handb Exp Pharmacol, 3-27.

Bunger, M.K., Wilsbacher, L.D., Moran, S.M., Clendenin, C., Radcliffe, L.A., Hogenesch, J.B., Simon, M.C., Takahashi, J.S., and Bradfield, C.A. (2000). Mop3 is an essential component of the master circadian pacemaker in mammals. Cell *103*, 1009-1017.

Cardone, L., Hirayama, J., Giordano, F., Tamaru, T., Palvimo, J.J., and Sassone-Corsi, P. (2005). Circadian clock control by SUMOylation of BMAL1. Science *309*, 1390-1394.

Cartwright, J.H., Piro, N., Piro, O., and Tuval, I. (2008). Fluid dynamics of establishing left-right patterning in development. Birth Defects Res C Embryo Today *84*, 95-101.

Chodobski, A., and Szmydynger-Chodobska, J. (2001). Choroid plexus: target for polypeptides and site of their synthesis. Microsc Res Tech *52*, 65-82.

Claudel, T., Cretenet, G., Saumet, A., and Gachon, F. (2007). Crosstalk between xenobiotics metabolism and circadian clock. FEBS Lett *581*, 3626-3633.

Coleman, G.J., and Francis, A.J. (1991). Food deprivation and reinstatement phase shifts rat activity rhythms in constant light but not constant dark. Physiol Behav *50*, 167-171.

Cserr, H.F., and Bundgaard, M. (1984). Blood-brain interfaces in vertebrates: a comparative approach. Am J Physiol *246*, R277-288.

Cserr, H.F., Depasquale, M., Patlak, C.S., and Pullen, R.G. (1986). Convection of cerebral interstitial fluid and its role in brain volume regulation. Ann N Y Acad Sci *481*, 123-134.

Damiola, F., Le Minh, N., Preitner, N., Kornmann, B., Fleury-Olela, F., and Schibler, U. (2000). Restricted feeding uncouples circadian oscillators in peripheral tissues from the central pacemaker in the suprachiasmatic nucleus. Genes Dev *14*, 2950-2961.

Damkier, H.H., Brown, P.D., and Praetorius, J. (2010). Epithelial pathways in choroid plexus electrolyte transport. Physiology (Bethesda) *25*, 239-249.

Dardente, H., and Cermakian, N. (2007). Molecular circadian rhythms in central and peripheral clocks in mammals. Chronobiol Int *24*, 195-213.

Davson, H., Hollingsworth, G., and Segal, M.B. (1970). The mechanism of drainage of the cerebrospinal fluid. Brain *93*, 665-678.

de Boer, A.G., and Gaillard, P.J. (2007). Drug targeting to the brain. Annu Rev Pharmacol Toxicol *47*, 323-355.

de Lange, E.C. (2004). Potential role of ABC transporters as a detoxification system at the blood-CSF barrier. Adv Drug Deliv Rev *56*, 1793-1809.

DeCoursey, P.J., and Buggy, J. (1989). Circadian rhythmicity after neural transplant to hamster third ventricle: specificity of suprachiasmatic nuclei. Brain Res *500*, 263-275.

Deery, M.J., Maywood, E.S., Chesham, J.E., Sladek, M., Karp, N.A., Green, E.W., Charles, P.D., Reddy, A.B., Kyriacou, C.P., Lilley, K.S*., et al.* (2009). Proteomic analysis reveals the role of synaptic vesicle cycling in sustaining the suprachiasmatic circadian clock. Curr Biol *19*, 2031-2036.

Del Bigio, M.R. (2010). Ependymal cells: biology and pathology. Acta Neuropathol *119*, 55-73.

Devarajan, K., Marchant, E.G., and Rusak, B. (2005). Circadian and light regulation of oxytocin and parvalbumin protein levels in the ciliated ependymal layer of the third ventricle in the C57 mouse. Neuroscience *134*, 539-547.

Dobson, P.D., and Kell, D.B. (2008). Carrier-mediated cellular uptake of pharmaceutical drugs: an exception or the rule? Nat Rev Drug Discov *7*, 205-220.

Drummond, I.A. (2012). Cilia functions in development. Curr Opin Cell Biol *24*, 24-30.

Eckel-Mahan, K.L., Patel, V.R., Mohney, R.P., Vignola, K.S., Baldi, P., and Sassone-Corsi, P. (2012). Coordination of the transcriptome and metabolome by the circadian clock. Proc Natl Acad Sci U S A *109*, 5541-5546.

Edgar, D.M., and Dement, W.C. (1991). Regularly scheduled voluntary exercise synchronizes the mouse circadian clock. Am J Physiol *261*, R928-933.

Ehrlich P. (1885). Das Sauerstoffbedürfnis des Organismus. In Eine farbenanalytische Studie, Hirschwald, Berlin.

Emerich, D.F., Skinner, S.J., Borlongan, C.V., Vasconcellos, A.V., and Thanos, C.G. (2005). The choroid plexus in the rise, fall and repair of the brain. Bioessays *27*, 262-274.

Espana, R.A., Baldo, B.A., Kelley, A.E., and Berridge, C.W. (2001). Wake-promoting and sleep-suppressing actions of hypocretin (orexin): basal forebrain sites of action. Neuroscience *106*, 699-715.

Frayling, C., Britton, R., and Dale, N. (2011). ATP-mediated glucosensing by hypothalamic tanycytes. J Physiol *589*, 2275-2286.

Freeman, G.M., Jr., and Herzog, E.D. (2011). Neuropeptides go the distance for circadian synchrony. Proc Natl Acad Sci U S A *108*, 13883-13884.

Fuxe, K., Dahlstrom, A.B., Jonsson, G., Marcellino, D., Guescini, M., Dam, M., Manger, P., and Agnati, L. (2010). The discovery of central monoamine neurons gave volume transmission to the wired brain. Prog Neurobiol *90*, 82-100.

Gachon, F., and Firsov, D. (2011). The role of circadian timing system on drug metabolism and detoxification. Expert Opin Drug Metab Toxicol *7*, 147-158.

Gachon, F., Fonjallaz, P., Damiola, F., Gos, P., Kodama, T., Zakany, J., Duboule, D., Petit, B., Tafti, M., and Schibler, U. (2004). The loss of circadian PAR bZip transcription factors results in epilepsy. Genes Dev *18*, 1397-1412.

Gachon, F., Olela, F.F., Schaad, O., Descombes, P., and Schibler, U. (2006). The circadian PAR-domain basic leucine zipper transcription factors DBP, TEF, and HLF modulate basal and inducible xenobiotic detoxification. Cell Metab *4*, 25-36.

Gerber, A., Esnault, C., Aubert, G., Treisman, R., Pralong, F., and Schibler, U. (2013). Blood-borne circadian signal stimulates daily oscillations in actin dynamics and SRF activity. Cell *152*, 492-503.

Ghersi-Egea, J.F., Strazielle, N., Murat, A., Jouvet, A., Buenerd, A., and Belin, M.F. (2006). Brain protection at the blood-cerebrospinal fluid interface involves a glutathione-dependent metabolic barrier mechanism. J Cereb Blood Flow Metab *26*, 1165-1175.

Gilliam, J.C., Chang, J.T., Sandoval, I.M., Zhang, Y., Li, T., Pittler, S.J., Chiu, W., and Wensel, T.G. (2012). Three-dimensional architecture of the rod sensory cilium and its disruption in retinal neurodegeneration. Cell *151*, 1029-1041.

Glaser, F.T., and Stanewsky, R. (2005). Temperature synchronization of the Drosophila circadian clock. Curr Biol *15*, 1352-1363.

Gordon, M.D., and Nusse, R. (2006). Wnt signaling: multiple pathways, multiple receptors, and multiple transcription factors. J Biol Chem *281*, 22429-22433.

Gray, J. (1930). Photographic and stroboscopic analysis of ciliary movement. In The mechanism of ciliary movement.

Grzybowski, D.M., Holman, D.W., Katz, S.E., and Lubow, M. (2006). In vitro model of cerebrospinal fluid outflow through human arachnoid granulations. Invest Ophthalmol Vis Sci *47*, 3664-3672.

Guilding, C., Hughes, A.T., Piggins, H.D. (2010). Circadian oscillators in the epithalamus. Neuroscience *169(4)* 1630-9.

Guilding, C., and Piggins, H.D. (2007). Challenging the omnipotence of the suprachiasmatic timekeeper: are circadian oscillators present throughout the mammalian brain? Eur J Neurosci *25*, 3195-3216.

Guirao, B., Meunier, A., Mortaud, S., Aguilar, A., Corsi, J.M., Strehl, L., Hirota, Y., Desoeuvre, A., Boutin, C., Han, Y.G*., et al.* (2010). Coupling between hydrodynamic forces and planar cell polarity orients mammalian motile cilia. Nat Cell Biol *12*, 341-350.

Guo, H., Brewer, J.M., Champhekar, A., Harris, R.B., and Bittman, E.L. (2005). Differential control of peripheral circadian rhythms by suprachiasmatic-dependent neural signals. Proc Natl Acad Sci U S A *102*, 3111-3116.

Guo H., Brewer, J.M., Lehman, M.N., Bittman, E.L. (2006). Suprachiasmatic regulation of circadian rhythms of gene expression in hamster peripheral organs: effects of transplanting the pacemaker. J Neuroscience, *26(27)*, 6406-12.

Hardin, P.E., and Panda, S. (2013). Circadian timekeeping and output mechanisms in animals. Curr Opin Neurobiol *23*, 724-731.

Harmar, A.J., Marston, H.M., Shen, S., Spratt, C., West, K.M., Sheward, W.J., Morrison, C.F., Dorin, J.R., Piggins, H.D., Reubi, J.C*., et al.* (2002). The VPAC(2) receptor is essential for circadian function in the mouse suprachiasmatic nuclei. Cell *109*, 497-508.

Hawkins, B.T., and Davis, T.P. (2005). The blood-brain barrier/neurovascular unit in health and disease. Pharmacol Rev *57*, 173-185.

Hediger, M.A., Romero, M.F., Peng, J.B., Rolfs, A., Takanaga, H., and Bruford, E.A. (2004). The ABCs of solute carriers: physiological, pathological and therapeutic implications of human membrane transport proteinsIntroduction. Pflugers Arch *447*, 465-468.

Hirayama, J., and Sassone-Corsi, P. (2005). Structural and functional features of transcription factors controlling the circadian clock. Curr Opin Genet Dev *15*, 548-556.

Hirota, T., and Fukada, Y. (2004). Resetting mechanism of central and peripheral circadian clocks in mammals. Zoolog Sci *21*, 359-368.

Hirota, Y., Meunier, A., Huang, S., Shimozawa, T., Yamada, O., Kida, Y.S., Inoue, M., Ito, T., Kato, H., Sakaguchi, M*., et al.* (2010). Planar polarity of multiciliated ependymal cells involves the anterior migration of basal bodies regulated by non-muscle myosin II. Development *137*, 3037-3046.

Hrabetova, S., and Nicholson, C. (2007). Biophysical Properties of Brain Extracellular Space Explored with Ion-Selective Microelectrodes, Integrative Optical Imaging and Related Techniques.

Huang, H.C., and Klein, P.S. (2004). The Frizzled family: receptors for multiple signal transduction pathways. Genome Biol *5*, 234.

Hughes, A.T., Guilding, C., and Piggins, H.D. (2011). Neuropeptide signaling differentially affects phase maintenance and rhythm generation in SCN and extra-SCN circadian oscillators. PLoS One *6*, e18926.

Hughes, A.T., and Piggins, H.D. (2012). Feedback actions of locomotor activity to the circadian clock. Prog Brain Res *199*, 305-336.

Husse, J., Zhou, X., Oster, H., Eichele, G. (2011a). Synaptotagmin10-Cre, a driver to disrupt clock genes in the SCN. J Biol Rhythms *26(5)* 379-89.

Husse, J. (2011b), Genetic disruption of the master pacemaker in the superchiasmatic nucleus sheds light on the hierarchical organization of the mammalian circadian timing system. http://hdl.handle.net/11858/00-1735-0000-000D-F1DF-F.

Ibanez-Tallon, I., Heintz, N., and Omran, H. (2003). To beat or not to beat: roles of cilia in development and disease. Hum Mol Genet *12 Spec No 1*, R27-35.

Ibanez-Tallon, I., Pagenstecher, A., Fliegauf, M., Olbrich, H., Kispert, A., Ketelsen, U.P., North, A., Heintz, N., and Omran, H. (2004). Dysfunction of axonemal dynein heavy chain Mdnah5 inhibits ependymal flow and reveals a novel mechanism for hydrocephalus formation. Hum Mol Genet *13*, 2133-2141.

Iliff, J.J., Lee, H., Yu, M., Feng, T., Logan, J., Nedergaard, M., and Benveniste, H. (2013). Brain-wide pathway for waste clearance captured by contrast-enhanced MRI. J Clin Invest *123*, 1299-1309.

Iliff, J.J., Wang, M., Liao, Y., Plogg, B.A., Peng, W., Gundersen, G.A., Benveniste, H., Vates, G.E., Deane, R., Goldman, S.A*., et al.* (2012). A paravascular pathway facilitates CSF flow through the brain parenchyma and the clearance of interstitial solutes, including amyloid beta. Sci Transl Med *4*, 147ra111.

Imhoff, O., Marion, V., Stoetzel, C., Durand, M., Holder, M., Sigaudy, S., Sarda, P., Hamel, C.P., Brandt, C., Dollfus, H*., et al.* (2011). Bardet-Biedl syndrome: a study of the renal and cardiovascular phenotypes in a French cohort. Clin J Am Soc Nephrol *6*, 22-29.

Inouye, S.T., and Kawamura, H. (1979). Persistence of circadian rhythmicity in a mammalian hypothalamic "island" containing the suprachiasmatic nucleus. Proc Natl Acad Sci U S A *76*, 5962-5966.

Jacquet, B.V., Muthusamy, N., Sommerville, L.J., Xiao, G., Liang, H., Zhang, Y., Holtzman, M.J., and Ghashghaei, H.T. (2011). Specification of a Foxj1-dependent lineage in the forebrain is required for embryonic-to-postnatal transition of neurogenesis in the olfactory bulb. J Neurosci *31*, 9368-9382.

Jansen, K., Van der Zee, E.A., and Gerkema, M.P. (1999). Organotypic suprachiasmatic nuclei cultures of adult voles reflect locomotor behavior: differences in number of vasopressin cells. Chronobiol Int *16*, 745-750.

Jansen, K., Van der Zee, E.A., and Gerkema, M.P. (2000). Being circadian or not: vasopressin release in cultured SCN mirrors behavior in adult voles. Neuroreport *11*, 3555-3558.

Jin, H., and Nachury, M.V. (2009). The BBSome. Curr Biol *19*, R472-473.

Jin, H., White, S.R., Shida, T., Schulz, S., Aguiar, M., Gygi, S.P., Bazan, J.F., and Nachury, M.V. (2010). The conserved Bardet-Biedl syndrome proteins assemble a coat that traffics membrane proteins to cilia. Cell *141*, 1208-1219.

Johanson, C., Stopa, E., Baird, A., and Sharma, H. (2011a). Traumatic brain injury and recovery mechanisms: peptide modulation of periventricular neurogenic regions by the choroid plexus-CSF nexus. J Neural Transm *118*, 115-133.

Johanson, C., Stopa, E., McMillan, P., Roth, D., Funk, J., and Krinke, G. (2011b). The distributional nexus of choroid plexus to cerebrospinal fluid, ependyma and brain: toxicologic/pathologic phenomena, periventricular destabilization, and lesion spread. Toxicol Pathol *39*, 186-212.

Johanson, C.E., Duncan, J.A., 3rd, Klinge, P.M., Brinker, T., Stopa, E.G., and Silverberg, G.D. (2008). Multiplicity of cerebrospinal fluid functions: New challenges in health and disease. Cerebrospinal Fluid Res *5*, 10.

Johanson, C.E., Duncan, J.A., Stopa, E.G., and Baird, A. (2005). Enhanced prospects for drug delivery and brain targeting by the choroid plexus-CSF route. Pharm Res *22*, 1011-1037.

Johnston, M., Zakharov, A., Papaiconomou, C., Salmasi, G., and Armstrong, D. (2004). Evidence of connections between cerebrospinal fluid and nasal lymphatic vessels in humans, non-human primates and other mammalian species. Cerebrospinal Fluid Res *1*, 2.

Keep, R.F., and Smith, D.E. (2011). Choroid plexus transport: gene deletion studies. Fluids Barriers CNS *8*, 26.

Kirchhausen, T. (2000). Three ways to make a vesicle. Nat Rev Mol Cell Biol *1*, 187-198.

Kishimoto, N., and Sawamoto, K. (2012). Planar polarity of ependymal cilia. Differentiation *83*, S86-90.

Knopf, P.M., Cserr, H.F., Nolan, S.C., Wu, T.Y., and Harling-Berg, C.J. (1995). Physiology and immunology of lymphatic drainage of interstitial and cerebrospinal fluid from the brain. Neuropathol Appl Neurobiol *21*, 175-180.

Koepsell, H., and Endou, H. (2004). The SLC22 drug transporter family. Pflugers Arch *447*, 666-676.

Kramer, A., Yang, F.C., Snodgrass, P., Li, X., Scammell, T.E., Davis, F.C., and Weitz, C.J. (2001). Regulation of daily locomotor activity and sleep by hypothalamic EGF receptor signaling. Science *294*, 2511-2515.

Kraves, S., and Weitz, C.J. (2006). A role for cardiotrophin-like cytokine in the circadian control of mammalian locomotor activity. Nat Neurosci *9*, 212-219.

Lamia, K.A., Storch, K.F., and Weitz, C.J. (2008). Physiological significance of a peripheral tissue circadian clock. Proc Natl Acad Sci U S A *105*, 15172-15177.

Lechtreck, K.F., and Witman, G.B. (2007). Chlamydomonas reinhardtii hydin is a central pair protein required for flagellar motility. J Cell Biol *176*, 473-482.

Lee, D.H., Maunsbach, A.B., Riquier-Brison, A.D., Nguyen, M.T., Fenton, R.A., Bachmann, S., Yu, A.S., and McDonough, A.A. (2013). Effects of ACE inhibition and ANG II stimulation on renal Na-Cl cotransporter distribution, phosphorylation, and membrane complex properties. Am J Physiol Cell Physiol *304*, C147-163.

Lee, J., Kim, M.S., Li, R., Liu, V.Y., Fu, L., Moore, D.D., Ma, K., and Yechoor, V.K. (2011). Loss of Bmal1 leads to uncoupling and impaired glucose-stimulated insulin secretion in beta-cells. Islets *3*, 381-388.

Lee, L. (2011). Mechanisms of mammalian ciliary motility: Insights from primary ciliary dyskinesia genetics. Gene *473*, 57-66.

LeSauter, J., Lehman, M.N., and Silver, R. (1996). Restoration of circadian rhythmicity by transplants of SCN "micropunches". J Biol Rhythms *11*, 163-171.

LeSauter, J., Romero, P., Cascio, M., and Silver, R. (1997). Attachment site of grafted SCN influences precision of restored circadian rhythm. J Biol Rhythms *12*, 327-338.

Li, J.D., Hu, W.P., Boehmer, L., Cheng, M.Y., Lee, A.G., Jilek, A., Siegel, J.M., and Zhou, Q.Y. (2006). Attenuated circadian rhythms in mice lacking the prokineticin 2 gene. J Neurosci *26*, 11615-11623.

Marion, V., Stoetzel, C., Schlicht, D., Messaddeq, N., Koch, M., Flori, E., Danse, J.M., Mandel, J.L., and Dollfus, H. (2009). Transient ciliogenesis involving Bardet-Biedl syndrome proteins is a fundamental characteristic of adipogenic differentiation. Proc Natl Acad Sci U S A *106*, 1820-1825.

Marpegan, L., Swanstrom, A.E., Chung, K., Simon, T., Haydon, P.G., Khan, S.K., Liu, A.C., Herzog, E.D., and Beaule, C. (2011). Circadian regulation of ATP release in astrocytes. J Neurosci *31*, 8342-8350.

Marshall, W.F., and Kintner, C. (2008). Cilia orientation and the fluid mechanics of development. Curr Opin Cell Biol *20*, 48-52.

Mathew, T.C. (1998). Supraependymal neuronal elements of the floor of the fourth ventricle in adult rat: a scanning electron microscopic study. J Submicrosc Cytol Pathol *30*, 175-181.

Maywood, E.S., Chesham, J.E., O'Brien, J.A., and Hastings, M.H. (2011). A diversity of paracrine signals sustains molecular circadian cycling in suprachiasmatic nucleus circuits. Proc Natl Acad Sci U S A *108*, 14306-14311.

Maywood, E.S., O'Neill, J.S., Chesham, J.E., and Hastings, M.H. (2007). Minireview: The circadian clockwork of the suprachiasmatic nuclei--analysis of a cellular oscillator that drives endocrine rhythms. Endocrinology *148*, 5624-5634.

McDearmon, E.L., Patel, K.N., Ko, C.H., Walisser, J.A., Schook, A.C., Chong, J.L., Wilsbacher, L.D., Song, E.J., Hong, H.K., Bradfield, C.A*., et al.* (2006). Dissecting the functions of the mammalian clock protein BMAL1 by tissue-specific rescue in mice. Science *314*, 1304-1308.

McCarthy, J.J., Andrews, J.L., McDearmon E.L., Campbell K.S., Barber, B.K., Miller, B.H., Walker, J.R., Hogenesch, J.B., Takahashi, J.S., Esser, K.A. (2007). Identification of the circadian transcriptome in adult mouse skeletal muscle. Physiol Genomics *31(1),* 86-95.

Meng, Q.J., Logunova, L., Maywood, E.S., Gallego, M., Lebiecki, J., Brown, T.M., Sladek, M., Semikhodskii, A.S., Glossop, N.R., Piggins, H.D*., et al.* (2008). Setting clock speed in mammals: the CK1 epsilon tau mutation in mice accelerates circadian pacemakers by selectively destabilizing PERIOD proteins. Neuron *58*, 78-88.

Millar, I.D., Bruce, J., and Brown, P.D. (2007). Ion channel diversity, channel expression and function in the choroid plexuses. Cerebrospinal Fluid Res *4*, 8.

Miller, B.H., McDearmon, E.L., Panda, S., Hayes, K.R., Zhang, J., Andrews, J.L., Antoch, M.P., Walker, J.R., Esser, K.A., Hogenesch, J.B*., et al.* (2007). Circadian and CLOCK-controlled regulation of the mouse transcriptome and cell proliferation. Proc Natl Acad Sci U S A *104*, 3342-3347.

Mirzadeh, Z., Han, Y.G., Soriano-Navarro, M., Garcia-Verdugo, J.M., and Alvarez-Buylla, A. (2010). Cilia organize ependymal planar polarity. J Neurosci *30*, 2600-2610.

Mohawk, J.A., Green, C.B., Takahashi, J.S. (2012). Central and peripheral clocks in mammals. Annu Rev Neurosci *35*, 445-62.

Montcouquiol, M., Rachel, R.A., Lanford, P.J., Copeland, N.G., Jenkins, N.A., and Kelley, M.W. (2003). Identification of Vangl2 and Scrb1 as planar polarity genes in mammals. Nature *423*, 173-177.

Moore, R.Y., and Eichler, V.B. (1972). Loss of a circadian adrenal corticosterone rhythm following suprachiasmatic lesions in the rat. Brain Res *42*, 201-206.

Mosko, S.S., and Moore, R.Y. (1979). Neonatal suprachiasmatic nucleus lesions: effects on the development of circadian rhythms in the rat. Brain Res *164*, 17-38.

Mrosovsky, N. (1999). Masking: history, definitions, and measurement. Chronobiol Int *16*, 415-429.

Muhlbauer, E., Gross, E., Labucay, K., Wolgast, S., and Peschke, E. (2009). Loss of melatonin signalling and its impact on circadian rhythms in mouse organs regulating blood glucose. Eur J Pharmacol *606*, 61-71.

Narita, K., Kawate, T., Kakinuma, N., and Takeda, S. (2010). Multiple primary cilia modulate the fluid transcytosis in choroid plexus epithelium. Traffic *11*, 287-301.

Nilsson, C., Kannisto, P., Lindvall-Axelsson, M., Owman, C., and Rosengren, E. (1990). The neuropeptides vasoactive intestinal polypeptide, peptide histidine isoleucine and neuropeptide Y modulate [3H]noradrenaline release from sympathetic nerves in the choroid plexus. Eur J Pharmacol *181*, 247-252.

Nilsson, C., Stahlberg, F., Thomsen, C., Henriksen, O., Herning, M., and Owman, C. (1992). Circadian variation in human cerebrospinal fluid production measured by magnetic resonance imaging. Am J Physiol *262*, R20-24.

O'Connor, A.K., Malarkey, E.B., Berbari, N.F., Croyle, M.J., Haycraft, C.J., Bell, P.D., Hohenstein, P., Kesterson, R.A., and Yoder, B.K. (2013). An inducible CiliaGFP mouse model for in vivo visualization and analysis of cilia in live tissue. Cilia *2*, 8.

Ohdo, S. (2007). Chronopharmacology focused on biological clock. Drug Metab Pharmacokinet *22*, 3-14.

Okoniewski, M.J., and Miller, C.J. (2008). Comprehensive analysis of affymetrix exon arrays using BioConductor. PLoS Comput Biol *4*, e6.

Oster, H., Damerow, S., Hut, R.A., and Eichele, G. (2006a). Transcriptional profiling in the adrenal gland reveals circadian regulation of hormone biosynthesis genes and nucleosome assembly genes. J Biol Rhythms *21*, 350-361.

Oster, H., Damerow, S., Kiessling, S., Jakubcakova, V., Abraham, D., Tian, J., Hoffmann, M.W., and Eichele, G. (2006b). The circadian rhythm of glucocorticoids is regulated by a gating mechanism residing in the adrenal cortical clock. Cell Metab *4*, 163-173.

Ostrowski, L.E., Hutchins, J.R., Zakel, K., and O'Neal, W.K. (2003). Targeting expression of a transgene to the airway surface epithelium using a ciliated cell-specific promoter. Mol Ther *8*, 637-645.

Ounjai, P., Kim, K.D., Liu, H., Dong, M., Tauscher, A.N., Witkowska, H.E., and Downing, K.H. (2013). Architectural insights into a ciliary partition. Curr Biol *23*, 339-344.

Panda, S., Antoch, M.P., Miller, B.H., Su, A.I., Schook, A.B., Straume, M., Schultz, P.G., Kay, S.A., Takahashi, J.S., and Hogenesch, J.B. (2002). Coordinated transcription of key pathways in the mouse by the circadian clock. Cell *109*, 307-320.

Partch, C.L., Green, C.B., and Takahashi, J.S. (2013). Molecular architecture of the mammalian circadian clock. Trends Cell Biol.

Paschos, G.K., Baggs, J.E., Hogenesch, J.B., and FitzGerald, G.A. (2010). The role of clock genes in pharmacology. Annu Rev Pharmacol Toxicol *50*, 187-214.

Pedersen, L.B., and Christensen, S.T. (2012). Regulating intraflagellar transport. Nat Cell Biol *14*, 904-906.

Pedersen, L.B., Veland, I.R., Schroder, J.M., and Christensen, S.T. (2008). Assembly of primary cilia. Dev Dyn *237*, 1993-2006.

Peek, C.B., Ramsey, K.M., Marcheva, B., and Bass, J. (2012). Nutrient sensing and the circadian clock. Trends Endocrinol Metab *23*, 312-318.

Praetorius, J. (2007). Water and solute secretion by the choroid plexus. Pflugers Arch *454*, 1-18.

Preston, J.E. (2001). Ageing choroid plexus-cerebrospinal fluid system. Microsc Res Tech *52*, 31-37.

Prosser, H.M., Bradley, A., Chesham, J.E., Ebling, F.J., Hastings, M.H., and Maywood, E.S. (2007). Prokineticin receptor 2 (Prokr2) is essential for the regulation of circadian behavior by the suprachiasmatic nuclei. Proc Natl Acad Sci U S A *104*, 648-653.

Purkinje, (1836). Über Flimmerbewegungen im Gehirn in Müller´s Archiv, 290-291.

Quay, W.B. (1972). Twenty-four-hour rhythmicity in carbonic anhydrase activities of choroid plexuses and pineal gland. Anat Rec *174*, 279-287.

Ramsey, K.M., Marcheva, B., Kohsaka, A., Bass, J. (2007). The clockwork of metabolism. Annu Rev Nutr *27,* 219-40.

Reddy, A.B., Karp, N.A., Maywood, E.S., Sage, E.A., Deery, M., O'Neill, J.S., Wong, G.K., Chesham, J., Odell, M., Lilley, K.S*., et al.* (2006). Circadian orchestration of the hepatic proteome. Curr Biol *16*, 1107-1115.

Redlin, U., and Mrosovsky, N. (1999). Masking by light in hamsters with SCN lesions. J Comp Physiol A *184*, 439-448.

Redzic, Z.B., and Segal, M.B. (2004). The structure of the choroid plexus and the physiology of the choroid plexus epithelium. Adv Drug Deliv Rev *56*, 1695-1716.

Reed, H.E., Meyer-Spasche, A., Cutler, D.J., Coen, C.W., and Piggins, H.D. (2001). Vasoactive intestinal polypeptide (VIP) phase-shifts the rat suprachiasmatic nucleus clock in vitro. Eur J Neurosci *13*, 839-843.

Reese, T.S., and Karnovsky, M.J. (1967). Fine structural localization of a blood-brain barrier to exogenous peroxidase. J Cell Biol *34*, 207-217.

Reick, M., Garcia, J.A., Dudley, C., and McKnight, S.L. (2001). NPAS2: an analog of clock operative in the mammalian forebrain. Science *293*, 506-509.

Reiter, J.F., Blacque, O.E., and Leroux, M.R. (2012). The base of the cilium: roles for transition fibres and the transition zone in ciliary formation, maintenance and compartmentalization. EMBO Rep *13*, 608-618.

Rennels, M.L., Blaumanis, O.R., Grady, P.A. (1990). Rapid solute transport throughout the brain via paravascular pathways. Adv Neurol *52*, 431-439.

Riquier-Brison, A.D., Leong, P.K., Pihakaski-Maunsbach, K., and McDonough, A.A. (2010). Angiotensin II stimulates trafficking of NHE3, NaPi2, and associated proteins into the proximal tubule microvilli. Am J Physiol Renal Physiol *298*, F177-186.

Robins, S.C., Stewart, I., McNay, D.E., Taylor, V., Giachino, C., Goetz, M., Ninkovic, J., Briancon, N., Maratos-Flier, E., Flier, J.S*., et al.* (2013). alpha-Tanycytes of the adult hypothalamic third ventricle include distinct populations of FGF-responsive neural progenitors. Nat Commun *4*, 2049.

Rodriguez, E.M., Blazquez, J.L., Pastor, F.E., Pelaez, B., Pena, P., Peruzzo, B., and Amat, P. (2005). Hypothalamic tanycytes: a key component of brain-endocrine interaction. Int Rev Cytol *247*, 89-164.

Roth, Y., Kimhi, Y., Edery, H., Aharonson, E., and Priel, Z. (1985). Ciliary motility in brain ventricular system and trachea of hamsters. Brain Res *330*, 291-297.

Rusak, B. (1979). Neural mechanisms for entrainment and generation of mammalian circadian rhythms. Fed Proc *38*, 2589-2595.

Rusak, B., and Zucker, I. (1979). Neural regulation of circadian rhythms. Physiol Rev *59*, 449-526.

Saini, C., Suter, D.M., Liani, A., Gos, P., and Schibler, U. (2011). The mammalian circadian timing system: synchronization of peripheral clocks. Cold Spring Harb Symp Quant Biol *76*, 39-47.

Saitoh, Y., Nihonmatsu, I., and Kawamura, H. (1987). Transplantation of the suprachiasmatic nucleus in the rat. Acta Neurochir Suppl (Wien) *41*, 41-45.

Saunders, N.R., Daneman, R., Dziegielewska, K.M., and Liddelow, S.A. (2013). Transporters of the blood-brain and blood-CSF interfaces in development and in the adult. Mol Aspects Med *34*, 742-752.

Saunders, N.R., Ek, C.J., Habgood, M.D., and Dziegielewska, K.M. (2008). Barriers in the brain: a renaissance? Trends Neurosci *31*, 279-286.

Sawaki, Y., Nihonmatsu, I., and Kawamura, H. (1984). Transplantation of the neonatal suprachiasmatic nuclei into rats with complete bilateral suprachiasmatic lesions. Neurosci Res *1*, 67-72.

Sawamoto, K., Wichterle, H., Gonzalez-Perez, O., Cholfin, J.A., Yamada, M., Spassky, N., Murcia, N.S., Garcia-Verdugo, J.M., Marin, O., Rubenstein, J.L.*, et al.* (2006). New neurons follow the flow of cerebrospinal fluid in the adult brain. Science *311*, 629-632.

Schreiber, G., Aldred, A.R., Jaworowski, A., Nilsson, C., Achen, M.G., and Segal, M.B. (1990). Thyroxine transport from blood to brain via transthyretin synthesis in choroid plexus. Am J Physiol *258*, R338-345.

Schroeder, A., Mueller, O., Stocker, S., Salowsky, R., Leiber, M., Gassmann, M., Lightfoot, S., Menzel, W., Granzow, M., and Ragg, T. (2006). The RIN: an RNA integrity number for assigning integrity values to RNA measurements. BMC Mol Biol *7*, 3.

Seeley, E.S., and Nachury, M.V. (2010). The perennial organelle: assembly and disassembly of the primary cilium. J Cell Sci *123*, 511-518.

Segal, M.B. (2000). The choroid plexuses and the barriers between the blood and the cerebrospinal fluid. Cell Mol Neurobiol *20*, 183-196.

Shah, A.S., Ben-Shahar, Y., Moninger, T.O., Kline, J.N., and Welsh, M.J. (2009). Motile cilia of human airway epithelia are chemosensory. Science *325*, 1131-1134.

Sharma, N., Kosan, Z.A., Stallworth, J.E., Berbari, N.F., and Yoder, B.K. (2011). Soluble levels of cytosolic tubulin regulate ciliary length control. Mol Biol Cell *22*, 806-816.

Shearer, K.D., Fragoso, Y.D., Clagett-Dame, M., and McCaffery, P.J. (2012). Astrocytes as a regulated source of retinoic acid for the brain. Glia *60*, 1964-1976.

Shinohara, K., Kawasumi, A., Takamatsu, A., Yoshiba, S., Botilde, Y., Motoyama, N., Reith, W., Durand, B., Shiratori, H., and Hamada, H. (2012). Two rotating cilia in the node cavity are sufficient to break left-right symmetry in the mouse embryo. Nat Commun *3*, 622.

Siepka, S.M., Yoo, S.H., Park, J., Song, W., Kumar, V., Hu, Y., Lee, C., and Takahashi, J.S. (2007). Circadian mutant Overtime reveals F-box protein FBXL3 regulation of cryptochrome and period gene expression. Cell *129*, 1011-1023.

Silver, R., LeSauter, J., Tresco, P.A., and Lehman, M.N. (1996). A diffusible coupling signal from the transplanted suprachiasmatic nucleus controlling circadian locomotor rhythms. Nature *382*, 810-813.

Simons, M., and Mlodzik, M. (2008). Planar cell polarity signaling: from fly development to human disease. Annu Rev Genet *42*, 517-540.

Skipor, J., and Thiery, J.C. (2008). The choroid plexus--cerebrospinal fluid system: undervaluated pathway of neuroendocrine signaling into the brain. Acta Neurobiol Exp (Wars) *68*, 414-428.

Smith, D.E., Johanson, C.E., and Keep, R.F. (2004). Peptide and peptide analog transport systems at the blood-CSF barrier. Adv Drug Deliv Rev *56*, 1765-1791.

Spassky, N., Merkle, F.T., Flames, N., Tramontin, A.D., Garcia-Verdugo, J.M., and Alvarez-Buylla, A. (2005). Adult ependymal cells are postmitotic and are derived from radial glial cells during embryogenesis. J Neurosci *25*, 10-18.

Spector, R. (2010). Nature and consequences of mammalian brain and CSF efflux transporters: four decades of progress. J Neurochem *112*, 13-23.

Spector, R., and Johanson, C. (2006). Micronutrient and urate transport in choroid plexus and kidney: implications for drug therapy. Pharm Res *23*, 2515-2524.

Stephan, F.K., and Zucker, I. (1972). Circadian rhythms in drinking behavior and locomotor activity of rats are eliminated by hypothalamic lesions. Proc Natl Acad Sci U S A *69*, 1583-1586.

Storch, K.F., Lipan, O., Leykin, I., Viswanathan, N., Davis, F.C., Wong, W.H., and Weitz, C.J. (2002). Extensive and divergent circadian gene expression in liver and heart. Nature *417*, 78-83.

Storch, K.F., Paz, C., Signorovitch, J., Raviola, E., Pawlyk, B., Li, T., and Weitz, C.J. (2007). Intrinsic circadian clock of the mammalian retina: importance for retinal processing of visual information. Cell *130*, 730-741.

Strazielle, N., Khuth, S.T., and Ghersi-Egea, J.F. (2004). Detoxification systems, passive and specific transport for drugs at the blood-CSF barrier in normal and pathological situations. Adv Drug Deliv Rev *56*, 1717-1740.

Sujino, M., Masumoto, K.H., Yamaguchi, S., van der Horst, G.T., Okamura, H., and Inouye, S.T. (2003). Suprachiasmatic nucleus grafts restore circadian behavioral rhythms of genetically arrhythmic mice. Curr Biol *13*, 664-668.

Tamanini, F., Yagita, K., Okamura, H., and van der Horst, G.T. (2005). Nucleocytoplasmic shuttling of clock proteins. Methods Enzymol *393*, 418-435.

Thanos, C.G., Bintz, B., and Emerich, D.F. (2010). Microencapsulated choroid plexus epithelial cell transplants for repair of the brain. Adv Exp Med Biol *670*, 80-91.

Thomas, S.A., Preston, J.E., Wilson, M.R., Farrell, C.L., and Segal, M.B. (2001). Leptin transport at the blood--cerebrospinal fluid barrier using the perfused sheep choroid plexus model. Brain Res *895*, 283-290.

Threadgill, D.W., Yee, D., Matin, A., Nadeau, J.H., and Magnuson, T. (1997). Genealogy of the 129 inbred strains: 129/SvJ is a contaminated inbred strain. Mamm Genome *8*, 390-393.

Tissir, F., Qu, Y., Montcouquiol, M., Zhou, L., Komatsu, K., Shi, D., Fujimori, T., Labeau, J., Tyteca, D., Courtoy, P*., et al.* (2010). Lack of cadherins Celsr2 and Celsr3 impairs ependymal ciliogenesis, leading to fatal hydrocephalus. Nat Neurosci *13*, 700-707.

Tosini, G., and Menaker, M. (1996). Circadian rhythms in cultured mammalian retina. Science *272*, 419-421.

Ukai-Tadenuma, M., Yamada, R.G., Xu, H., Ripperger, J.A., Liu, A.C., and Ueda, H.R. (2011). Delay in feedback repression by cryptochrome 1 is required for circadian clock function. Cell *144*, 268-281.

Vigh-Teichmann, I., and Vigh, B. (1983). The system of cerebrospinal fluid-contacting neurons. Arch Histol Jpn *46*, 427-468.

Vigh, B., Manzano e Silva, M.J., Frank, C.L., Vincze, C., Czirok, S.J., Szabo, A., Lukats, A., and Szel, A. (2004). The system of cerebrospinal fluid-contacting neurons. Its supposed role in the nonsynaptic signal transmission of the brain. Histol Histopathol *19*, 607-628.

Vigh, B., and Vigh-Teichmann, I. (1998). Actual problems of the cerebrospinal fluid-contacting neurons. Microsc Res Tech *41*, 57-83.

Vitaterna, M.H., King, D.P., Chang, A.M., Kornhauser, J.M., Lowrey, P.L., McDonald, J.D., Dove, W.F., Pinto, L.H., Turek, F.W., and Takahashi, J.S. (1994). Mutagenesis and mapping of a mouse gene, Clock, essential for circadian behavior. Science *264*, 719-725.

Vladar, E.K., Bayly, R.D., Sangoram, A.M., Scott, M.P., and Axelrod, J.D. (2012). Microtubules enable the planar cell polarity of airway cilia. Curr Biol *22*, 2203-2212.

Vorbrodt, A.W., and Dobrogowska, D.H. (2003). Molecular anatomy of intercellular junctions in brain endothelial and epithelial barriers: electron microscopist's view. Brain Res Brain Res Rev *42*, 221-242.

Vosko, A.M., Schroeder, A., Loh, D.H., and Colwell, C.S. (2007). Vasoactive intestinal peptide and the mammalian circadian system. Gen Comp Endocrinol *152*, 165-175.

Wallingford, J.B. (2010). Planar cell polarity signaling, cilia and polarized ciliary beating. Curr Opin Cell Biol *22*, 597-604.

Wallingford, J.B., and Mitchell, B. (2011). Strange as it may seem: the many links between Wnt signaling, planar cell polarity, and cilia. Genes Dev *25*, 201-213.

Wang, Q., Maillard, M., Schibler, U., Burnier, M., and Gachon, F. (2010). Cardiac hypertrophy, low blood pressure, and low aldosterone levels in mice devoid of the three circadian PAR bZip transcription factors DBP, HLF, and TEF. Am J Physiol Regul Integr Comp Physiol *299*, R1013-1019.

Welsh, D.K., Yoo, S.H., Liu, A.C., Takahashi, J.S., and Kay, S.A. (2004). Bioluminescence imaging of individual fibroblasts reveals persistent, independently phased circadian rhythms of clock gene expression. Curr Biol *14*, 2289-2295.

Werner, M.E., Hwang, P., Huisman, F., Taborek, P., Yu, C.C., and Mitchell, B.J. (2011). Actin and microtubules drive differential aspects of planar cell polarity in multiciliated cells. J Cell Biol *195*, 19-26.

Westlake, C.J., Baye, L.M., Nachury, M.V., Wright, K.J., Ervin, K.E., Phu, L., Chalouni, C., Beck, J.S., Kirkpatrick, D.S., Slusarski, D.C.*, et al.* (2011). Primary cilia membrane assembly is initiated by Rab11

and transport protein particle II (TRAPPII) complex-dependent trafficking of Rabin8 to the centrosome. Proc Natl Acad Sci U S A *108*, 2759-2764.

Whelan, G., Kreidl, E., Wutz, G., Egner, A., Peters, J.M., and Eichele, G. (2012). Cohesin acetyltransferase Esco2 is a cell viability factor and is required for cohesion in pericentric heterochromatin. EMBO J *31*, 71-82.

Wittkowski, W. (1998). Tanycytes and pituicytes: morphological and functional aspects of neuroglial interaction. Microsc Res Tech *41*, 29-42.

Wostyn, P., De Groot, V., Van Dam, D., Audenaert, K., and De Deyn, P.P. (2013). Senescent changes in cerebrospinal fluid circulatory physiology and their role in the pathogenesis of normal-tension glaucoma. Am J Ophthalmol *156*, 5-14 e12.

Yamadori, T. (1972). A scanning electron microscopic observation of the choroid plexus in rats. Arch Histol Jpn *35*, 89-97.

Yamadori, T., and Yagihashi, S. (1975). A scanning and transmission electron microscopic observation of the fourth ventricular floor in the mouse. Arch Histol Jpn *37*, 415-432.

Yamaguchi, S., Isejima, H., Matsuo, T., Okura, R., Yagita, K., Kobayashi, M., and Okamura, H. (2003). Synchronization of cellular clocks in the suprachiasmatic nucleus. Science *302*, 1408-1412.

Yamazaki, S., Numano, R., Abe, M., Hida, A., Takahashi, R., Ueda, M., Block, G.D., Sakaki, Y., Menaker, M., and Tei, H. (2000). Resetting central and peripheral circadian oscillators in transgenic rats. Science *288*, 682-685.

Yan, J., Wang, H., Liu, Y., and Shao, C. (2008). Analysis of gene regulatory networks in the mammalian circadian rhythm. PLoS Comput Biol *4*, e1000193.

Yaylaoglu, M.B., Titmus, A., Visel, A., Alvarez-Bolado, G., Thaller, C., and Eichele, G. (2005). Comprehensive expression atlas of fibroblast growth factors and their receptors generated by a novel robotic in situ hybridization platform. Dev Dyn *234*, 371-386.

Yoo, S.H., Yamazaki, S., Lowrey, P.L., Shimomura, K., Ko, C.H., Buhr, E.D., Siepka, S.M., Hong, H.K., Oh, W.J., Yoo, O.J.*, et al.* (2004). PERIOD2::LUCIFERASE real-time reporting of circadian dynamics reveals persistent circadian oscillations in mouse peripheral tissues. Proc Natl Acad Sci U S A *101*, 5339-5346.

Zakharov, A., Papaiconomou, C., Koh, L., Djenic, J., Bozanovic-Sosic, R., and Johnston, M. (2004). Integrating the roles of extracranial lymphatics and intracranial veins in cerebrospinal fluid absorption in sheep. Microvasc Res *67*, 96-104.

Zappaterra, M.W., and Lehtinen, M.K. (2012). The cerebrospinal fluid: regulator of neurogenesis, behavior, and beyond. Cell Mol Life Sci *69*, 2863-2878.

Zariwala, M.A., Knowles, M.R., and Omran, H. (2007). Genetic defects in ciliary structure and function. Annu Rev Physiol *69*, 423-450.

Zlokovic, B.V. (2008). The blood-brain barrier in health and chronic neurodegenerative disorders. Neuron *57*, 178-201.

Zlokovic, B.V., Jovanovic, S., Miao, W., Samara, S., Verma, S., and Farrell, C.L. (2000). Differential regulation of leptin transport by the choroid plexus and blood-brain barrier and high affinity transport systems for entry into hypothalamus and across the blood-cerebrospinal fluid barrier. Endocrinology *141*, 1434-1441.

Zvonic,S., Ptitsyn, A.A., Conrad, S.A., Scott, L.K., Floyd, Z.E., Kilroy, G., Wu, X., Goh,B.C., Mynatt, R.L., Gimble, J.M. (2006). Characterization of peripheral circadian clocks in adipose tissues. Diabetes *55(4)*, 962-70.

Acknowledgement

First, I would like to thank Gregor Eichele that he offered me the opportunity to work on such an interesting project. I appreciate a lot the atmosphere of freedom and support that he offered. I am grateful for the trust he set in my ideas and my work and for the fruitful and inspiring discussions we had during all stages of my work.

Next, I would like to thank Eberhard Bodenschatz who opened the doors to his department for me and my project. He generously shared equipment, knowledge, and enthusiasm. The fruits of our cooperation are a central part of my work.

Also, I would like to thank my cooperation partners that strongly supported me with computational tasks. Thanks to Wenchao Hu and Jun Yan that you for your work on my array data and for the interesting discussions we had! And thanks to Christian Westendorf who did a great job whenever I asked for programming with Matlab. Thanks for your patience, your great help, and for being a friend.

The students Jana Renziehausen and Shoba Kapoor were a good help in lab with qRT-PCR, Immunostaining, and discussion partners for my projects. Thanks for your support and interest!

Further, I wish to express thanks to Christina Thaller, Gregor Eichele, Esther Kuhney, and Donald Hunneman for corrections and discussions of my thesis text.

Thanks to Ute Kunze, Simone Brauer, and Denise Brödner that you took care of our mice with so much passion and for discussion and support with my animal experiments.

Thanks to Maren Brockstett and Frauke Grabbe for help with sectioning, ISH, and much more.

I appreciate a lot the discussions during coffee breaks with my colleagues in the “genes and behavior” and the “dynamics and self-organization”. Especially at the beginning of my thesis, Ana Martinez-Hernandez, Jana Husse, and Henrik Oster have strongly supported, encouraged, and inspired my work. To you and all the other colleagues that hopefully feel addressed even though not mentioned individually: Thanks!

I wish to express thanks especially to my parents, my three brothers, my “parents in law”, and my friends that always encouraged me, shared good times and bad times, and always believed in me.

My daughter is the most important in my life and she accepted me spending weekends and nights in lab. Thanks for that, Lea! The time with you has always been my highlight of the day! I appreciate your joyful and strong character, your imagination, (thanks for your ideas about the experiments!). You are perfect the way you are.

Regina Faubel

Curriculum Vitae

Name: Regina Johanna Faubel

Date of birth: 14.05.1981

Place of birth: Göttingen

Education

2008-2013	PhD student in the Department Genes and Behavior, Max-Planck-Institute for Biophysical Chemistry, Göttingen.
2007-2008	Diploma thesis in the Department of Molecular Biology and Physiology of Plants; Albrecht von Haller Institute for plant science, Georg August Universität Göttingen.
2007	student job at the Albrecht von Haller Institute for plant science, Georg August Universität, Göttingen.
2005/2006	Project work and student job in the Department of Molecular Cell Differentiation; Max-Planck-Institute for Biophysical Chemistry, Göttingen.
2002-2008	Student of Biology Georg August Universität Göttingen.
2001-2002	Student of Medicine Université Louis Pasteur, Strasbourg, France.
2001	School leaving examination at the Theodor-Heuss-Gymnasium Göttingen,